AD

FLUID AMPLIFICATION

12. Binary Counter Design

Final Report

by
T. A. Shook
T. F. Chen
T. D. Reader

30 November 1964

U.S. ARMY MATERIEL COMMAND
HARRY DIAMOND LABCRATORIES
WASHINGTON, D.C. 20438

Prepared by:
UNIVAC, DIVISION OF SPERRY RAND CORP.
Under contract number:
DA-49-186-AMC-34(X)
UEC Project No. 240

AVAILABILITY/LIMITATION NOTICES

Qualified requesters may obtain copies of this report from DDC. DDC release to Clearinghouse for Federal Scientific and Technical Information is authorized.

AD

HDL Proj No. 31100
AMCMS CODE: 5011.11.71200
DA-1P010501A001

FLUID AMPLIFICATION

12. Binary Counter Design

Final Report

by
T. A. Shook
T. F. Chen
T. D. Reader

30 November 1964

U.S. ARMY MATERIEL COMMAND
HARRY DIAMOND LABORATORIES
WASHINGTON, D.C. 20438

Prepared by:
UNIVAC, DIVISION OF SPERRY RAND CORP.
Under contract number:
DA-49-186-AMC-34(X)
UEC Project No. 240

CONTENTS

ILLUSTRATIONS

ILLUSTRATIONS—Cont'd

APPENDICES

ABSTRACT

The following report is a detailed account of the work carried out by UNIVAC pursuant to Contract Number DA-49-186-AMC-34(X). It is of special interest in this contract to develop analytical tools which indicate circuit values in the construction of an all-fluid system, and which then predict its operating characteristics. In short, a circuit theory is to be formulated. An n-stage binary counter is selected for analysis, the foundations of which are the analogous equations of fluid flow and electrical current, and empirically formulated element characteristics.

1. INTRODUCTION

The primary goal of this investigation is the formulation of analytical techniques which allow a circuit to be constructed by defining and giving values to its relevant parameters, and which then predict its limits of operation. The term "analytical" is used here in its broadest sense: like most "theories," the analytical techniques developed here derive, in part, from a great deal of experimental data. It is this experimental data (most of it, steady state) which, although unspectacular, is really the backbone of the first portion of the investigation, for it is the characteristics of the elements and circuit components which permit the fashioning of a workable "DC" circuit. It remains for the more sophisticated (but less well developed) AC analysis to predict the frequency limits and other transient effect.

In addition, this contract is concerned with several other areas of interest which are related to, or come as by-products of the main investigation described above. These include design optimization, generalization of results, documentation of laboratory experience, particularly with dynamic instrumentation, scaling effects, sealing techniques, and control of spurious oscillation.

The circuit chosen for analysis was the binary counter circuit described in ref 1. Subsequent investigation of this circuit disclosed characteristics that made it appear inadvisable to continue with it. Several different designs were then considered, and one selected for study--one which gave promise of working quite satisfactorily, which presented a quite interesting and general type of circuit, and which was amenable to mathematical analysis.

Following this decision, the characteristics of the additional elements to be used in this circuit were obtained, and a 3-stage counter constructed and tested over a wide range of control signal inputs and power jet flows. Concurrently, the theoretical analysis was being developed which sought to determine a transfer function for

the flip-flop from an equivalent synthesized electrical network, predict frequency limits, predict the variation in output wave shape with changing loads--in a word, to describe the dynamic operation of the circuit.

2. TEST EQUIPMENT—INSTRUMENTATION

2.1 Mechanical Pulse Generator

Rapid generation of flow pulses was achieved by the use of a rotating disc with cutout slots on its periphery (fig. 1). In use, an air jet from a nozzle is aimed at the periphery, and the slots allow the the passage of the jet in rapid step-like fashion. Interchangeable discs with different size slots and variable motor speed make possible the independent variation of frequency and pulse duration. This apparatus produces rise times on the order of 0.1 msec. In terms of usual rise times encountered in fluid circuitry, this is a near-perfect step. Of course, receiver tubes or other impedances may be placed immediately downstream of the rotating disc to produce almost any desired signal.

2.2 Steady-State Instrumentation

The usual methods of steady-state measurement of flow and pressure were employed. Static pressures and total pressures (using a Pitot or stagnation tube) were indicated on conventional manometers. Air flow was measured using a variety of instruments--a few purchased flow meters, and a number of nozzles and orifice-type meters, machined and calibrated in our department.

2.3 Dynamic Instrumentation

The hot-wire anemometer is an indispensible tool in fluid amplifier research. Notwithstanding its drawbacks, it remains the obvious choice when transient flow measurements are required. One inherent problem in hot-wire anemometry is the nonlinearity of the mass flow-voltage output relationship. If one wishes to view the character of a wave form, he sees a distorted picture; the slope at low velocities is, of course, too high. If precise rise-time measurements are required, say between 10 and 90 percent points in velocity, the corresponding voltage points may be deduced with good accuracy, but this is a very great annoyance, especially where considerable quantities of data are being gathered.

Because of the great advantage in a linear system, our instrumentation section expended a considerable effort in the development of an anemometer with a linearized voltage output. This is a constant temperature system. Two such systems were built, tested, and put into operation in our laboratory.

Figure 1. Test apparatus

A few notes on our operating experience are worthwhile to record here. The units were built with the circuitry immersed in an oil bath for the primary purpose of damping out variations in the temperature of the surroundings. A subsequent test showed that the drift could be further reduced by maintaining the oil bath itself at a constant temperature. At this point, the systems were considered quite "useable" although there still occurred, from time to time, some unaccountable changes in the calibration curve of a particular probe--a phenomenon which was then interpreted as drift in some portion of the circuit. A short time later, it was to be discovered that the hot-wire probes exhibited "one-sidedness"--that is, in general, a probe exhibited different characteristics depending on its orientation to the direction of air flow. From this point on, all probes were carefully marked, and always calibrated and used with the same side subjected to the air flow. It was then evident that the actual electronic drift was at a tolerable level.

Naturally, where any changes at all can be expected, and when doing precise quantitative work, it is prudent to calibrate a probe before and after each such test. This is a practice which we have adopted in all of our test programs involving dynamic instrumentation. Following this practice, accuracy limits not exceeding ±5% in velocity are obtained.

In fluid systems, pressure is an equally important variable. A number of pressure transducers of various types has been introduced on the market, but the more desirable (capacitive type) has not been developed quite to the extent of hot-wire anemometry. Reference 2 gives an excellent pressure transducer survey, and discusses the general problem of pressure measurements in unsteady flow.

3. LARGE-SCALE TESTS

The first series of tests was directed toward obtaining the steady-state pressure and flow characteristics of the most important element in the circuit--the flip-flop. This series was performed in two parts, the complete description of which comprises Appendix A. The critical dimensions of this element (as supplied by HDL under the terms of the contract) are seen in figure A-1, Appendix A.

A nozzle width of 0.120 in. was chosen for the initial tests, and was prompted by two main considerations: (1) to observe scale effects, for by the use of the 0.120 in. size and the more conventional 0.030 in. size, a Reynolds Number range of 1,000 to 24,000 (based on nozzle width could be covered conveniently, and (2) accuracy of measurements. These tests were run with great attention to detail. Both pressure and flow were measured at all five ports for a number of input conditions, and a premium was placed upon accuracy of measurements. (See notes in section 4 about the difficulties involved in measurements on smaller apparatus.)

Part I of Appendix A, describing one phase of the work, is concerned with a representation of the flip-flop performance under changing load conditions. The load was simulated by a restriction in the form of an orifice located on each output leg of the flip-flop. Similar orifices were placed in the control ports to note what effect, if any, this had on performance. The test ranges of these geometric parameters, as well as the flow and pressure parameters, are shown below.

Parameter	Symbol	Test Range
Output load orifices	d_3, d_4	0.3125-0.52 in.
Normalized output load orifices	$(d_3/d_n)^2$, $(d_4/d_n)^2$	1.78-4.94
Control port orifices	d_2, d_5	0.1-0.52 in.
Normalized control port orifices	$(d_2/d_n)^2$, $(d_5/d_n)^2$	0.182-4.94
Supply pressure	P_1	5-45 in. H_2O
Nozzle velocity	V_1	124-400 fps
Power jet flow	Q_1	2.25-7 CFM
Mach Number	M	0.1-0.35
*Reynolds Number	R	7,440-24,000

*Based on nozzle width = 0.120 in.

The conclusions may be summarized as follows:

(1) The element may be operated without control input restrictions. The performance characteristics favor slightly this configuration. Operation is very stable and digital.

(2) The element is essentially insensitive to supply pressure in the range tested. Results are, therefore, simplified by normalization of pressures.

(3) A proportional range is exhibited for the load orifice value, $d_3 = d_4 = 0.3124$ in., or $(d_3/d_n)^2 = 1.78$

(4) The range of bistable operation is $d_3 = d_4 \geq 0.325$ in. or $(d_2/d_n)^2 \geq 1.93$.

(5) The estimated load range for useful operation is $0.338 \leq d_3 \leq 0.3725$ in., or $2.09 \leq (d_3/d_n)^2 \leq 2.54$

(6) At $d_3 = d_4 = 0.348$ in. (with control ports open)

Pressure gain	3.0
Pressure recovery	31.5%
Efficiency	43 %
Percent of power jet flow to switch (Q_5/Q_1)	22 %

Part II of Appendix A discusses "Presteering." The successful operation of the originally suggested binary counter is dependent on the induced flow in the "loop" (see figure below) to presteer an incoming pulse in the proper direction.

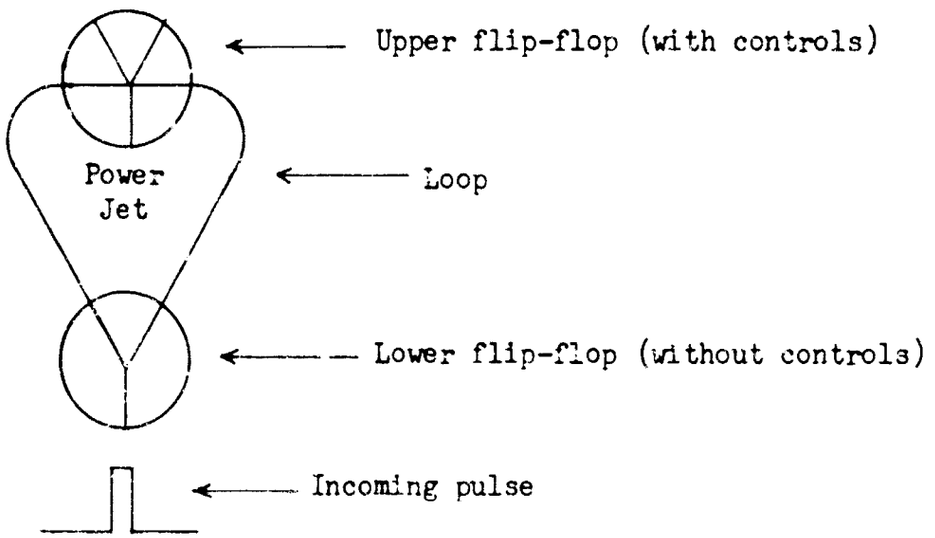

The jet stream in the upper flip-flop being asymetrical, establishes a pressure difference across the control ports, which in turn, accounts for the circulatory flow in the loop joining the two elements. This pressure difference, and the flow it induces were the subjects of investigation in this sequence of tests. Two typical load orifices were inserted in the output legs of the upper flip-flop, and measurements taken over a range of power jet flows.

The pressure difference across the control ports when blocked, or with a clamped loop, may be regarded as a measure of the "flow inducing capability" of the upper flip-flop. Of course, the actual flow which results depends on the resistance of the complete loop configuration, which embodies the lower element, and the lines connecting its outputs to the upper element inputs. For this reason, it is impossible to specify a value of flow until the entire configuration has been fixed. These tests used a simple loop with different orifices inserted to provide artificial resistance, and also to measure the flow.

The conclusions from these tests may be summarized as follows:

(1) The control port pressures were insensitive to the load orifices used.

(2) The induced loop flows ranged from 2 to 4 percent of the power jet flow for the line resistances used. It is estimated that the 4 percent figure is attainable (and probably necessary) in a practical configuration, when used in conjunction with the large element tested.

4. SMALL-SCALE TESTS

The critical dimensions of the 0.030-in. nozzle flip-flop remained the same (referring to fig. A-1), but the control port widths were changed from 5W to 3W, and the power jet port width from 10W to 3W. This was done to allow the use of our standard fittings, thereby facilitating the interconnecting of these and other circuit elements. These changes necessitated the making of a new template, from which a new brass master was machined. Several rubber molds were poured, and from these, several dozens of epoxy castings made.

Essentially, the same sequence of tests was performed as on the 0.120-in. element. The range of geometric, pressure, and flow parameters is given below:

		Test Range
Output load orifices	d_3 , d_4	0.079-0.110 in.
Normalized output load orifices	$(d_3/d_n)^2$, $(d_4/d_n)^2$	1.82-3.50
Control port orifices	d_5 , d_6	none used
Supply pressure	P_1	10-30 in H_2O
Nozzle width	V_1	200-350 fps
Power jet flow	Q_1	0.23-0.39 CFM

Mach Number	M	0.18-0.30
*Reynolds Number	R	3000-5200

*Based on nozzle width = 0.030 in.

The purpose of this section is to merely report the results of the small scale tests, and to compare them with the large scale performance. The differences are noted but not analyzed. A later section on scale effects attempts to introduce factors which account for these differences.

Figures 2 through 6 indicate and compare the performance of 0.03 and 0.12 in. nozzle scale models. Figure 2 shows the characteristics obtained for a single element, and may be compared with figure A-3. Figures 2, 3 and 4 compare the two sizes with respect to efficiency, pressure gain, and pressure recovery, respectively. Figure 5 shows the variation in pressure recovery and switching pressure exhibited by a number of small flip-flops.

The curves of figure 7 may be consulted to show the general variation in flow, velocity, and Reynolds Number at given supply pressures for both 0.03 and 0.12 in. nozzle flip-flops. They are approximate, since a slight variation with load orifices exists; however, this variation is less than ±5 percent.

There are several rather obvious differences in the performance characteristics of the two sizes. They may be summarized as follows:

(1) There is a definite "load-shift," as seen on figure 5, in particular. That is to say, the useful operating range of the 0.030-in. nozzle element has shifted to the left by about 10 percent in the $(d_o/d_n)^2$ load parameter. The useful operating range is defined as the range bounded on the right by the intersection of the on-side and switching-pressure curves, and on the left by the intersection of the off-side and switching pressure curves, or the limit of bistability, whichever occurs first.

(2) The small flip-flop appears to be more pressure sensitive; that is, normalized pressures vary a bit more over the supply pressure range investigated--a fact due partly to the practice used herein plotting static, rather than total pressures. See fuller description under "Scale Effects."

(3) Obtaining accurate and consistent results becomes a real problem when working with elements of the 0.030-in. nozzle class. Perhaps the most difficult problem is that of accurately machining the small load-simulating orifices in the output legs. It must be appreciated that the diameter range corresponding to the useful operating range is 0.081 to 0.089 in. An error as small as 0.001 in. is reflected in apparent inconsistencies in the load characteristics. It is evident that such inconsistencies do appear in the experimental data.

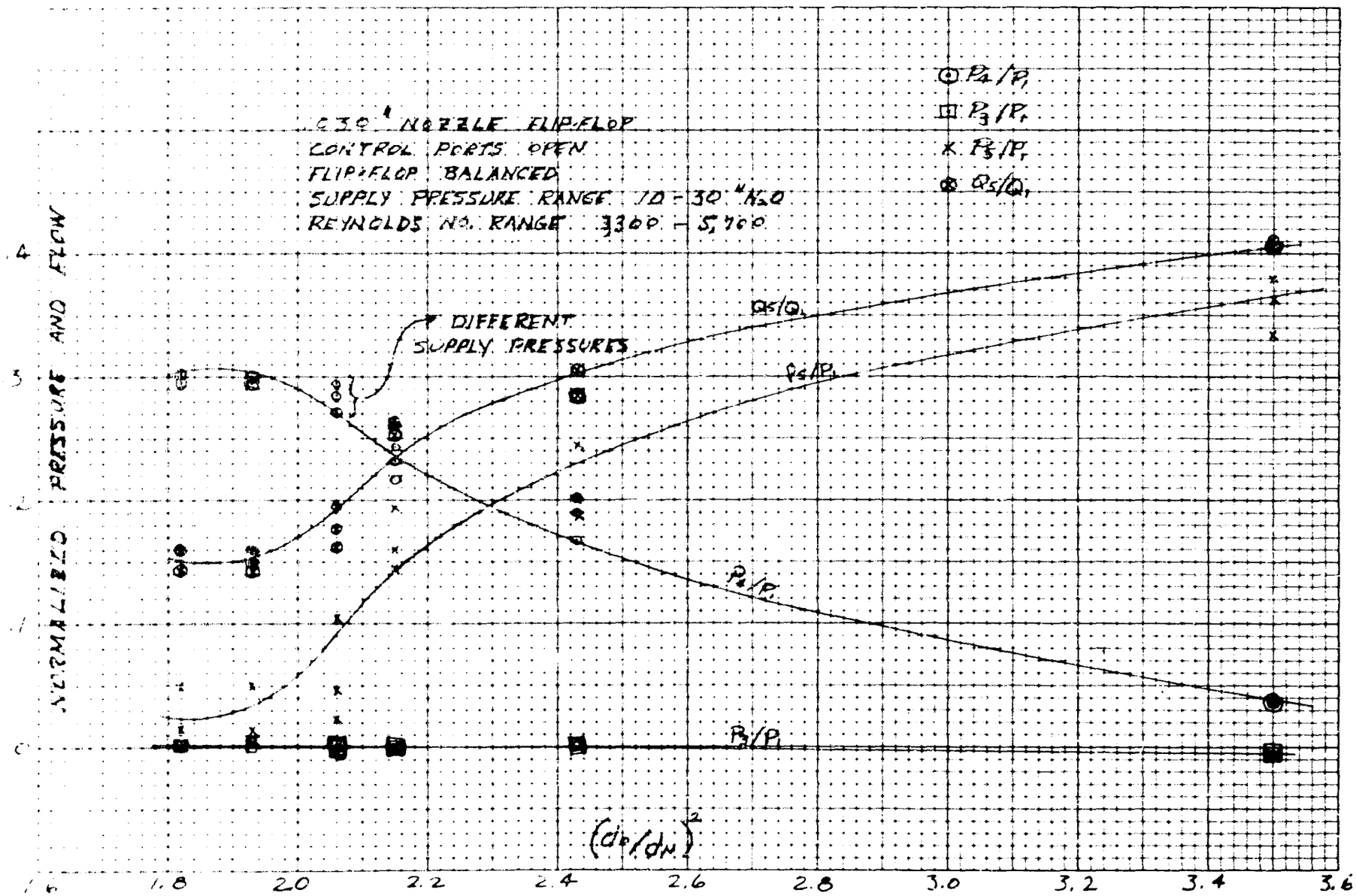

Figure 2. Performance comparison of 0.03- and 0.12-in. nozzle scale models.

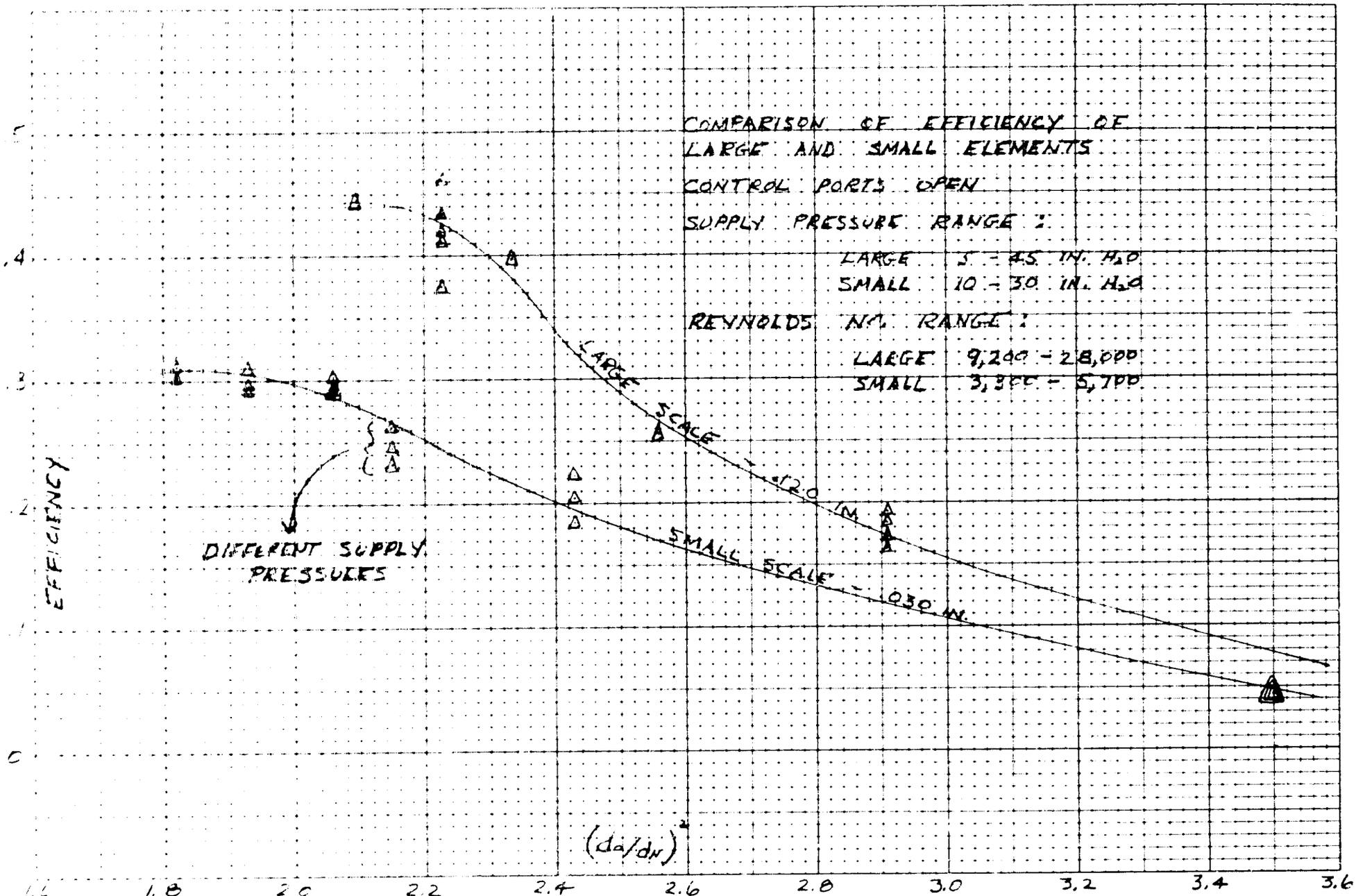

Figure 3. Comparison of efficiency of large and small elements.

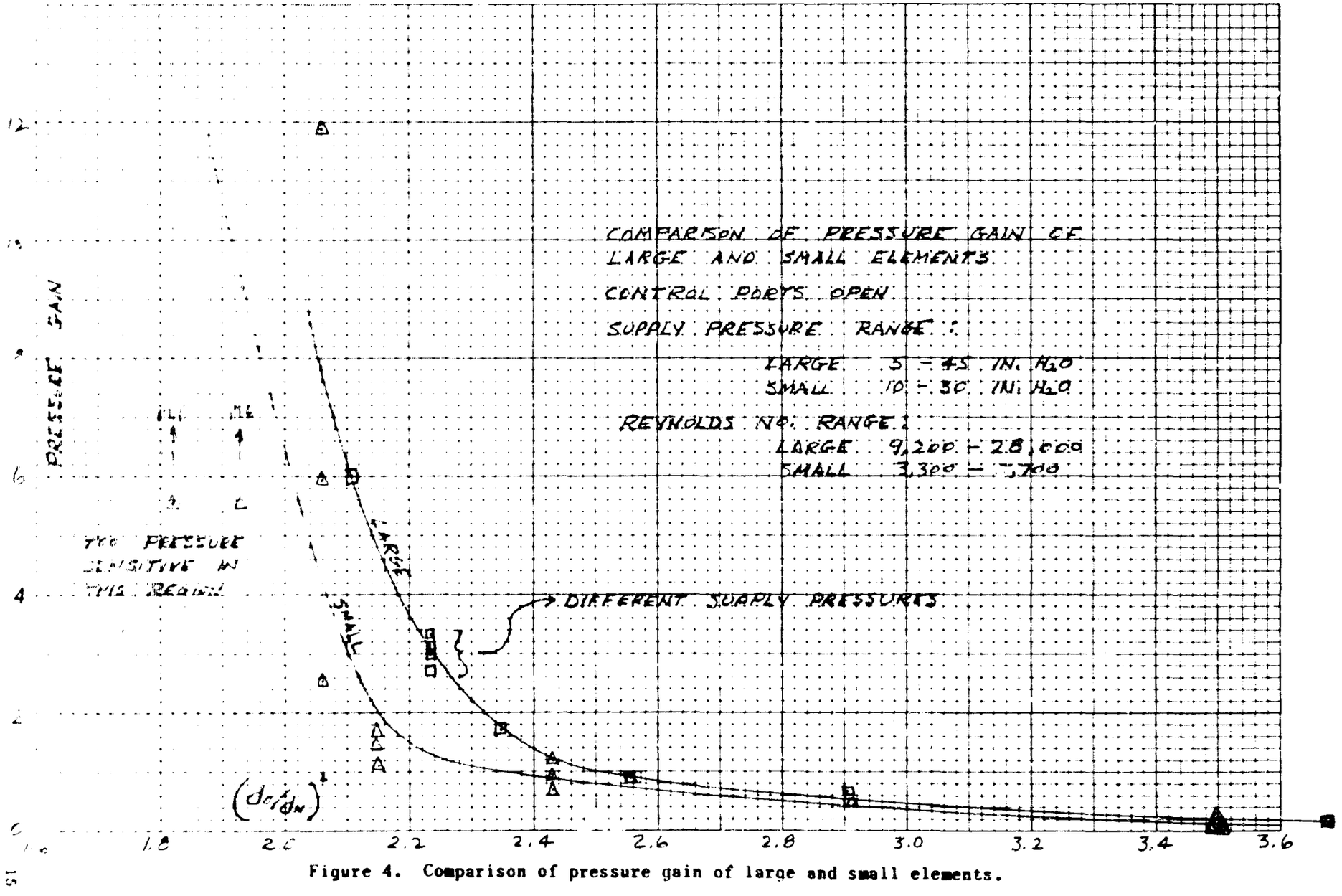

Figure 4. Comparison of pressure gain of large and small elements.

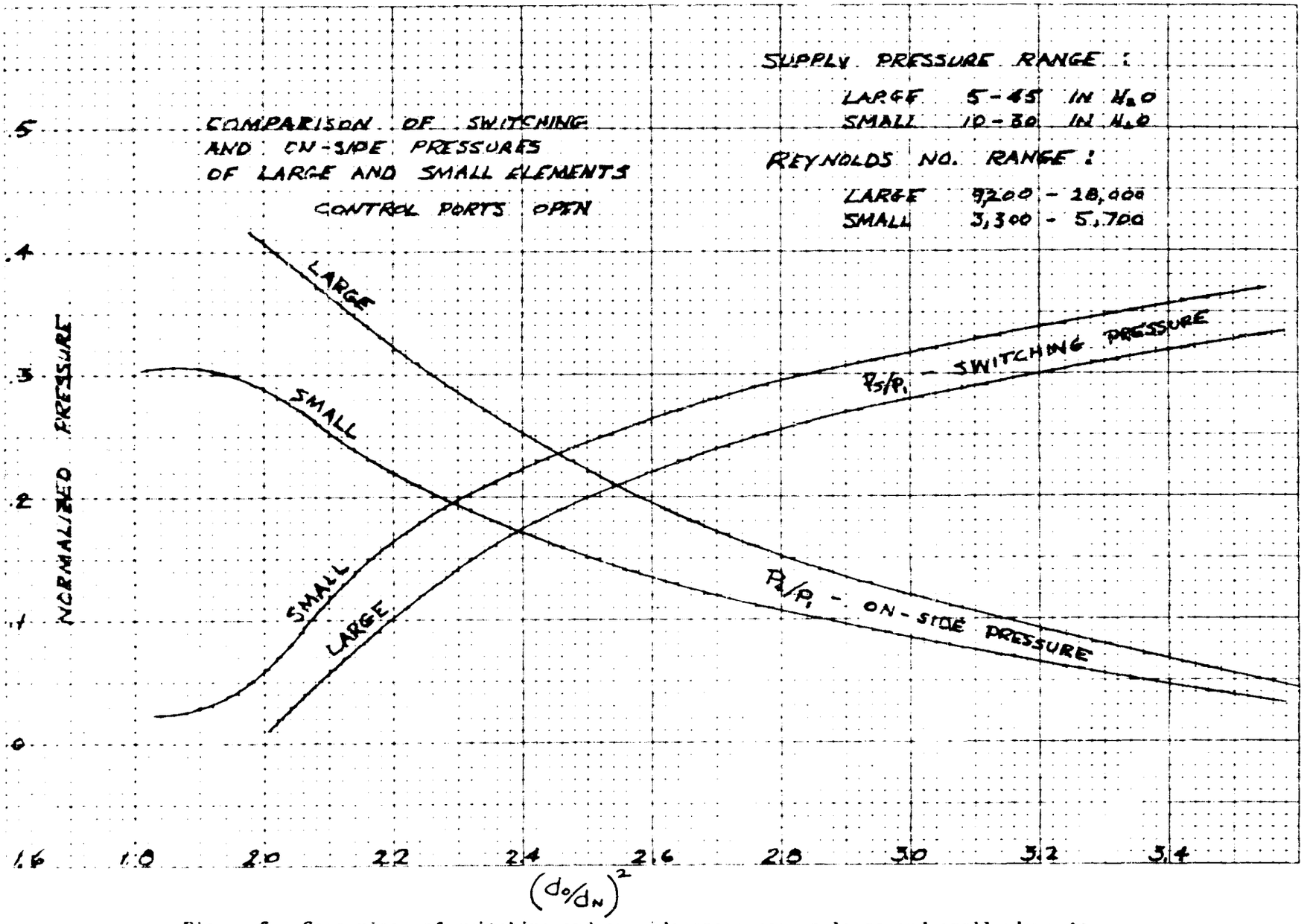

Figure 5. Comparison of switching and on-side pressures on large and small elements.

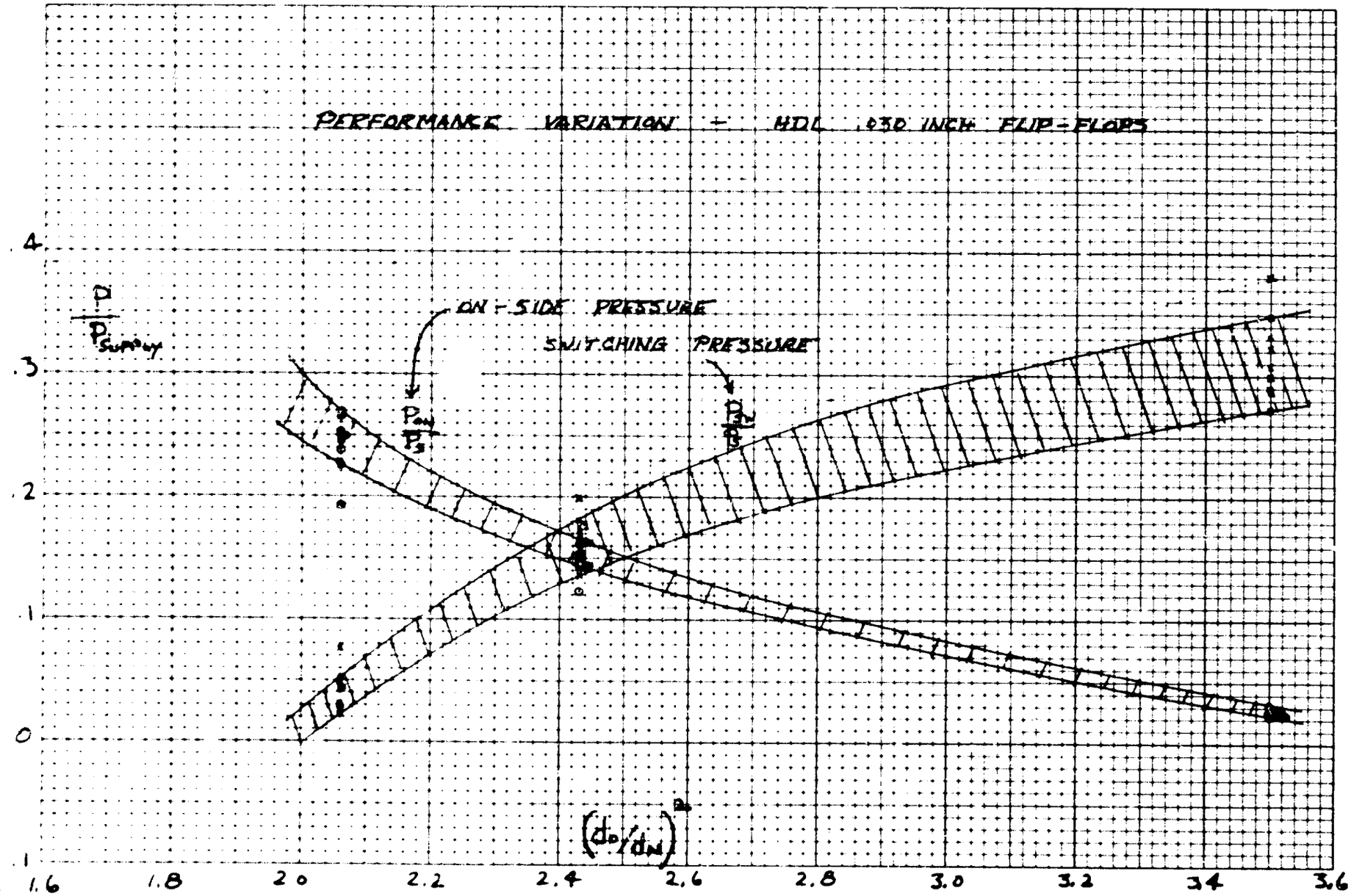

Figure 6. Performance variation—HDL 0.030-in. flip-flop.

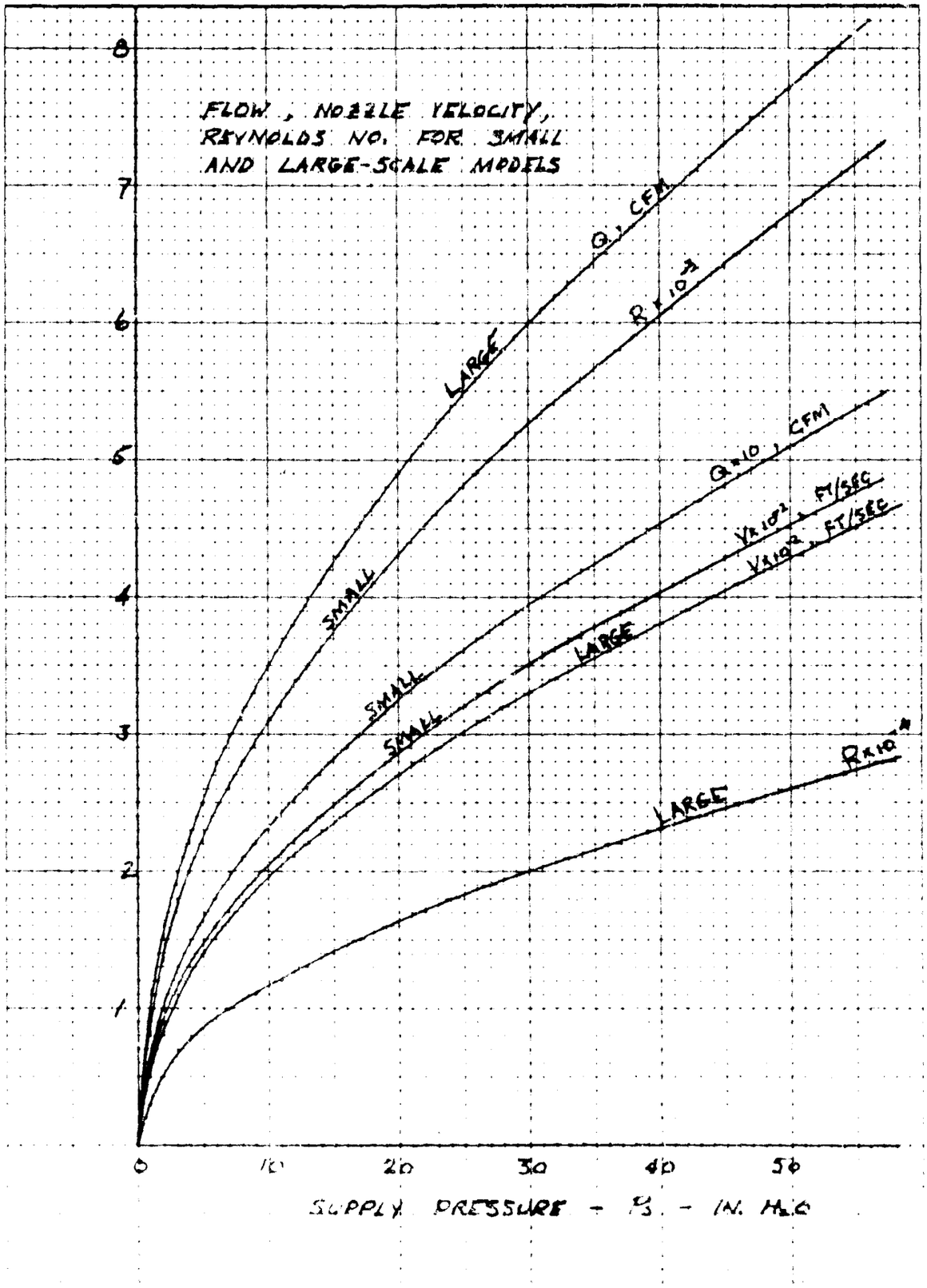

Figure 7. Curves showing variations in flow, nozzle velocity, and Reynolds number versus supply pressures for 0.03- and 0.12-in. nozzle flip-flops.

(4) The maximum efficiency and pressure gain of the small element is less than that of its big brother. In the case of efficiency, both the pressure and flow recovery is reduced; in fact, the flow recovery is very little more than 1, which means almost no entrainment. All these factors are probably related to the surface effects which will be discussed later more fully.

(5) The most disturbing fact of all is the very much decreased "loop" flow in the configuration described in Part II of Appendix A, and summarized in the last section. Because of the great dependence on this flow in the successful operation of the proposed counter circuit, this subject is discussed in more detail in the following section.

5. CIRCULATION IN LOWER LOOP

Measurements of the circulation flow in the standard size 0.030-in. element indicated an upper limit of 1.5 percent of the power jet flow, a substantial reduction from the 4 percent seen in the 0.120 in. size. This is a very difficult measurement in small sizes, and hot-wire techniques were employed to verify the correctness of the above figure. (The flow is about 6×10^{-3} CFM or 10^{-4} CFS.)

Apart from the scale effect, which will be discussed later, there arose the obvious question of the applicability of this particular flip-flop design to the proposed binary counter circuit. To gain more concrete evidence, we checked several other flip-flops in similar configurations, and found quite different values of circulation flow in the lower loop. In fact, there appeared to be a correlation with the amount of channel "setback" (dimension "X" in the figure below).

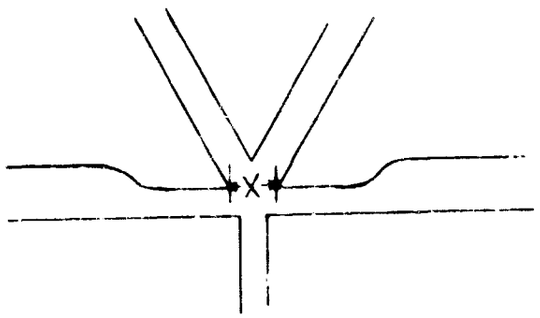

Dimension "X" for the HDL design being studied in this contract is 1.'W (for which the loop flow is 1.5 percent). For X = 3W (old HDL type), we get 3.5-4 percent.

Evidently, the flip-flop and the circuit for which it was intended in this study are seen to be ill-matched, and two remedial possibilities immediately suggest themselves:

(1) Substitute a different flip-flop in the same binary counter circuit.

(2) Continue with the same flip-flop, changing the circuit to one that is not dependent on this loop flow for its successful operation.

The first possibility was not particularly attactive, in view of the fact that a large portion of the work already completed would have had to be repeated. Changing the circuit appeared to cause the least disruption in the program, and had the added advantage of allowing us to continue with the same flip-flop, which certainly is superior in gain, efficiency and clean switching, notwithstanding its poor potential flow-inducing ability. The above change was agreed to in a meeting with HDL during the course of the program, and it was decided that UNIVAC would investigate several other possible counter circuits, and select one from these for experimental and theoretical analysis. The results of this investigation are reported in a later section.

6. SCALE EFFECTS

The problem of scaling is one which confronts the experimenter at every turn. An adequate knowledge of the classical scaling laws and a keen eye for new or unexpected effects is indispensable if data are to be interpreted properly. Scale effects are of great importance in fluid amplifier work since practical test sizes differ by at least one order of magnitude from hoped-for miniaturized production sizes. It is almost a certainty, that in bridging this gap, we pass through one or more changing flow regimes characterized by some Reynolds Number whose value we do not yet know. There have been a number of investigations directed toward shedding some light on this problem, and progress has been made; but devices have not yet been standardized to the point where it can be said that a single value of Reynolds Number (or some other parameter) may be considered critical for all designs.

The Reynolds Number, however, is not the only dimensionless parameter to be considered. The general condition for flow similarity requires that, at geometrically similar points, the forces acting on a fluid particle must bear a fixed relationship at every instant in time. This includes forces such as pressure, gravitational, elastic, and surface, as well as viscous forces. It is important to recognize that group of forces which predominate, as well as those which do not affect the fluid behavior. We begin by considering the latter group.

6.1 Nonpredominating Forces

In the test range, compressibility effects are undoubtedly of little importance for the steady-state case as the flow is very definitely subsonic. Certainly, this is true in the region where Reynolds No. effects begin to take place. If there are Mach No. effects, then they should be the same for both large and small models, because both were tested over essentially the same velocity range, and for a given air temperature; Mach No. is a function of velocity only.

6.2 Predominating Forces

We naturally think of Reynolds No. first. The test ranges have already been given for both scales, but now, for the purpose of noting scale effects, it is of interest to examine the maximum Reynolds No. of the small scale tests and the minimum Reynolds No. of the large scale tests. The following table gives this information:

	Small Scale	Large Scale
P_{supply}, $"H_2O$	30	5
Q_{nozzle}, CFM	0.39	2.5
V_{nozzle}, fps	348	140
R_{nozzle}	5200	8500
D_{loop}, in.	0.125	0.5
Q_{loop}, CFM	0.0054	0.096
R_{loop}	66	293

We cannot overlook the fact that the coefficient of discharge (of the load orifices) is a Reynolds No. dependent parameter, and we may therefore expect some change in the load performance plot with varying Reynolds No. In the range investigated, this change is such as to narrow the margin in the performance of the two models.

We next turn to geometric similarity, which has been presumed to have been satisfied. Actually, a small departure from perfect geometric scaling was introduced with the change to 3W of the power nozzle and control entry ports. We may, however, take account of this change by plotting total pressures rather than

static, if the (quite reasonable) assumption may be made that the total energy losses associated with the accelerating flow into the power and control nozzles are negligible.

$$\text{The ratio of total pressures is } \frac{P_{4_T}}{P_{1_T}} = \frac{P_4 + V_4^2/2g}{P_1 + V_1^2/2g}$$

The velocity heads at points 1 and 4 may be expressed in terms of the nozzle velocity head, and hence, in terms of the inlet static pressure, P_1. The ratio of total pressures, therefore, may be uniquely expressed in terms of the ratio of static pressures (as plotted in the figures) for a given geometry. The final expressions are as follows:

$$0.120\text{-in. size:} \quad P_{4_T}/P_{1_T} = 0.99\ (P_4/P_{1_S} + 0.112)$$

$$0.030\text{-in. size:} \quad P_{4_T}/P_{1_T} = 0.889\ (P_4/P_{1_S} + 0.125$$

The latter two equations are, for convenience, plotted in figure 8.

Unfortunately, perfect geometric scaling implies more than simply maintaining similarity of macroscopic dimensions. Surface finish plays an important part in determining the behavior of flowing fluids. A number of studies have shown a relationship between flow separation (from a wall), and a parameter, h/δ, where h is the height of a surface irregularity, and therefore a measure of surface roughness, and δ is the local boundary layer thickness. It is also true, that to a very close approximation, $\delta \sim L$, where L is an arbitrary linear dimension denoting the scale of the model. It follows then, that $h/L = \text{const}$ should be a condition for maintaining surface similarity. Unfortunately, when scaling to different sizes, this parameter is seldom held constant, for L changes with scale, and it is likely that h will remain about the same, unless particular attention is paid to surface finish details.

Also, the importance of the parameter h/L depends on the flow regime, and in particular, the nature of the boundary layer. Flow at very low Reynolds No. is insensitive to surface roughness. At higher Reynolds No., increased surface roughness is usually detrimental, unless the boundary layer itself is in a transitional state, in which case a roughened surface will trigger turbulence, thereby inhibiting separation, and reducing losses. For example, the reduced circulation flow found in the small model is not likely a result of surface phenomena, since the flow there is quite laminar,

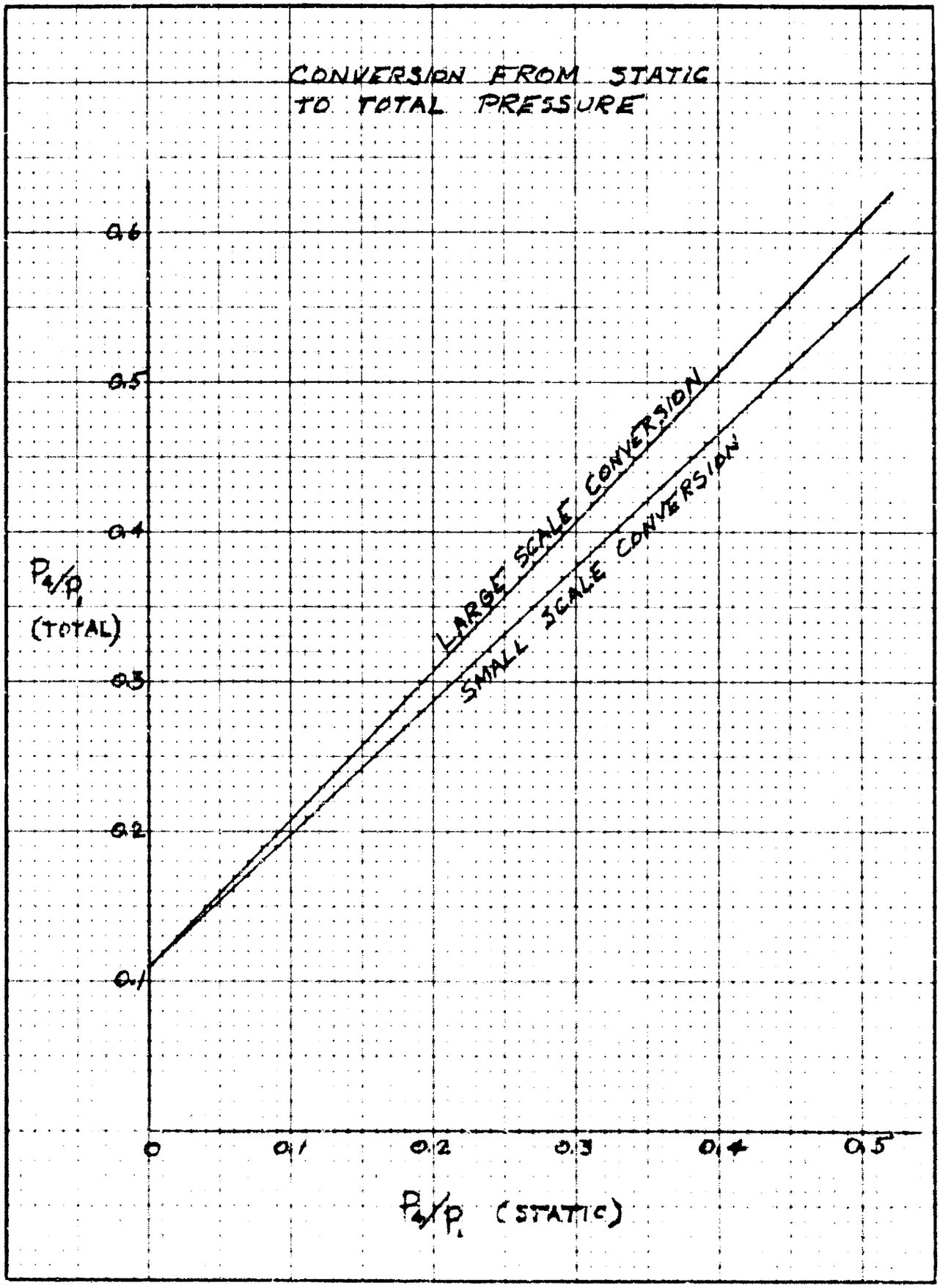

Figure 8. Graph showing conversion from static to total pressure.

and losses are negligible. On the other hand, surface effects may have considerable influence on the behavior of the flow in the output channels of the flip-flop, particularly in the diffuser region.

Having introduced the various factors which may account for performance variation, we attempt now to summarize the relative predominance of these effects.

6.3 Circulation Flow

The discrepancy in results between large and small scales is difficult to explain. Surface effects are not responsible. General geometric scaling was preserved. Reynolds No. seems the only answer. Certainly, the very low numbers are characterized by a transitory region. Actually, the ranges may be said to overlap if one wishes to put faith in the extrapolated portion of the large scale test down to 0 (see fig. A-22). But in this region, if the extrapolation is correct, the ratio of circulation to power jet flow remains about the same, and therefore differs from that of the small scale test at the same Reynolds No. This implies a dependence on something other than Reynolds No.

6.4 Load Characteristics

The Reynolds No. ranges do not quite overlap, but come close. One does not expect substantial changes in performance due to Reynolds No. at this level of turbulence, but it is possible, in fact probable that the variation in the discharge coefficient gives rise to a significant change--one that tends to draw the results closer together.

Comparing the two scales on the more equitable basis of total, rather than static pressure results in a widening of the gap. See the equations for this correction, or figure 5.

Surface finish quite probably plays an important role, especially in the region of the diffuser section of the output flip-flop channels. Were surface similarity preserved, the 0.030-in. size performance would probably be improved.

7. INVESTIGATION OF DIFFERENT COUNTER CIRCUITS

The discovery of the poor circulation flow associated with the flip-flop design under consideration raised doubts as to the wisdom of its incorporation into the suggested binary counter circuit. Brief, informal tests were conducted on this and several other binary counter circuits, the results of which tended to support this hypothesis.

The suggested circuit was erratic in operation, and "difficult to make work." It also posed uncertainties in connection with the analytical phase of the work. A consultation was held in Washington with HDL representatives, and it was agreed upon that UNIVAC should investigate several different binary counter circuits, and select, from these, one for theoretical and experimental analysis.

Accordingly, two circuits were selected for study, one, a variation of the original circuit with two feedback loops added, one from each output to the opposite control port, which serve the purpose of supporting the "loop" flow established by the pressure differential across the jet. Thus, the feedback flow becomes predominant in directing the incoming signal to the proper channel. The loop flow, at best, a small percentage of the power jet flow, is no longer a critical parameter.

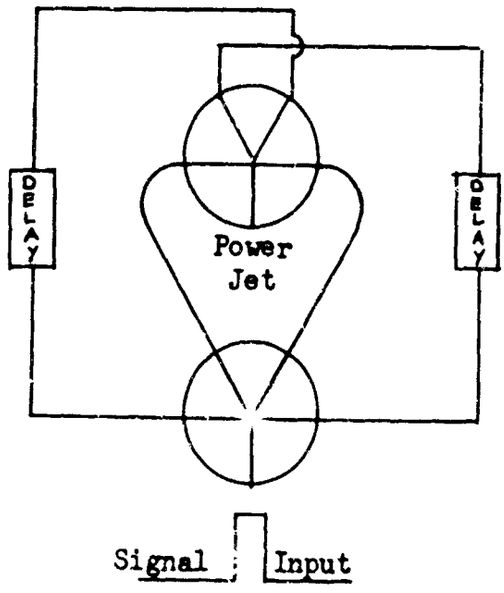

This circuit (shown above) was constructed in the laboratory, using the small size HDL flip-flops with standard connections and tubing. The circuit was instrumented with pressure transducers and hot-wire probes in such a manner that the signal at any critical point in the circuit could easily be monitored. Bleeds were used at the outputs.

This circuit, while better than the one without feedback lines, was very difficult to make operate consistently. Short leads were used to the controls of the active element, but various lengths of feedback lines were experimented with. Surprisingly, the longer feedback lines (which permit a longer input pulse duration) hindered successful operation more than shorter lines.

The main difficulty with this circuit is its predilection to oscillate. Aside from greatly increasing the impedance of a return line, there is no way to completely shut off an undesirable signal which may prematurely switch the element. (Note that in the AND gate circuit discussed later, this disadvantage is not present.) Another possibility is the redesign of the lower element, or associated lines, so they are more suited to their purpose in the circuit, namely, to "presteer" an incoming signal in a particular direction without allowing stray internal signals to gain such magnitude that they may switch the unit.

Upon adjusting the various circuit parameters to achieve the best performance, a single stage of the counter was made to operate in the range of 14 to 30 input pulses per second. The table below gives the pertinent information at the extremes of the range:

Pulses/sec	On time (msec)	Feedback delay (msec)	Input pulse duration (msec)
14	71.5	2	12.0
30	33.3	2	5.5

It was noted that the circuit operation was very sensitive to the amount of bleed, controlled at the output legs of the upper element.

In this operating range, the switching seemed quite clean to the "ear" as it was sensed through the bleed, but the observed waveform was somewhat jagged; in short, it left much to be desired in terms of the type of signal one would want entering the next stage. In fact, a second stage was added, and could not be made to operate successfully. Bleed control of the second stage in attempting to make it work caused even the first stage to break down.

The chief advantage of this circuit appears to be the fact that the pulse duration may not have to be a critical parameter. Note from the above table that the duration is considerably longer than the delay time associated with the feedback loop. The reason for this is not entirely clear. At times the circuit oscillates under controlled pulse operation, implying that the input pulse was not "off" by the time feedback flow returned. Yet, oscillation is present in the complete absence of an input signal, implying a quite different mechanism by which oscillation occurs. Again, it seems clear that if such a circuit were to be used, a differently designed lower element would be appropriate.

The second circuit tested was the AND gate circuit shown below:

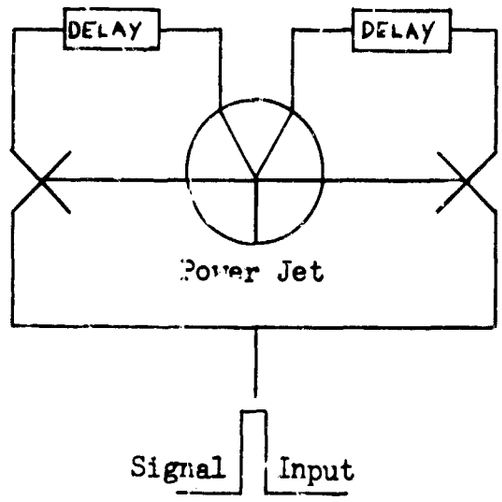

The incoming pulse is divided, ANDS with the feedback flow from the on output and switches the power jet. Note that this circuit is not a natural oscillator as is the other one, subject only to the condition that the signal be off by the time the feedback flow reaches the AND gate. A steady input flow, or a pulse of too-long duration will put the circuit into oscillation. The table shown below indicates the capabilities of this configuration:

No. of stages	Pulses/sec	On time (msec)	Feedback delay (msec)	Input pulse duration (msec)	Comments
2	50 (max)	20	10	3.5	Strong Input Signal
2	20 (min)	50	10	8	Strong Input Signal
1	5 (min)	200	10	34	Weak Input Signal
1	8 (min)	125	5	22	Weak Input Signal

The upper frequency attainable is limited by the first stage. The lower limit is probably set by the second, or succeeding stages, unless the output pulses are reshaped.

Clearly, this circuit seems more manageable than the one previously described. It has a much wider frequency range, two stages operate

together quite nicely, and the bleed adjustment is not nearly as critical. No difficulty was experienced using different feedback delays, though the pulse duration limit, of course, changes. It is significant that for the first stage, using a "strong" signal, the maximum possible pulse duration is of similar magnitude to the time delay in the feedback loop. It is only with a reduced signal that lower frequency, or longer pulse duration may be achieved. This indicates that the steady state pressure is not sufficient to switch. A similar mechanism may account for the successful operation of the second stage. Evidently, the on time of the first stage represents the duration of the second stage signal input. This is obviously too long, in theory, to permit successful operation of the second stage. Thus, the "effective pulse width," in terms of switching capability is, quite clearly, within a reasonable limit.

Since each stage in a binary counter must operate at one-half the frequency of its predecessor, we may eventually reach a point where the pulse width must be decreased. This can be done using a simple "pulse-former" in the connecting lines.

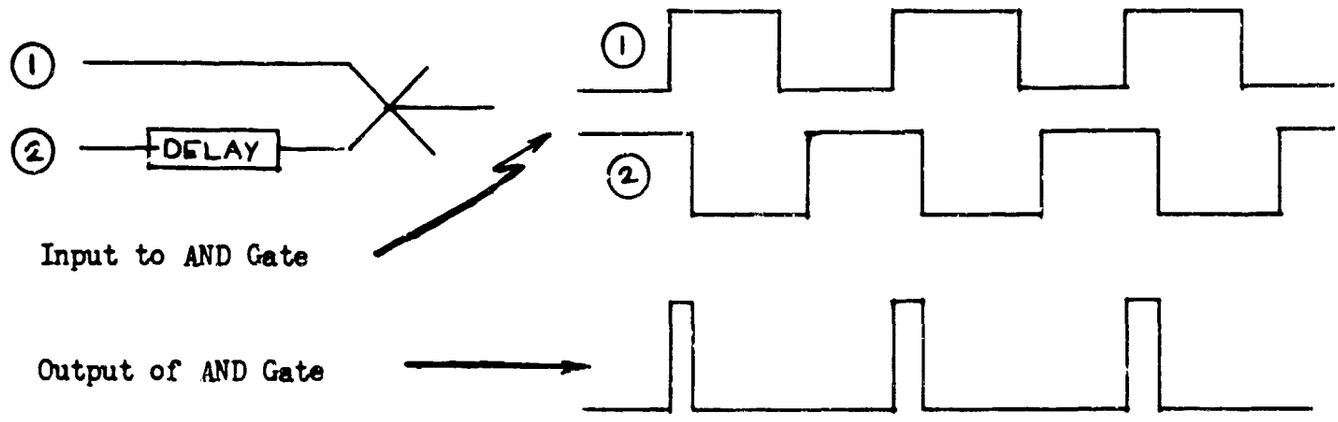

(1) and (2) are outputs from the flip-flops. One of the two is delayed so that the wave forms overlap by any desired amount. The output of the AND gate is then a pulse of shorter duration. One disadvantage of such a procedure is the weakened output signal which results. In some cases, an amplifier may be necessary to build up this signal.

Having tested the two binary counter circuits, the latter, or AND gate circuit seemed to be the wiser selection for study. The preliminary tests showed that it could be made to work satisfactorily; in addition, it appeared to be a representative circuit posing a reasonably comprehensive problem in analysis.

8. ISOLATION STUDY

The subject of isolation has been studied with considerable interest at UNIVAC. The attractiveness of the isolation or self-adaptive element is its ability (if designed properly) to operate over a wide range of imposed loads with negligible feedback effects. There are several ways to isolate an element from the rest of the circuit. One is to simply place an isolator, or isolating element in the output leg of the element in question. Another is to "build in" the necessary isolation.

The relative merits of the above mentioned possibilities were investigated early in the contract period. It was suspected at that time (although not yet verified by test) that it was advantageous to isolate as far upstream as possible (say in the output leg of a flip-flop). This is followed by diffusion, if necessary, which is accomplished at a lower velocity, and therefore with less loss. (Later test results of various isolator configurations supported the theory that it is more efficient to isolate first, and then diffuse, rather than diffuse first, and then isolate.)

Having established the goal of producing a reasonably well optimized element containing isolation, the initial task became clear. A fundamental study, on a large scale, of several different isolator configurations was undertaken. The complete description and results of this series of tests are set forth in Appendix B.

Stated briefly, the test explored a cylindrical gap-type isolator, the flow being axi-symmetric. Three types of recovery port configurations were analyzed, and pressures and flows measured under various load conditions. (The limiting load conditions prevail with the output tube blocked, and unblocked.) Data were taken at gaps up to 2.4 diameters. It was seen that perfect isolation could be obtained when employing the right combination of gap size and recovery port configuration. Flow and pressure recoveries were noted.

The value of this series of tests is evident. Using the results as guidelines, one may design an element to be used specifically for isolating purposes, or an element, say a flip-flop, with built-in isolation, by placing in the output channel a gap of appropriate configuration. The latter project was, in fact, undertaken.

9. OPERATION OF A THREE-STAGE BINARY COUNTER CONSTRUCTED ACCORDING TO STEADY-STATE CALCULATIONS

9.1 Constructing the Circuit

The first step in the analytical procedure is to represent the binary counter in terms of an equivalent fluid circuit. The resistance

of each element of this circuit must be experimentally determined, whereupon, the necessary load-matching orifices may be calculated using straightforward procedures.

The steady-state aspects of the circuit theory are detailed in Appendix C. It is expedient to express the resistance of a fluid element as an equivalent area--general expressions may then be derived for combining areas in series and in parallel. The appendix gives these derivations as well as the complete calculations pertinent to the construction of an n-stage binary counter.

Based on these calculations, a three-stage counter was constructed. The "breadboard" model of this counter is seen in figure 9. As a matter of interest, we note that the circuit consists of flip-flops, bleeds, delay lines, flow dividers, orifices, and AND gates. It is necessary to determine the steady-state characteristics of each of these elements. The flip-flop is the most complicated of these, and has already been discussed in detail. All the others, with the exception of the AND gate are relatively simple elements, whose resistance to flow may be quickly ascertained. The AND gate is a very important element in logic circuits, and, being a three-terminal device, its characteristics are slightly more complicated to specify uniquely.

It is therefore constructive to refer to figure 10, which is a plot of the characteristics of a typical UNIVAC AND gate. The following points of interest are noted:

(1) The maximum output does not occur at equal inputs, but at a ratio of about 1.15.

(2) The fact that the two curves shown do not coincide indicates a sensitivity to pressure level (or Reynolds Number).

(3) The elements are not perfectly symmetrical. This is proven by reversing signals A and B and noting the slightly different output C.

(4) Because of conclusions 2 and 3, we cannot uniquely characterize an "AND" gate by abscissas in the range $0 \leq P_B/P_A \leq 1$, for when $P_B/P_A > 1$, the high and low sides are reversed (asymmetry changes result), and operation is at a higher pressure level (Reynolds Number changes result).

A typical load was used at the output of the "AND" gate. For this load, the pressure recovery is seen to be 57 percent for

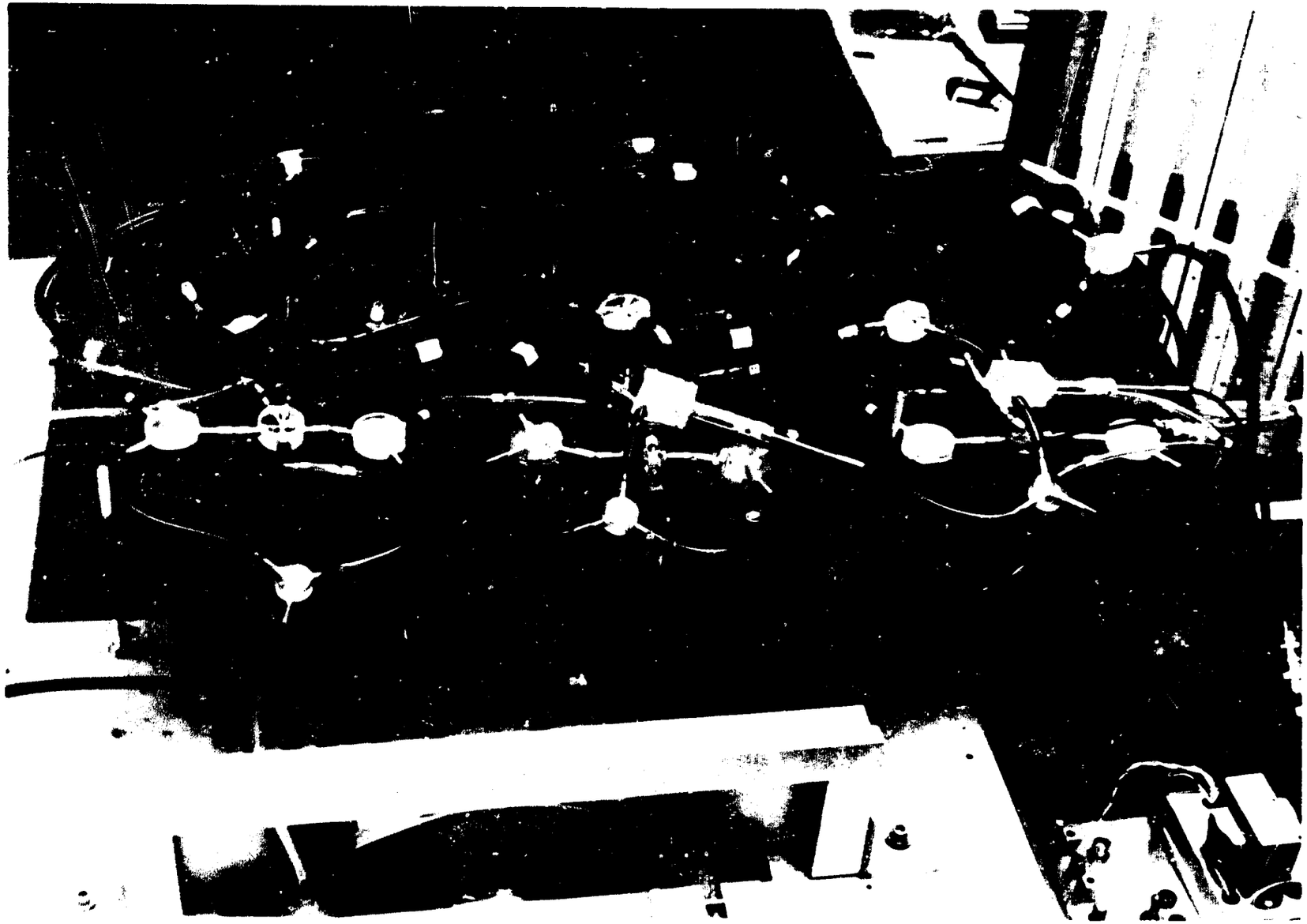

Figure 9. Breadboard construction of three-stage binary counter circuit.

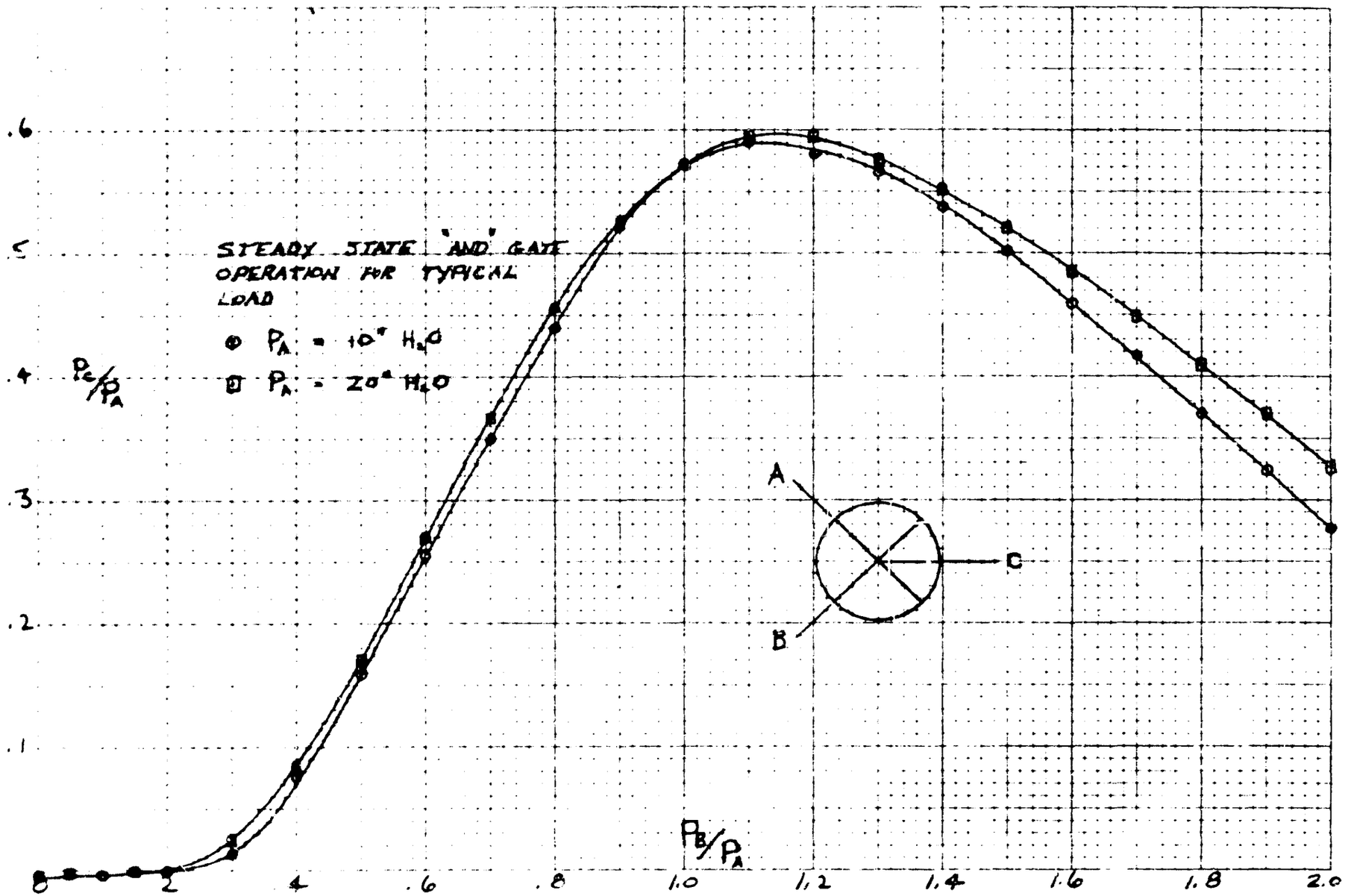

Figure 10. Curves showing steady-state AND gate operation for typical load.

equal inputs. Tests conducted on numerous gates with equal inputs, and with the output blocked off completely, indicated total pressure recoveries in the range of 70 to 80 percent. From the gates available, three well matched pairs were selected for use in the feedback lines of the three-stage counter circuit. Three more having good recovery were used in the pulse-former sections of the circuit.

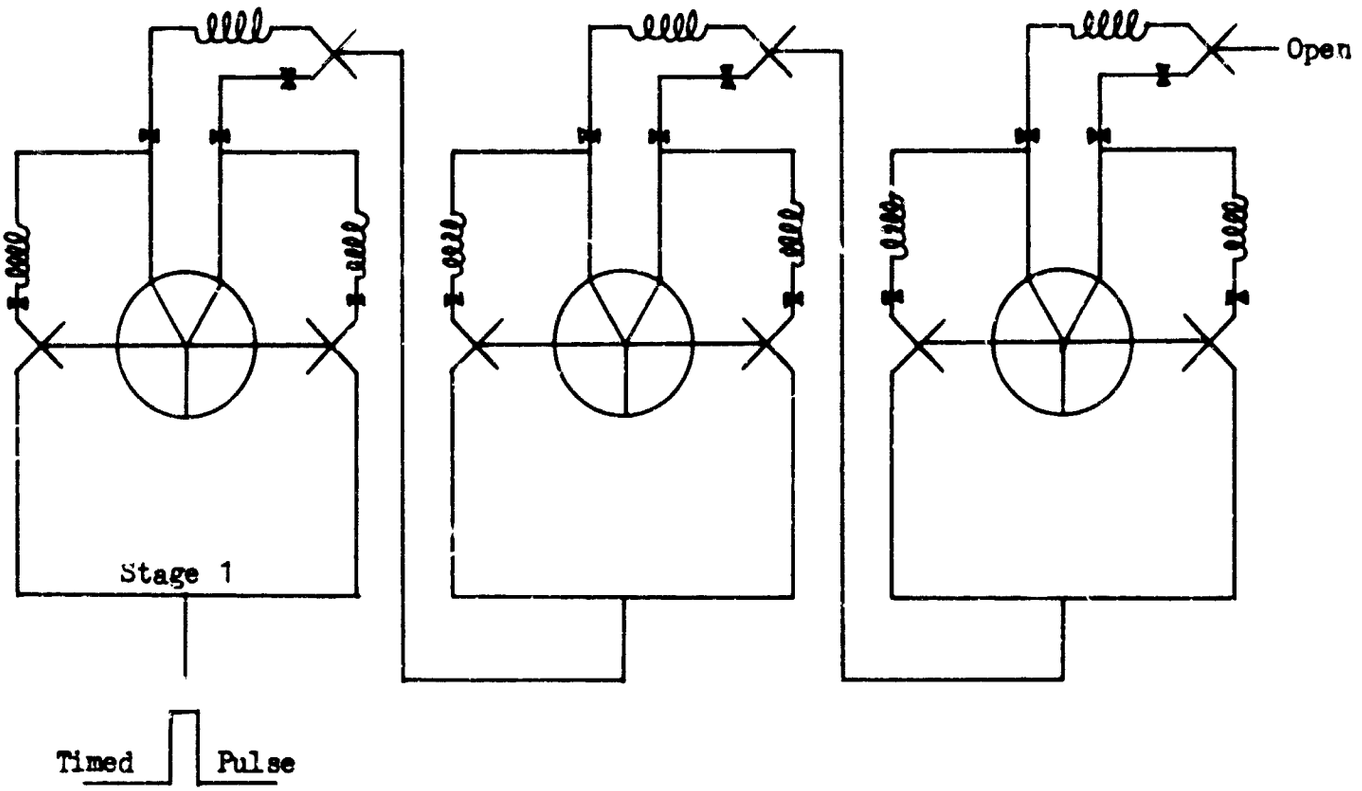

Orifice

Delay Line

AND Gate

The operation of the three-stage counter, a diagram of which appears above, may be termed successful. Only one fundamental change was made; the delay line in the pulse-former circuit was increased from 5 to 10 ft. This is a critical length--the line must be long enough to permit a signal of sufficient duration to activate the next stage. But it must be short enough so that the signal will cease by the time the feedback from the output reaches the "AND" gate. Of course, a longer feedback line could be used, but is not desirable, since impedance is thereby increased. This may be especially harmful when high frequency operation is reached. The increase in length was compensated for by suitable changes in orifice diameters.

9.2 Operation of the Counter Circuit

The first stage operated successfully as an oscillator (80 cps), and drove the second and third stage at 40 and 20 cps respectively. Using mechanically timed pulses at the first stage input, the circuit operated successfully over a range of frequencies dictated by acceptable pulse width limits. Three slotted generator wheels of 10, 20, and 30 degree cut outs were used.

The maximum permissible pulse width is dictated by the length of the feedback lines, as described earlier. For this circuit, the maximum width is about 10 msec. This corresponds to lower frequency limits of 7, 11, and 17 pulses/sec for the 10-, 20-, and 30-deg wheels, respectively. The limits of actual operation matched these figures very closely, with the exception of the 10-deg wheel, where the limit was 3 or 4 pulses/sec. This is explained by the inability of the wheel slot to produce a perfect flow step at very slow rotating speeds. The rise-time shortens the effective pulse duration, and permits lower speed operation.

The minimum permissible pulse width is difficult to predict accurately, but our switching tests show a sharp knee in the pressure-to-switch versus pulse duration curve (see Appendix D), starting at a pulse duration of about 3 msec. The upper frequency limits achieved with 10-, 20-, and 30-deg wheels were about 18, 30, and 45 cps, respectively. These frequencies correspond to pulse widths in the 3- to 4-msec range.

10. SWITCHING TESTS

A number of tests were performed to determine various switching characteristics. These tests may be categorized as follows:

(1) Determination of leading edge wave shape as seen at output leg of flip-flop.

(2) Correlation of minimum control pressure to switch and pulse duration.

(3) Switching time.

The first two items are explored in detail in Appendix D. Item 1 represents a part of the experimental portion of the transient circuit analysis. One purpose of this analysis is to predict by means of an equivalent flip-flop circuit its output wave shape. The supporting experimental evidence is a portion of the work of Appendix D, wherein are shown oscillograms of output wave shapes. The duration of the control pulse and the output load is varied.

The results of the control pressure-pulse duration tests are seen in figures D-3, D-4, and D-5. Different size cut-out slots in the pulse generator wheel allowed frequency and pulse duration to be varied independently. Figure D-4 shows the nondependence of frequency.

Item 3 is simply an experimental determination of the switching time of a flip-flop, which is here defined as the time necessary to switch from one output to the other with zero feedback length in the simple oscillator circuit indicated in figure 11. Since zero feedback length is physically unattainable, we simply plot the cycle period for different lengths, and extrapolate the curve to zero. This gives a full cycle time of 0.5 msec, or a switching time of 0.25 msec. The curve bends a bit in the region of the extrapolation, however, and it seems wiser to consider an average switching time inferred from the rest of the data, taking into account the delay in the feedback length. Considering the equation:

$$T = 2\ell + 2s$$

Where:

T = cycle period msec.

ℓ = delay in 1/2 cycle $\cong$ length of feedback line in ft.

s = switching time in msec.

We get an average s of 0.32 msec for the seven test points. The range was 0.25 to 0.40 msec.

11. TRANSIENT CIRCUIT ANALYSIS

The purpose of this portion of the analysis is, in a word, to predict the transient behavior of a fluid circuit. It starts with perhaps the most complex element in the circuit--the flip-flop--and attempts to derive its transfer function. The steps in this procedure may be outlined briefly here:

(1) Draw an equivalent flip-flop circuit, using AC type impedances as well as DC type resistances. (The placing of elements in this circuit is, to some degree arbitrary, and may have to be modified later.)

(2) Write the circuit equations

(3) Solve the equations for p(t) or q(t). These equations will have the form:

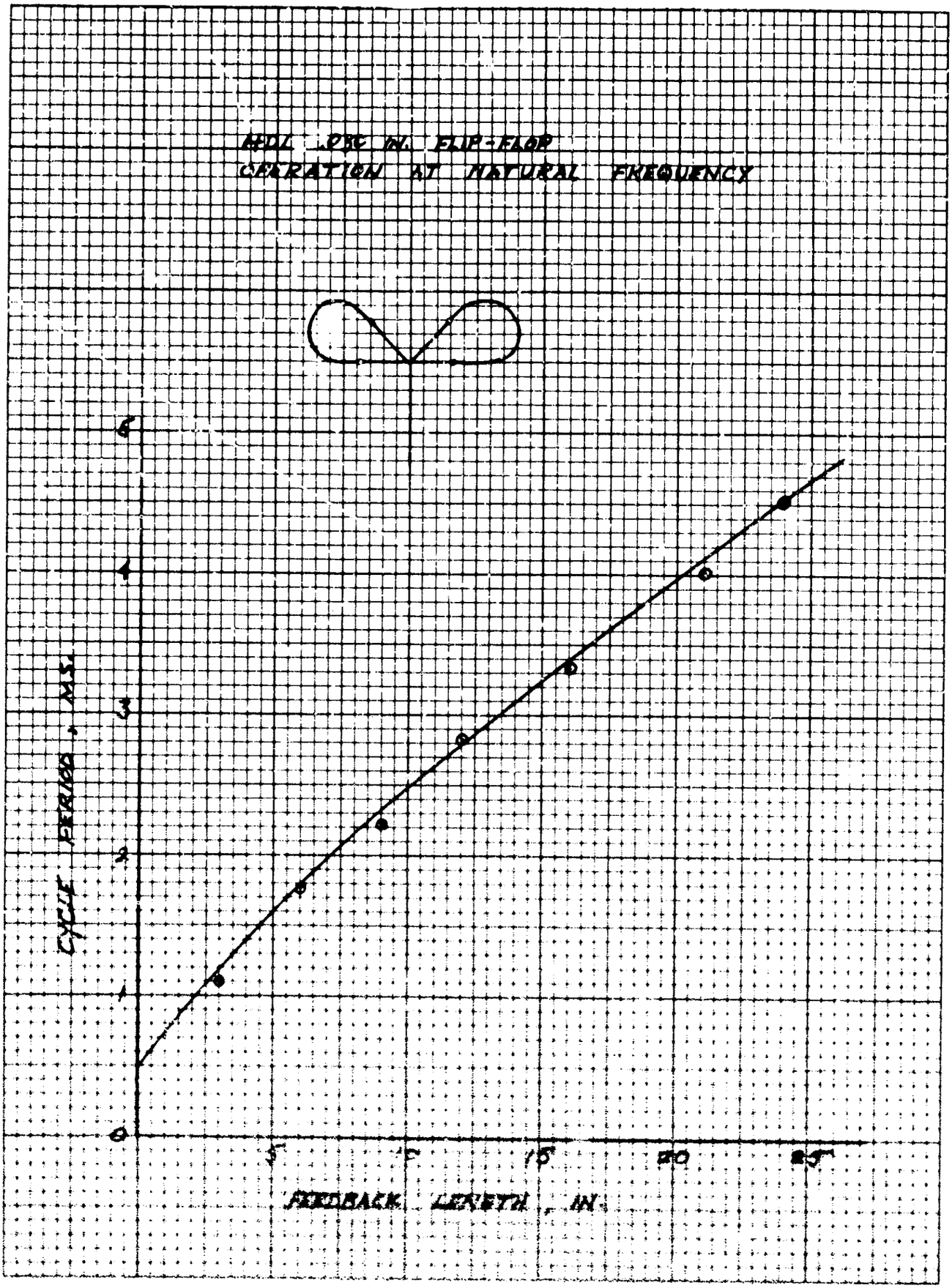

Figure 11. HDL 0.030-in. flip-flop operation at natural frequency.

$$p(t) = f(R, L, C, t)$$

where R, L, and C are arbitrary constants, any values of which will satisfy the initial equations.

(4) Select values of R, L, and C which will give p(t) which concides most closely with the experimentally determined p(t).

(5) Use this equation to predict the output wave form when different values of R, L, and C prevail.

The above procedure was described for, but is not limited to, a flip-flop, Any circuit may be handled in this fashion, assuming that the equations may be solved (see Appx E for detailed theory of fluid circuits). The equations, of course, are the well-known electrical circuit equations expressing voltage drop across resistive, inductive, and capacitive type elements:

$$e = L\frac{di}{dt} + Ri + \frac{1}{C}\int_o^t idt$$

But for a fluid circuit, we substitute pressure for voltage and flow for current, and get

$$p = L\frac{dq}{dt} + Rq + \frac{1}{C}\int_o^t qdt$$

Equations of this type are easily solved since they are linear. But the relationship between pressure and flow in a fluid resistive type element (say, an orifice) is not linear. We may solve the linear equations and have only an approximate solution--or attempt to solve the nonlinear equations and have exact solutions.

Each of these two approaches has been given considerable thought. Appendix F is a complete accounting of the linear analysis. Herein is described the assumed circuits, their equations, and solutions. The flip-flop is considered first, and a mathematical curve is derived which closely fits its known output wave shape. The analysis is then extended to a complete circuit, and culminates in a theoretical determination (confirmed by experiment) of the natural frequency of a stage of the experimental binary counter.

The second course--that of investigating the possibility of nonlinear solutions--failed to yield solutions in closed form. In general graphical or computer techniques are necessary.

12. A THREE-STAGE BINARY COUNTER USING THE ISOLATION FLIP-FLOP

The knowledge gained as a result of the fundamental investigation

of flow isolation (described in Appendix B) laid the ground work for the development of a flip-flop with "built-in" isolation. The design philosophy is described in detail in Appendix G, along with a dimensioned drawing, and performance curves. It is clear, from the nature of the curves, that feedback effects have virtually been eliminated in this element.

To demonstrate the utility of this new element, we have fabricated a 3-stage (single plane per stage) integrated binary counter. The planes are separated by short spacers to permit the necessary bleed from the isolation gap. The circuit used is a modification of the AND gate circuit which was investigated in the previous analyses. The circuit is so designed that its operation is independent (above a certain minimum time) of the duration of the incoming control pulse. This is a great advantage for any type of construction, but particularly so for an integrated plane-type construction, since it eliminates the need for space consuming delay lines that are normally necessary in the feedback and pulse-former sections of standard circuits.

A description of this circuit, as well as the details of the counter construction, is presented in Appendix G.

13. CONCLUSIONS

(1) The steady-state performance characteristics of a large and a small scale HDL flip-flop was the first task accomplished. A two-fold purpose was served; the tests provided the operating characteristics necessary to match the flip-flop to the rest of the circuit, and scale effects were noted.

(2) The small (0.030-in. nozzle) element characteristics were, in general, inferior to those of the large (0.120-in. nozzle) element. Reynolds Number changes are, in part, responsible, particularly insofar as the discharge coefficients of the various orifices are concerned. Equally important are surface phenomena. These are less predictable, but under certain conditions, may have a significant effect on performance.

(3) The low circulation flow found in the loop connecting the control ports of the upper flip-flop caused an investigation into several alternate binary counter circuits. Following a brief period of study, one of these (the AND gate circuit) was selected for analysis.

(4) Following the substitute counter selection, the steady-state resistance of all the necessary elements in the circuit were obtained; matching load orifices were prescribed by steady-state circuit theory, and a 3-stage "breadboard" counter was built and successfully operated.

(5) The transient circuit analysis took two forms: a linear, and a nonlinear study. The nonlinear study was not fruitful, due to the mathematical complexities involved. The linear analysis, although an approximation at the outset, produced more satisfactory results. An equivalent flip-flop circuit was drawn, and a transfer function deduced. Later, a complete circuit, including the flip-flop was considered, and the theory used to predict the natural frequency of oscillation.

(6) Switching tests on the small scale flip-flop produced the following information:

(a) Oscillograms of output wave shapes under varying conditions of load and control pulse duration.

(b) A correlation between the minimum control pressure to switch and the pulse duration.

(c) Switching time, as determined by varying the feedback length of a simple oscillator circuit, and extrapolating to zero.

(7) Following a fundamental study of axisymmetric flow isolation by gap, an isolation flip-flop was constructed which proved capable of operating in a circuit, and being virtually unaffected by feedback effects. A 3-stage integrated binary counter (in three planes) was fabricated using this flip-flop in a modified circuit, whose successful operation is independent of the duration of the control pulse. The need for space consuming delay lines is thereby eliminated.

14. REFERENCES AND BIBLIOGRAPH.

References

(1) Warren, R. W.; Fluid Amplification--3. Fluid Flip-Flops and a Counter TR-1061, DOFL, 25 August 1962.

(2) Symposium on Measurement in Unsteady Flow, pp 3-21, ASME, May, 1962

Bibliography

Schenck, Jr.; Theories of Engineering Experimentation, McGraw-Hill, 1961.

Schlichting, H.; Boundary Layer Theory, McGraw-Hill, 1960, Fourth Edition.

Oldenburger, Rufus; Mathematical Engineering Analysis, Dover Publications, Inc., New York, pages 357-359.

NOMENCLATURE

a, b, c, d, α	constants
A	area
C	capacitance
d, D	diameter
e	voltage
f	friction factor
g	gravitational acceleration
i	current
L	inductance
M	Mach No.
p, P	pressure
q, Q	flow
R	Reynolds No., resistance
s	switching time
t	time
T	period
V	velocity, volume
γ	weight density
ρ	mass density

Subscripts

o	initial
1, 2, 3, 4, 5	flip-flop terminals (See Figure)
j	jet
n	nozzle
s	supply
T	total

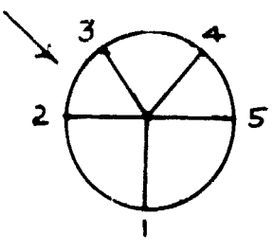

APPENDIX A.—STEADY-STATE CHARACTERISTICS OF HDL FLIP-FLOP

Part I - T. A. Shook

Part II - T. F. Chen

I L L U S T R A T I O N S

APPENDIX A.—STEADY-STATE CHARACTERISTICS OF HDL FLIP-FLOP

INTRODUCTION

The problems inherent in describing the performance of a five-terminal device, such as a flip-flop (fig A-1)*, are manifold. No one method appears to be unique, nor even the best under all circumstances. Rather, we must keep in mind the use for which the element is intended, and be content with a method of presentation which is the most instructive for this purpose.

In a word, the method used here shows the variation of the output characteristics of the device as a function of load. This method has the advantage of giving immediate insight into the useful operating range. For example, this flip-flop is not called upon to "fan-out," or drive a number of other units. Therefore, flow gain is of little importance. But pressure gain is of great importance, and we can by inspection of, say figure A-2, see that the operating point must lie within the intersection of the switching and off-side pressure curves, and the intersection of the switching and on-side pressure curves.

Loads are simulated by the placing of orifices of different sizes in the output channels. A function of this load is plotted as the abscissa, and normalized flows and pressures as the ordinate. Some investigators in the field find it expedient to use orifices in the control inputs. This flip-flop, accordingly, was tested over a range of such input restrictions.

The unit was tested in air with supply pressures ranging to 45 in. of water. At each supply pressure and configuration of orifices, performance data were taken with the control ports open to atmosphere in the absence of a control signal. A line was then connected to one control port, and air introduced in "quasi-steady" fashion to the point of switching. At this point, another complete set of performance data was taken, but with particular emphasis on the switching pressure and flow. A third configuration involved connecting the control ports by a line (to form a closed loop). The latter configuration is of interest in connection with the proper functioning of this element as a binary counter. Measurements of the pressure difference across the jet and the circulation this establishes comprise a division of this investigation which is described in Part II of this report.

*Figures for appendix A appear on pp 53 to 64.

PART I

1. DESCRIPTION OF TEST APPARATUS AND MEASUREMENT OF FUNDAMENTAL QUANTITIES

The line diagram of figure A-3 shows how the flip-flop is instrumented. Orifice type flow meters are inserted in the supply line and the line to the left control port. Each terminal has four static pressure taps manifolded to a common line leading to a manometer. Thus, the possibility of erratic readings due to asymmetry in the flow is minimized. The orifices in the output legs used to simulate varying load conditions, conveniently double for flow measurement devices. Each orifice used was calibrated for this purpose to give output flows as well as pressures.

The entrainment flows in the control ports and in the "off-side" output leg are, of course, small, and not suitably measured by the pressure drop across an orifice. For this purpose, hot-wire anemometry was employed, probes being situated at terminals 2 and 3. Thus, flow and pressure are quite adequately monitored at each of the five terminal points.

2. DEFINITION OF TERMS

Pressure recovery	$R_P = P_4/P_1$
Flow recovery	$R_Q = Q_4/Q_1$
Efficiency	$\eta = R_P R_Q$

Pressure gain is defined as the change in pressure at one output leg prior to and after switching divided by the corresponding change at the control port.

For a symmetrical device, this reduces to

$$\frac{P_{\text{on side}} - P_{\text{off side}}}{P_{\text{switch}} - P_c}$$

where P_c is the pressure at the control port on the jet side in the absence of control flow. For a jet in state 4, the gain would be

$$G_p = \frac{P_4 - P_3}{P_{5(sw)} - P_5}$$

Flow gain, G_Q is defined similarly, as

$$G_Q \quad \frac{Q_4 - Q_3}{Q_{5(sw)} - Q_5}$$

The power gain is $G_p \times G_Q$

3. DISCUSSION OF TEST RESULTS

A brief explanation concerning the abscissa parameter in figures A-3 through A-10 is in order. d_o is simply the diameter of the orifices used in the output legs. d_N is the diameter of a circle whose area is the same as that of the nozzle. In other words,

$$\text{Nozzle area} = .120\ (.360) = \frac{\pi}{4}\ d_N^2$$

$$d_N^2 = \frac{4}{\pi}\ (.12)(.36),\ d_N = .234 \text{ in.}$$

In general, for flow through an orifice,

$$Q = KCA\sqrt{\Delta P}$$

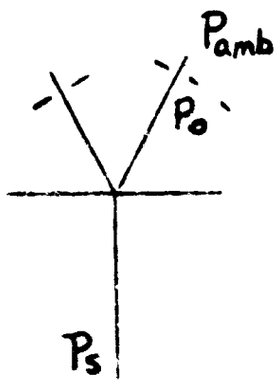

Specifically, $Q_N = KC_N A_N \sqrt{P_s - P_{amb.}}$

and $Q_o = KC_o A_o \sqrt{P_o - P_{amb.}}$

But, if P_{amb} is atmospheric, and all pressures are gauge,

$$Q_N = KC_N A_N \sqrt{P_s} \text{ and } Q_o = KC_o A_o \sqrt{P_o}$$

Admittance, defined as Q^2/P is an oft-used parameter to characterize a hydraulic load. Note, that for the specific cases above,

$$\text{Output admittance} = Q_o^2/P_o = K^2 C_o^2 A_o^2$$

$$\text{Input admittance} = Q_N^2/P_s = K^2 C_N^2 A_N^2$$

$$\text{Admittance ratio} = \left(\frac{C_o}{C_N}\right)^2 \left(\frac{A_o}{A_N}\right)^2 = \left(\frac{C_o}{C_N}\right)^2 \left(\frac{d_o}{d_N}\right)^4$$

(if d_N is defined as above).

It is seen that the term $(d_o/d_N)^2$ is related to the square root of the admittance ratio by the ratio of discharge coefficients. The attractiveness of this term as a load parameter is apparent when one considers its simplicity and its fundamental relation to load. Its nondimensional form allows direct comparison of characteristics of flip-flops of differing size and design.

Figures A-2 to A-7 show the performance characteristics of the flip-flop for a series of control input restrictions ranging from 0.1 in. to 0.52 in. (open). Inspection of these curves does not indicate a clear-cut advantage in operating the element with the controls restricted. The element is quite stable with the inputs unrestricted, and quite "digital" (note the off-side pressures). The pressure recovery and pressure gain are good, and seem little affected by changes in the input orifice size, until a diameter of 0.1 in. is reached. Here, switching pressures are somewhat erratic, and quite low--in fact, comparable to the off-side pressure.

The area of interest is, of course, to the left of the intersection of the switching and on-side pressure curves (P_5/P_1 and P_4/P_1), since it is in this region that pressure gain is obtained. The limit of stable circuit operation is the intersection of the switching and off-side pressure curves (P_5/P_1 and P_3/P_1), since an off-side pressure equal to the switching pressure of a downstream

flip-flop would trigger it. We seek an operating point somewhere between these two limits. Note that the operating point will also closely coincide with the point of maximum efficiency.

Output orifices of 0.325 in., or $(d_o/d_N)^2 = 1.93$, represent the approximate limit of bistable operation. There is a slight dependence on supply pressure here, but nominally, the output of the element is divided when using output restrictions less than 0.325 in. A later paragraph describes a brief test in the proportional range of this amplifier.

The curves in figures A-2 to A-7 were taken with the element in state 4. For comparison, figure A-8 shows the characteristics in state 3 (the preferred side). The difference in performance is seen to be small. Compare figures A-2 and A-8, which are both for open inputs.

The device is essentially pressure insensitive, in the range tested, a fact which greatly simplifies the presentation of the results, since it allows normalization of all pressures. The supply pressure range for each input configuration is noted on the curves. Most tests were run at more than one value of supply pressure, and the data are indicated as discrete points (same abscissa, different points on the ordinate). It is seen that in general, the points are close enough to assume that pressures scale quite well in the range tested. What dependence there is on supply pressure seems more pronounced as the limit of stability is reached.

Figures A-9 and A-10 show the pressure and power gain for the control inputs open, and for $d_2 = d_5 = 0.3$ in.

Figure A-11 shows the input power as a function of the supply pressure. It is essentially independent of the orifice configurations tested.

Figure A-12 shows a proportional range of this element. Not a concern for the present application, it seems fitting, nevertheless to comment briefly on its existence for possible future reference. The range in output load giving these results was not fully investigated, but appears to be quite limited. Similar results obtain when orifices are placed in the control ports.

4. CONCLUSIONS

(1) The element may be operated without control input restrictions. The performance characteristics favor slightly this configuration. Operation is very stable and digital.

(2) The element is essentially insensitive to supply pressure in the range tested. Results are, therefore, simplified by normalization of pressures.

(3) While perhaps not the best design for an analogue device, the element exhibits a proportional range when using output orifices of 0.3125 in.

(4) The range of bistable operation was found to be $d_3 = d_4 \geq 0.325$ in.

(5) The estimated load range for useful operation is $0.338 \leq d \leq 0.3725$ in. At d = 0.348 in. (with control ports open),

Pressure gain	3.0
Pressure recovery	31.5%
Efficiency	43%
Percent of power jet flow to switch (Q_5/Q_1)	22%

5. BIBLIOGRAPHY

Warren, R. W., "Fluid Amplification - Part 3, Fluid Flip-Flops and a Counter" TR-1061, 25 August 1962, DOFL

Peperone, S. J., Katz, S., and Goto, J. M., "Gain Analysis of the Proportional Fluid Amplifier," Fluid Amplification Symposium, October, 1962, Volume 1, DOFL

NOMENCLATURE

See figure A-3 for terminal numbering.

A	Area
C	Discharge coefficient
d	Orifice diameter
G	Gain
K	Constant
P	Pressure
ΔP	Pressure difference
Q	Volume flow
R	Recovery
η	Efficiency

Subscripts

1 to 5	Flip-flop terminals
o	Output
amb.	Ambient
c	Control
N	Nozzle
P	Pressure
Q	Volume flow
s	Supply
sw	Switch

PART II.

STEADY-STATE LOOP TESTS

1. INTRODUCTION

The operating principles of the binary counter under investigation in this contract are explained in detail in the report "Fluid Flip-Flops and Counter" by R. W. Warren[1]. For convenience in the following discussion the key operating principles are listed below:

(1) The successful operation of the binary counter depends on the ability of a small induced flow in the loop (fig. A-13) to guide the pulse stream properly in the correct direction.

(2) If there exist waves of sufficient magnitude in the power stream, they must be attenuated to eliminate their effect, acting as an undesired signal to switch the power stream from one output to the other in the absence of an input pulse.

In order to get a better understanding of these principles and to provide a basis for the development of an analytical formulation of the input and output relationship, steady-state loop tests, to be reported below, were carried out.

In this test the prime objective was to find out the amount and characteristics of the small induced flow in the loop since the first of the two key operating principles is totally dependent on this flow. Though the wave phenomenon described by Warren[1] was not included in this test--the test results give some clue to this question.

2. DESCRIPTION OF THE STEADY-STATE LOOP TEST ARRANGEMENT

A 0.120-in. nozzle size, dual-input flip-flop of HDL design was constructed and used in this test. This is the flip-flop to be used in constructing a binary counter. The two control ports were connected with tygon tubing to form a loop. An orifice flow meter was placed in the loop to measure the inducted flow. It is evident that the orifice flow meter constitutes a load in the loop and that the induced flow may vary with respect to this load, therefore different size orifice flow meters were used. To vary the loads at the outputs, several pairs of different size orifices were prepared. These orifices can be inserted and replaced with other size orifices at ease. Figure A-14 shows the details of the orifice adapter. The details of the test arrangement are shown in the figures.

---

[1] HDL Report No. TR-1061, "Fluid Amplification--No. 3: Fluid Flip-Flops and a Counter," R. W. Warren, 25 Aug 1962.

A transition section was constructed and placed upstream of the power jet nozzle to insure the absence of large scale unsteady turbulence in the power stream. It is important from the fluid dynamical point of view to provide a consistent approaching flow of known characteristics to the power nozzle, especially in connection with the investigation of the second key operating principle described in the introduction. The detail of the transition section is shown in figure A-15. In figure A-16 the dimensions of the loop are shown.

3. STEADY-STATE LOOP TEST

For the characterization of the induced flow in the loop several variables are considered. They are the independent variables which can be varied individually under control, and the dependent variables which we observe.

The independent variables considered are:

a. Output loads--denoted by d_3 and d_4, the diameter of the orifices placed at the output channels 3 and 4. The flow paths in the flip-flop are numbered as follows:

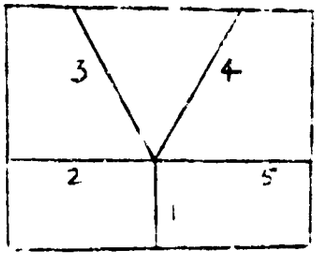

Facing the cover plate of the device

b. Load in the loop--denoted as "OFM 0.150," means orifice flow meter of size 0.150 in. in diameter.

c. Power jet flow rate--denoted by Q_1.

d. State of power jet--denoted by "State 3" and "State 4" indicating the output through which the power jet flows.

The dependent variables considered are:

a. Entrainment flow--denoted by Q_l.

b. Static pressure at points in the flow path--denoted by P_1, P_2--P_5.

c. Jet velocity at the exits of the output channels--denoted by V_3 and V_4.

Several sets of test conditions were selected, and these are summarized in Table A-1

4. TEST RESULTS AND DISCUSSION

(1) Characteristics of the lowest induced pressure at the control ports. Referring to Table 1.1, when the loop condition is "clamped," the pressure at the control ports drops to the lowest value for a given power jet flow due to the entrainment of air by the power jet. This minimum pressure is a measure of the entrainment capability of the power jet.

Figures A-17 and A-18 show the pressure at the control ports at various Q_1 for chosen loads at the outputs and in the loop.

The following points are worth mentioning:

(a) Each of the figures indicates a clear trend of decrease in pressure at the control ports with increasing Q_1.

(b) In changing the output loads d_3 and d_4 from 0.348 in. to 0.398 in. the relation between lowest induced static pressure and Q_1 remains essentially the same. Therefore, the lowest induced static pressure is determined practically by Q_1.

(c) The difference in the lowest induced static pressure at the two control ports which may be called the "potential maximum pressure differential," determines the potential inducible flow in the loop. The size and length of the loop, and the design at the pulse input will influence significantly the rate and pattern of the induced flow in the loop. A plot of the potential maximum pressure differential against Q_1 is shown in figure A-19.

(2) Characteristics of the Induced Flow in the Loop

When the clamp on the loop is released, the pressure differential across the power jet is reduced from the potential maximum value to a lower value as steady state is reached. At the same time the induced flow begins to flow through the loop in the direction of decreasing pressure and reaches a steady rate. The time in which the induced pressure and flow rate reach steady-state values plays an important role in determining the upper limit of frequency of the binary counter.

In figure A-20 the induced flow is plotted against power jet flow Q_1 for different loads at the output and the loop.

(a) The data indicate a clear trend of increase in Q_ℓ with increasing Q_1.

(b) The degree of dependence of the induced flow on the output loads is negligible compared with the effect of the loads in the loop. Q_ℓ increases with decreased load in the loop. The load in the loop is dependent on the length and diameter of the loop, and the size of the orifice used to measure the induced flow.

(c) Referring to figure 2 in Warren's report[1], the location of the pulse input port is in the middle of the induced flow path. This means that in a multistage binary counter the induced flow loop in each counter will not be entirely closed from the ambient, except possibly the first stage where a valve might be used. Entrainment through the pulse input port should be fully utilized.

(3) The Symmetry of the Test Unit

As noticed in Table A-1, one of the independent variables, namely, the state of power jet is considered in order to test the symmetry of the test unit. The results of careful dimensional check disclosed that the tolerances are equal or superior to those given on the drawing submitted by HDL. This is substantiated also in the test results shown in figures A-17, A-18, and A-19.

(4) The turbulence waves in the power jet do not influence the steady-state stability with the output loads of 0.34 in. and 0.398 in. However, as the output loads $d_{3,4}$ are reduced to smaller than 0.325 in. the power jet is no longer bistable. The power jet becomes divided into two streams and begins to oscillate at higher rates of power jet flow.

5. CONCLUSIONS

A test scheme has been described by which an estimation of the potential inducible flow in the loop-shaped passage of the binary counter can be made.

The test results with 0.120 in. size (power nozzle) flip-flop have been presented. Within the test range of velocity (Mach No. $\geq$ 0.3) an induced flow of 2-4 percent of the power of jet flow exists in the loop-shaped passage. In order to operate the binary counter successfully the induced flow must be able to direct the resultant flow (induced flow plus the input pulse) in the correct direction. A further investigation of this interaction is highly desirable.

---

[1] Ibid.

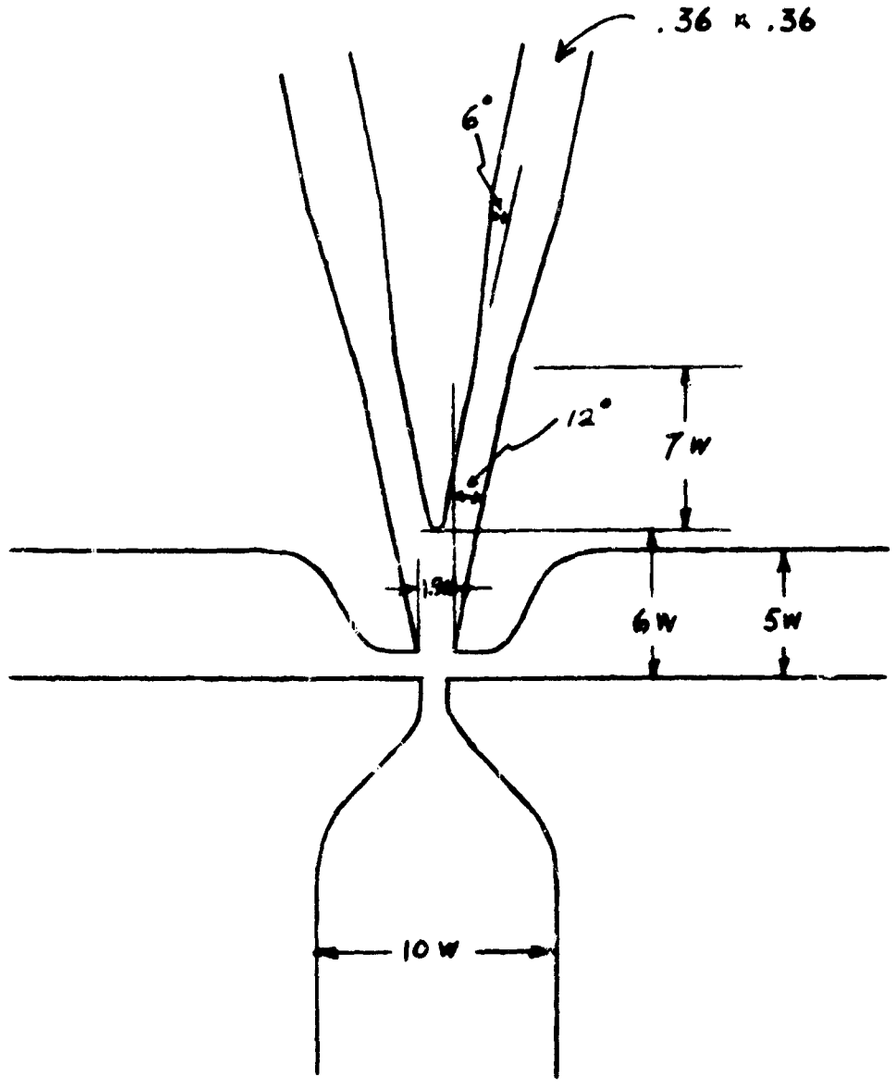

Figure A-1. Critical dimensions of large scale HDL flip-flop.

Nozzle width: 0.120 in.

Nozzle depth: 0.360 in.

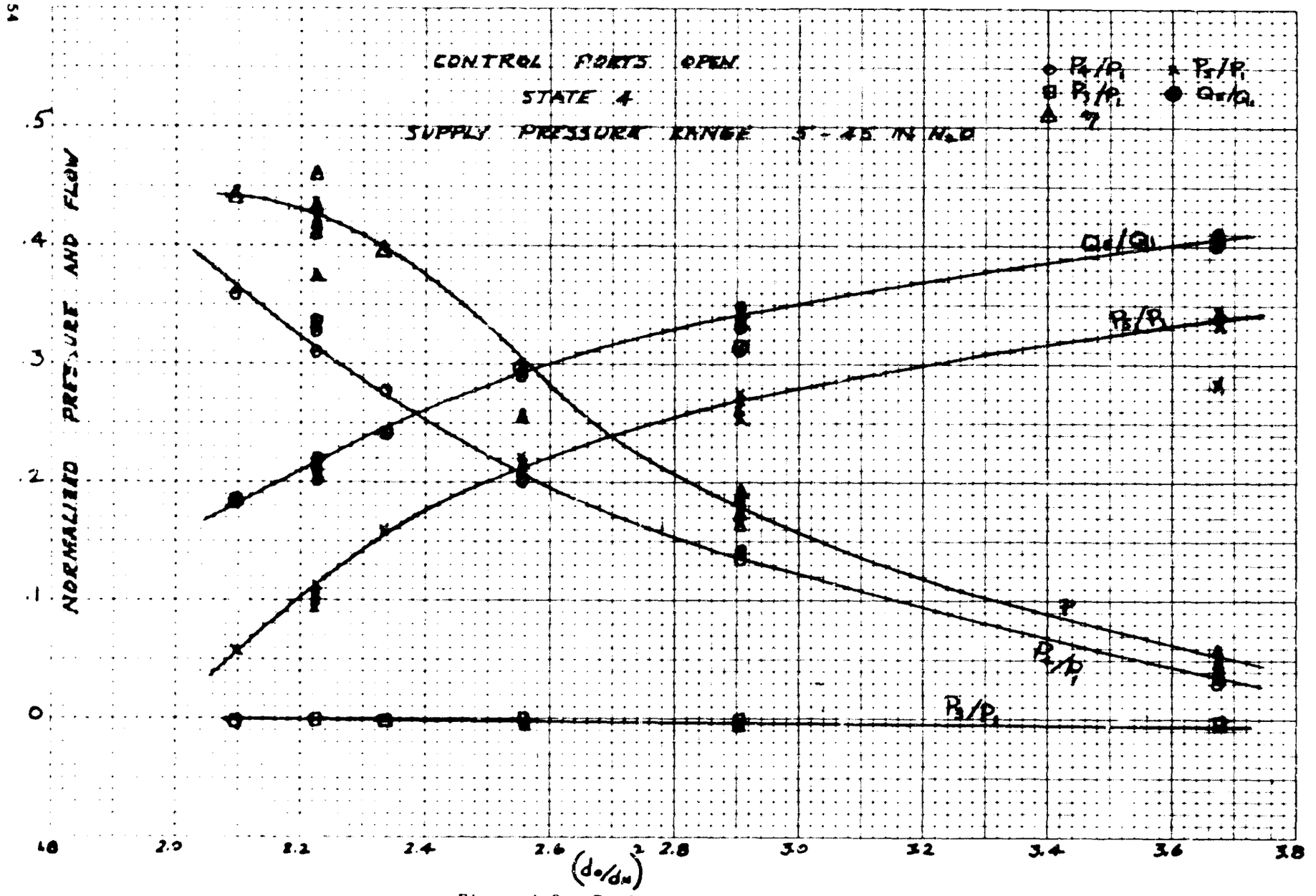

Figure A-2. Performance characteristics.

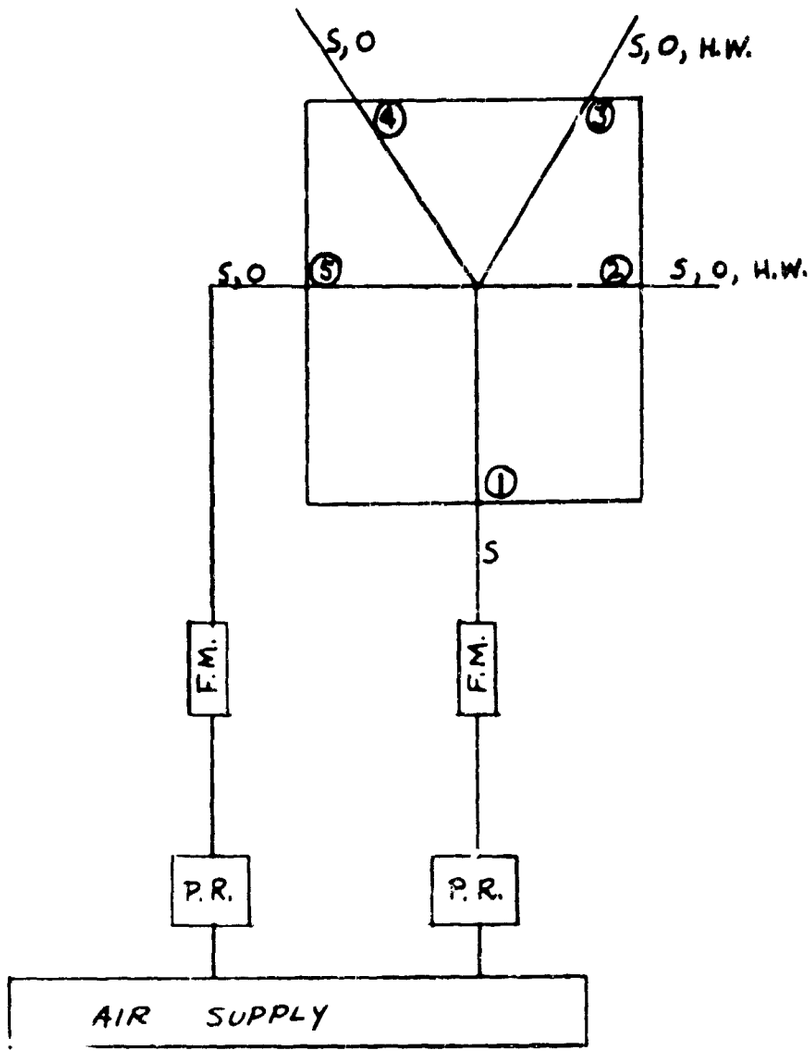

Figure A-3. Line diagram of test apparatus.

Legend

S = Static pressure measuring station

O = Orifice location

HW = Hot-wire anemometer probe location

FM = Flow meter (orifice type)

PR = pressure regulator

Supply pressure, P_1 - - - 5-45 in. H_2O

Nozzle velocity - - - - - 124-400 fps

Power jet flow - - - - - 2.25-7 CFM

Mach number - - - - - - - 0.1-0.35

Reynolds number - - - - - 7,440-24,000

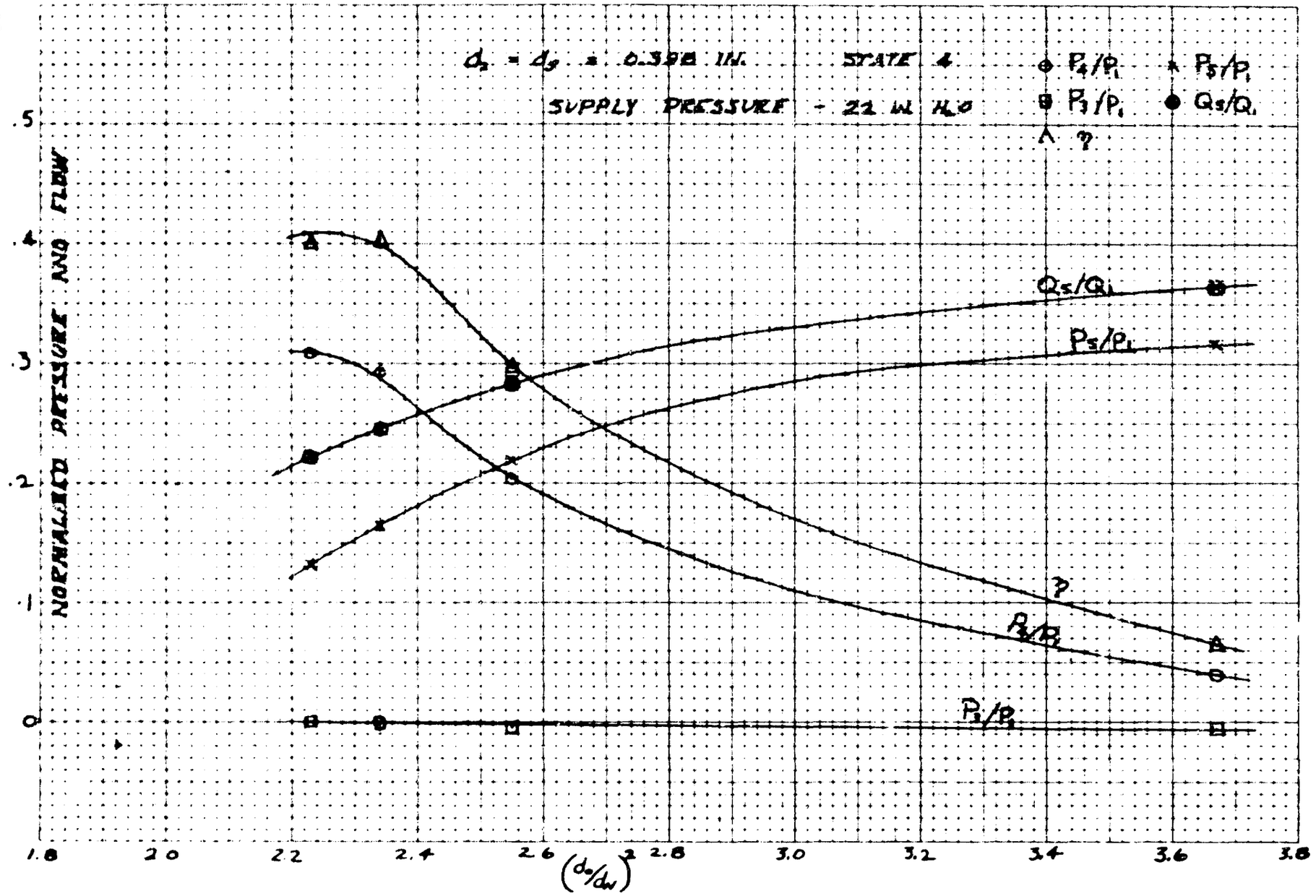

Figure A-4. Performance characteristics of flip-flops.

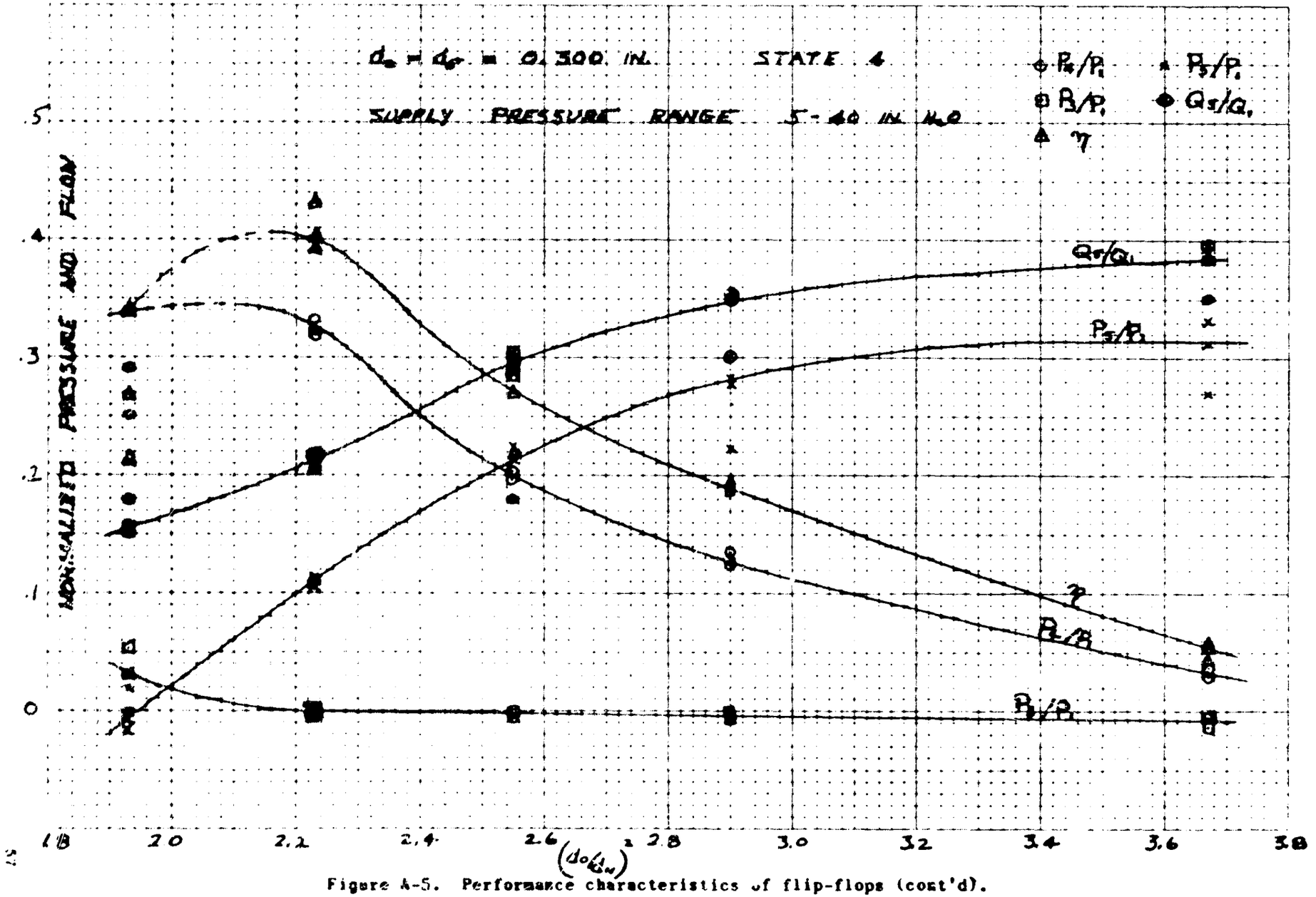

Figure A-5. Performance characteristics of flip-flops (cont'd).

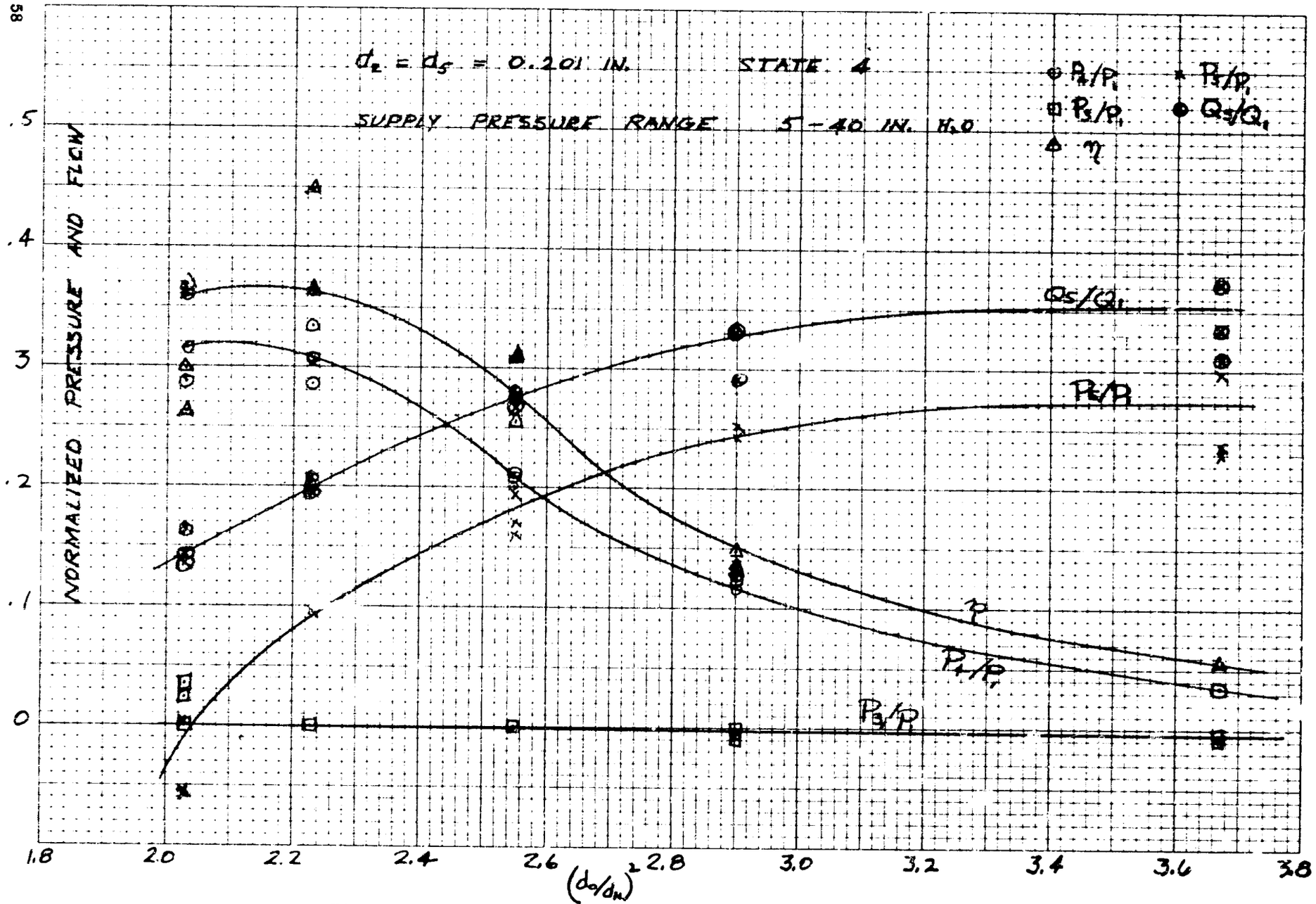

Figure A-6. Performance characteristics of flip-flops (cont'd).

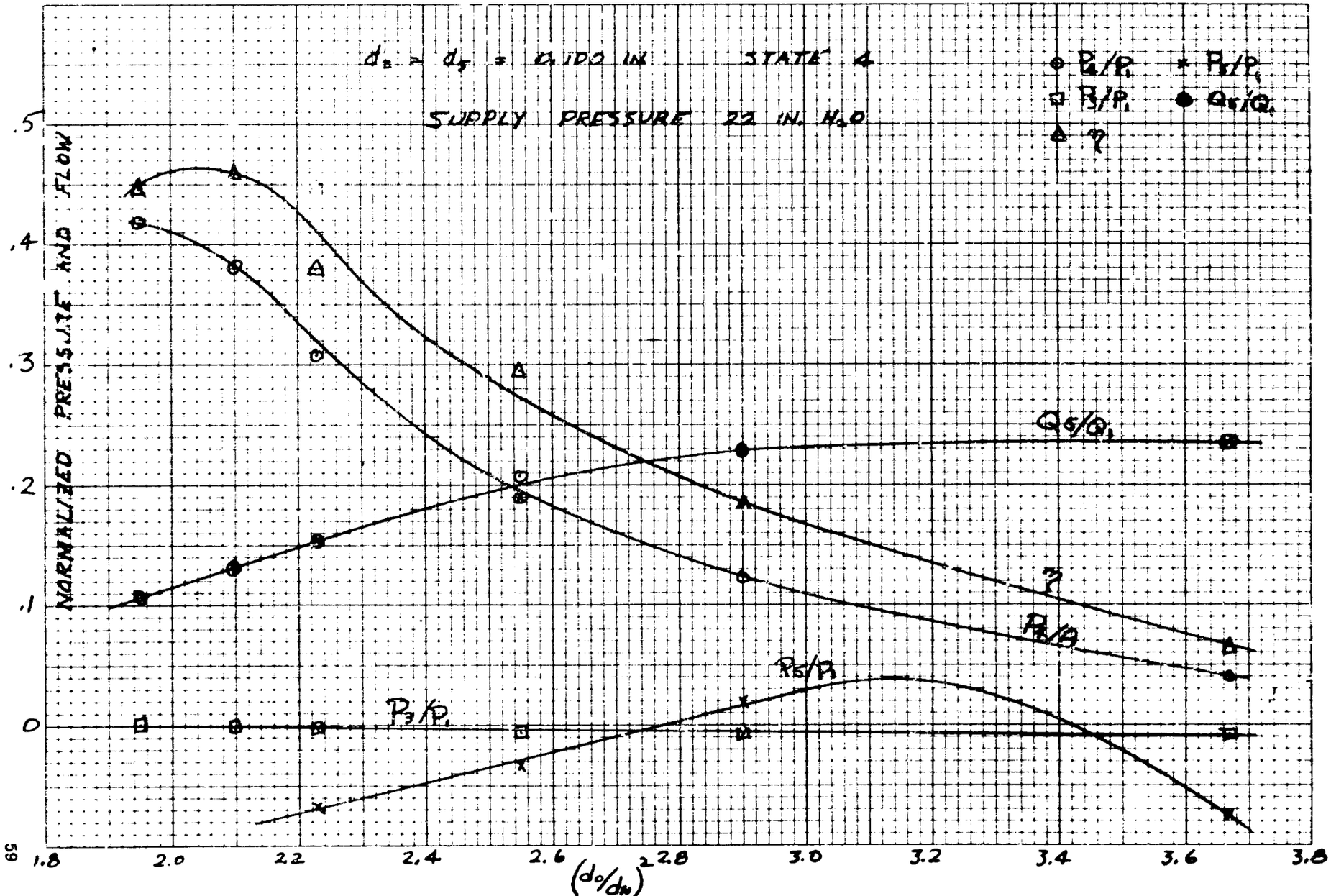

Figure A-7. Performance characteristics of flip-flops (cont'd).

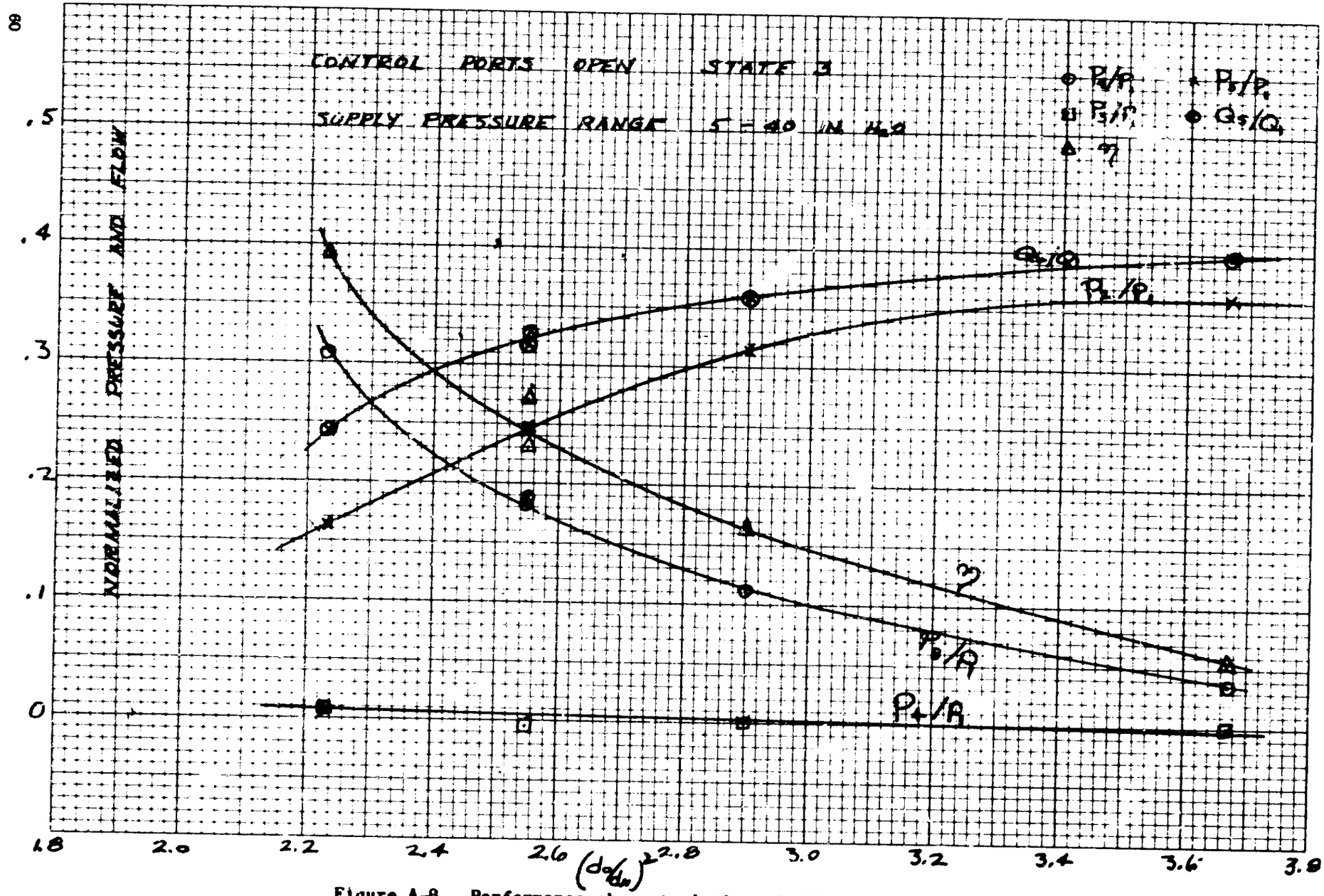

Figure A-8. Performance characteristics of flip-flops (cont'd).

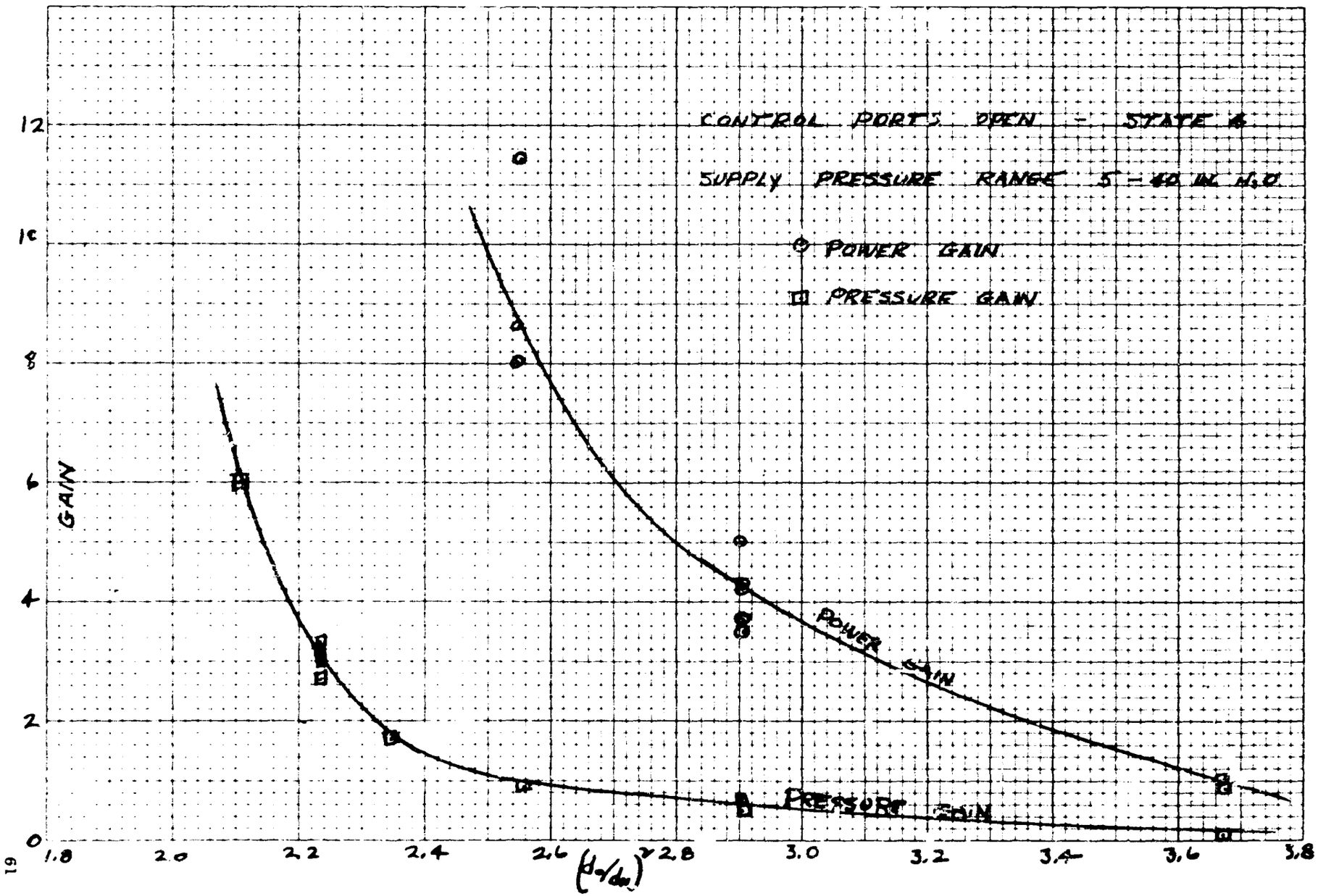

Figure A-9. Performance characteristics of flip-flops (cont'd).

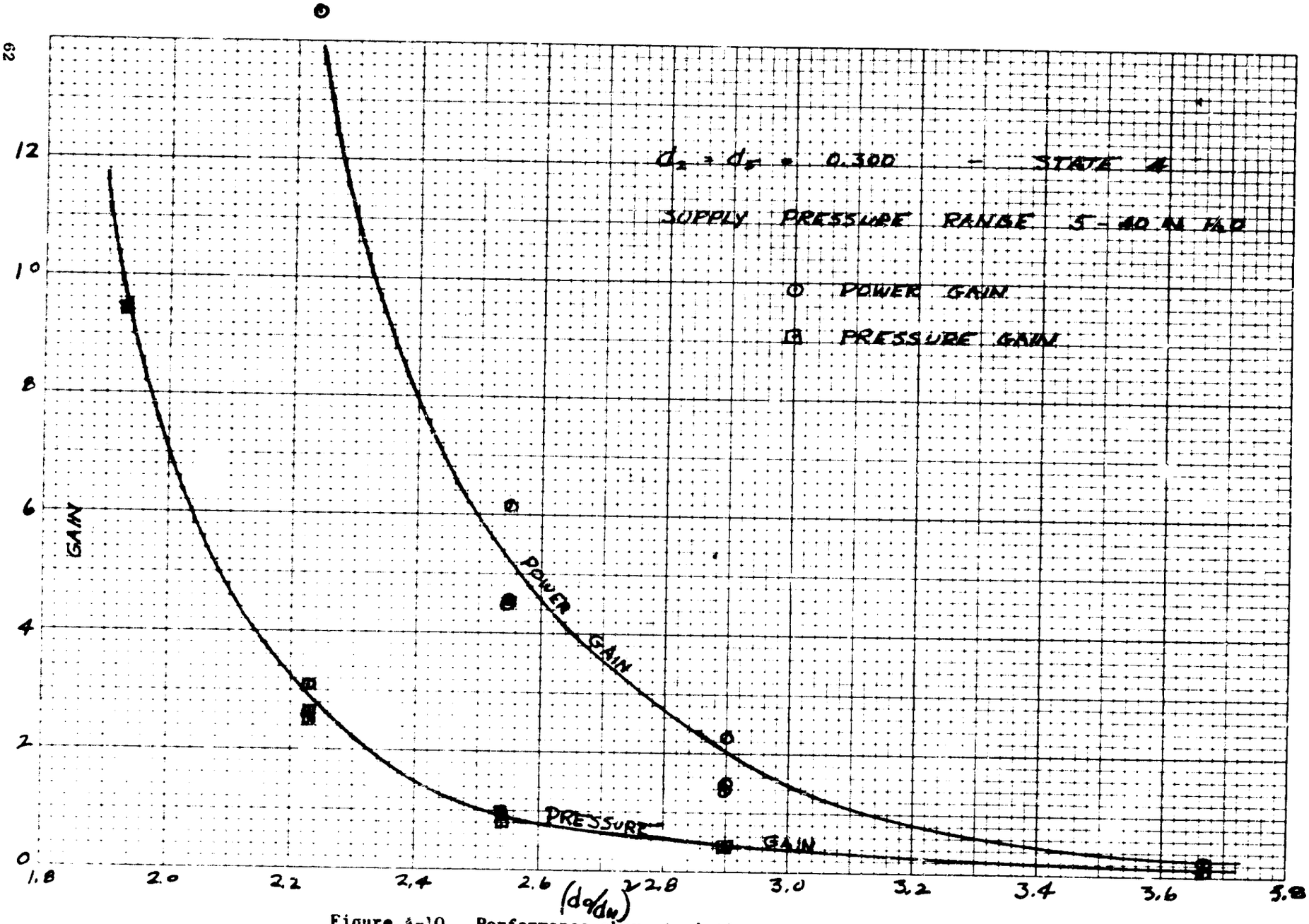

Figure A-10. Performance characteristics of flip-flops (cont'd).

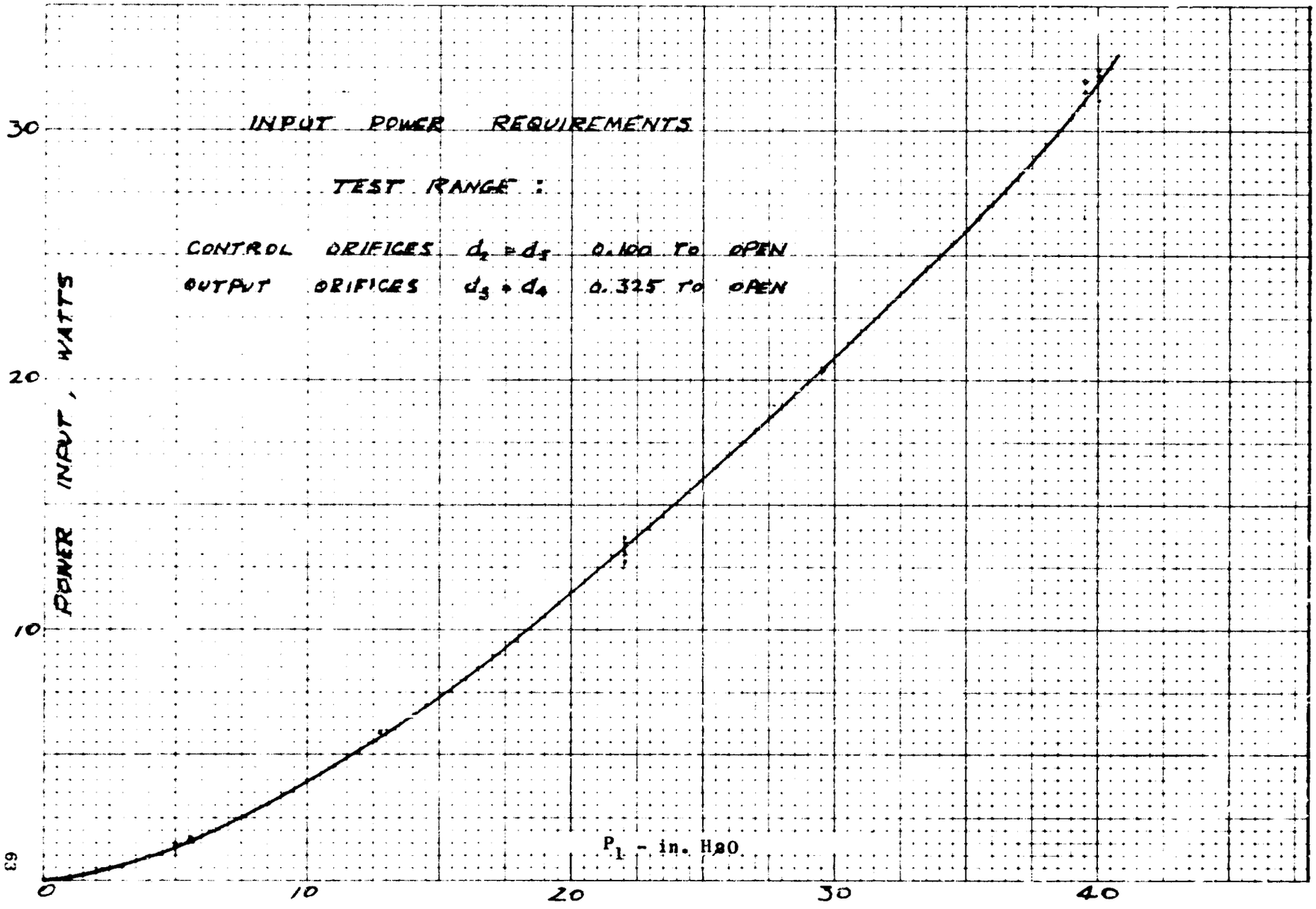

Figure A-11. Performance characteristics of flip-flops (cont'd).

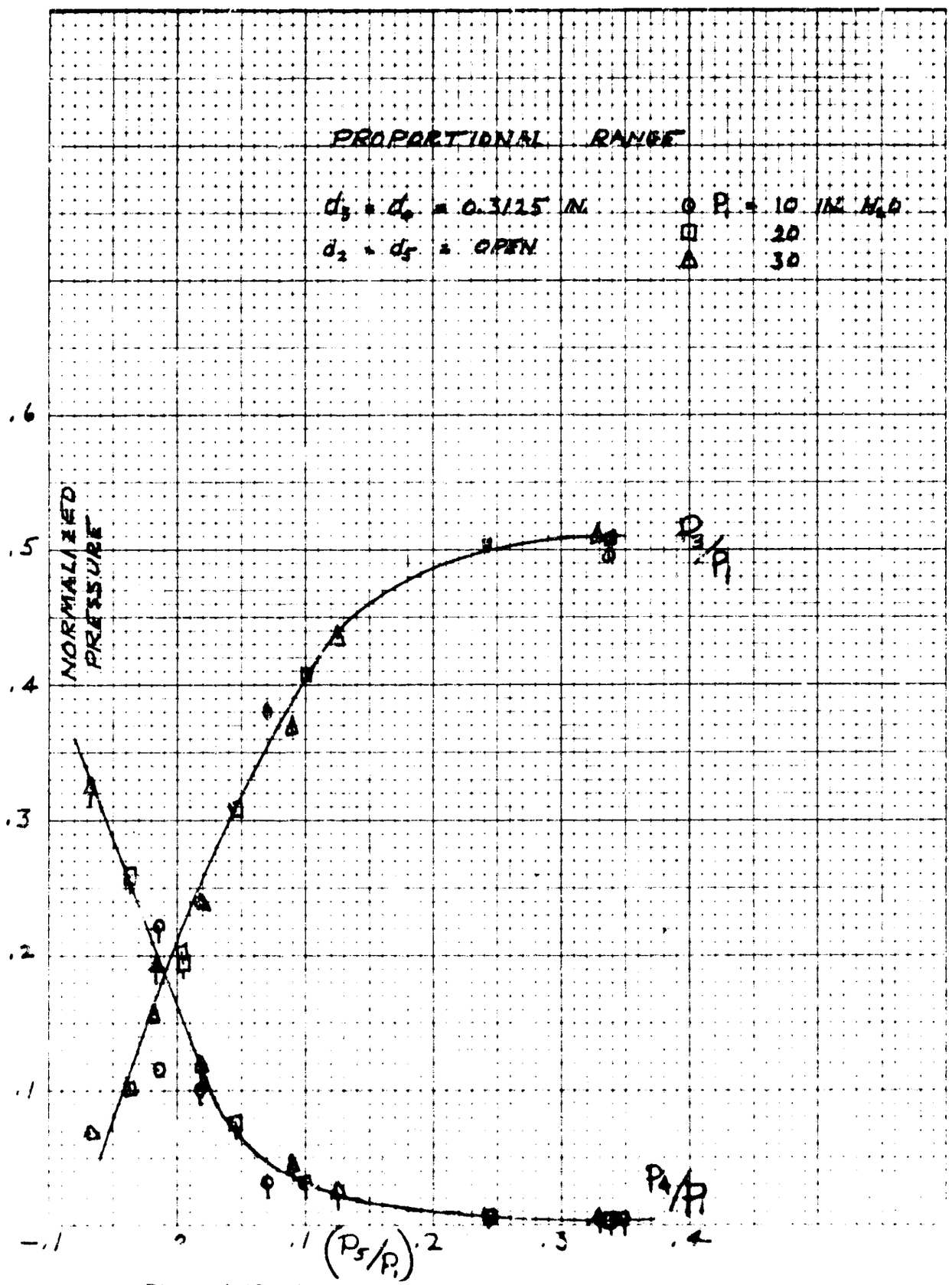

Figure A-12. Last graph showing performance characteristics of flip-flops.

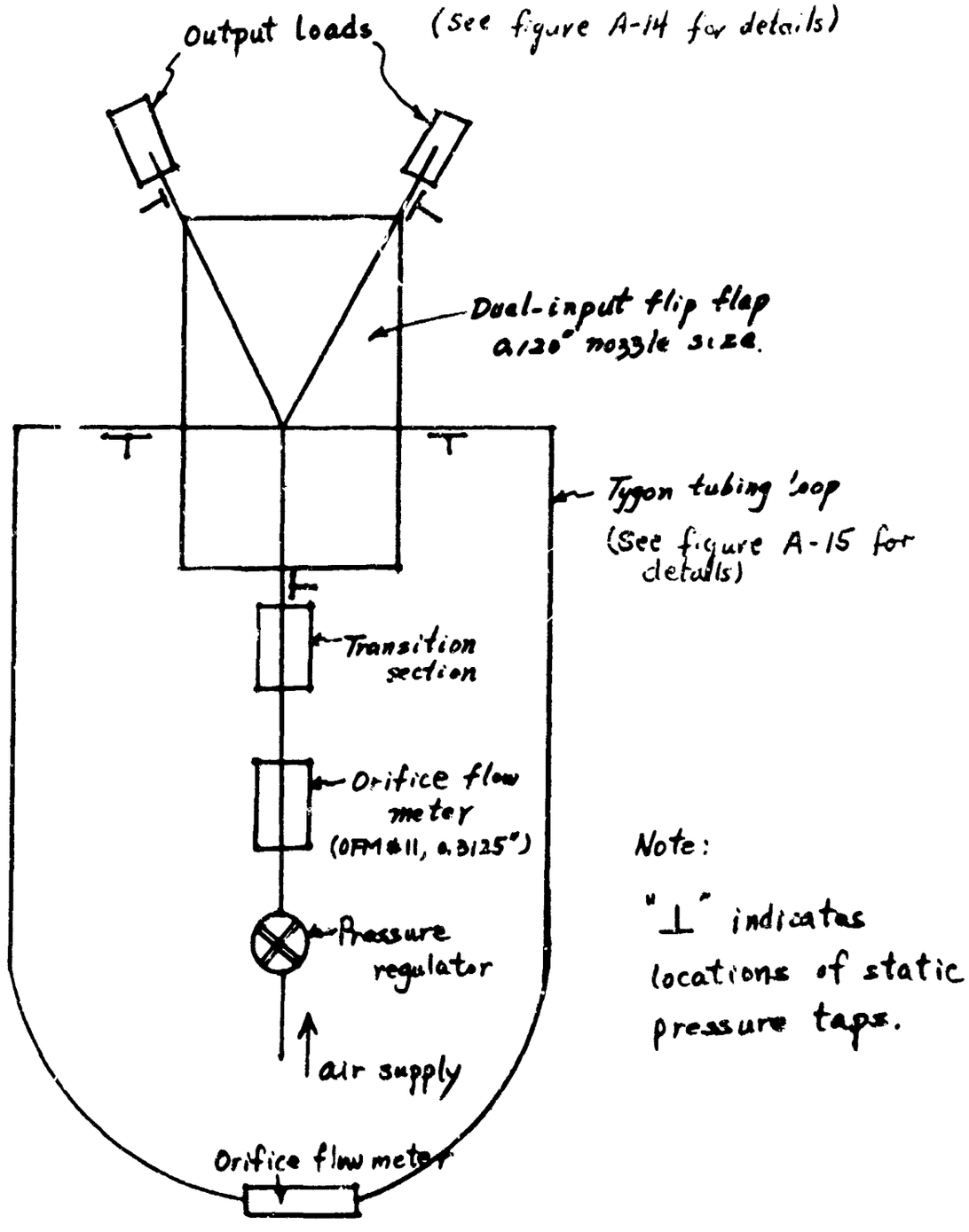

Figure A-13. Schematic diagram of the complete test arrangement.

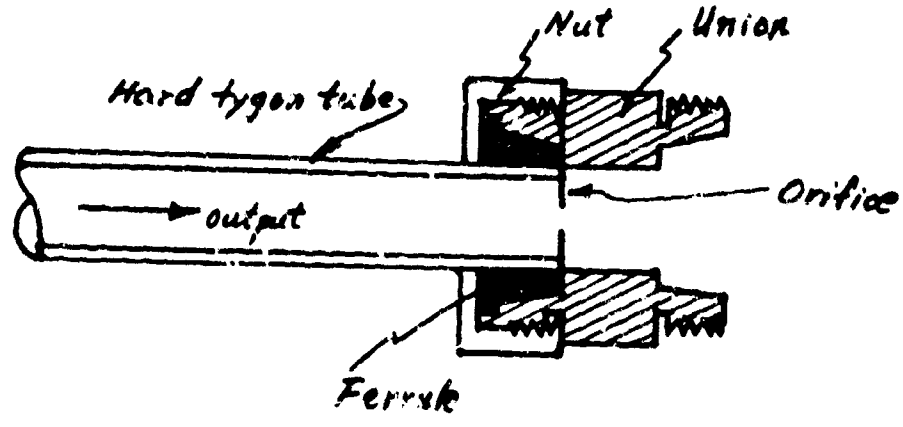

Figure A-14. Orifice adaptor.

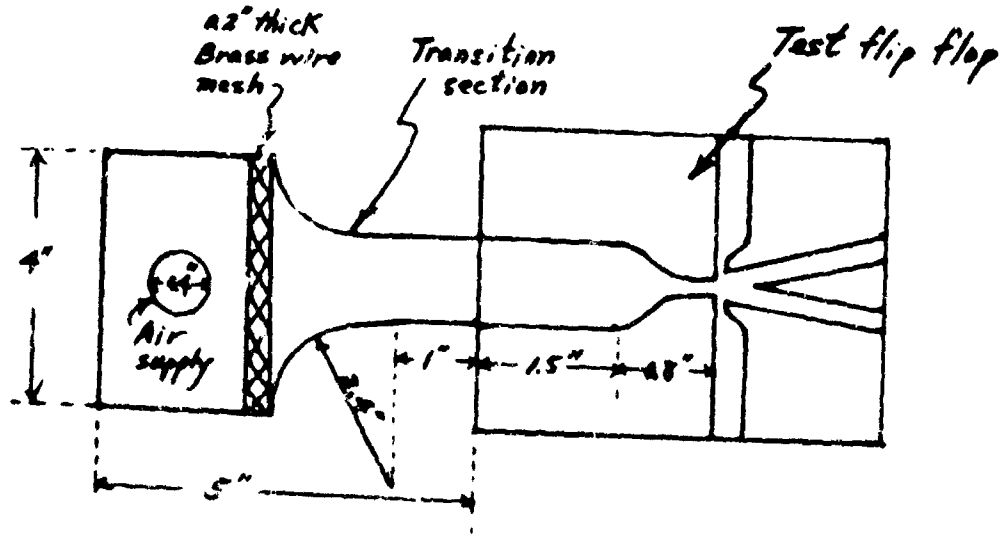

Figure A-15. Transition section.

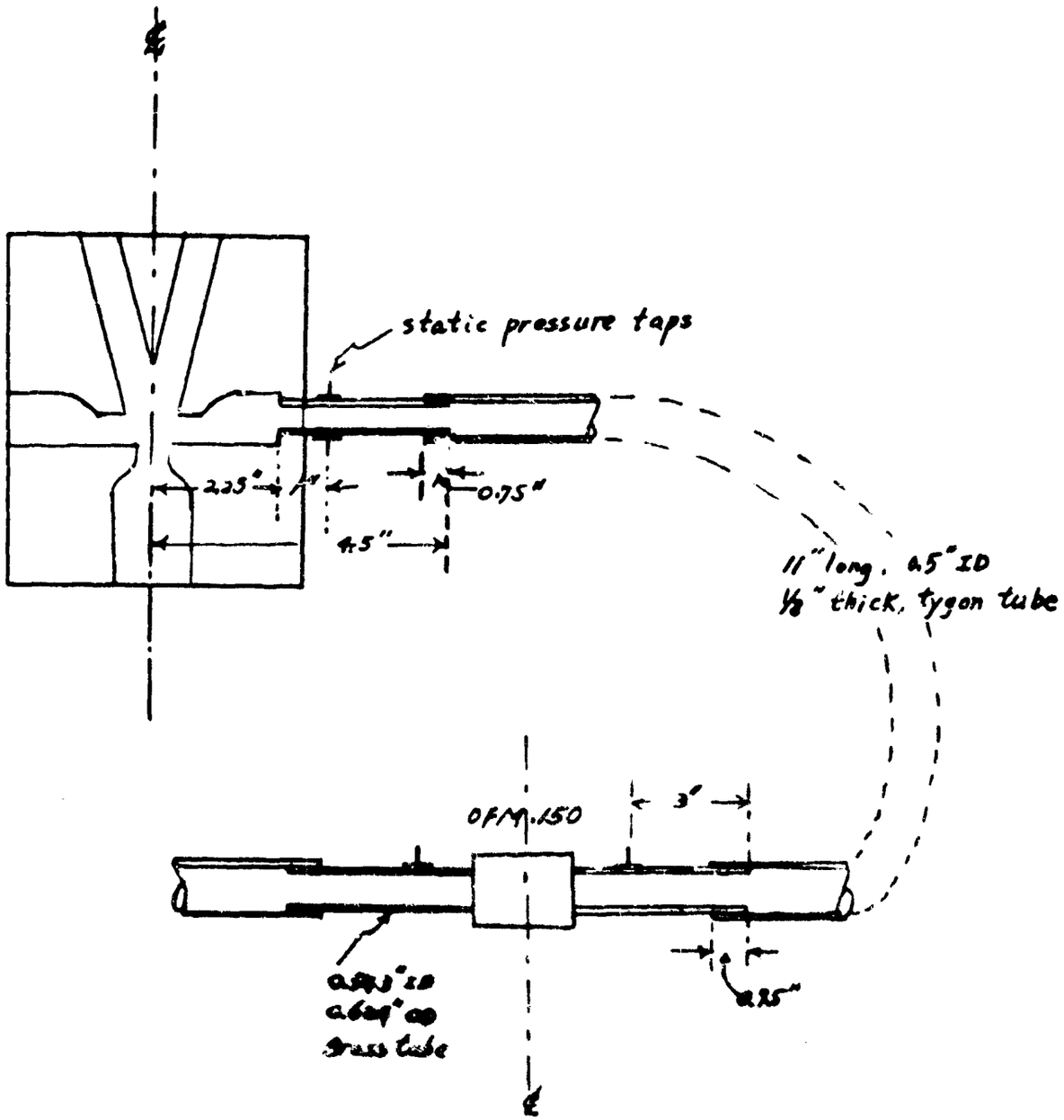

Figure A-10. Details of the tygon tubing loop.

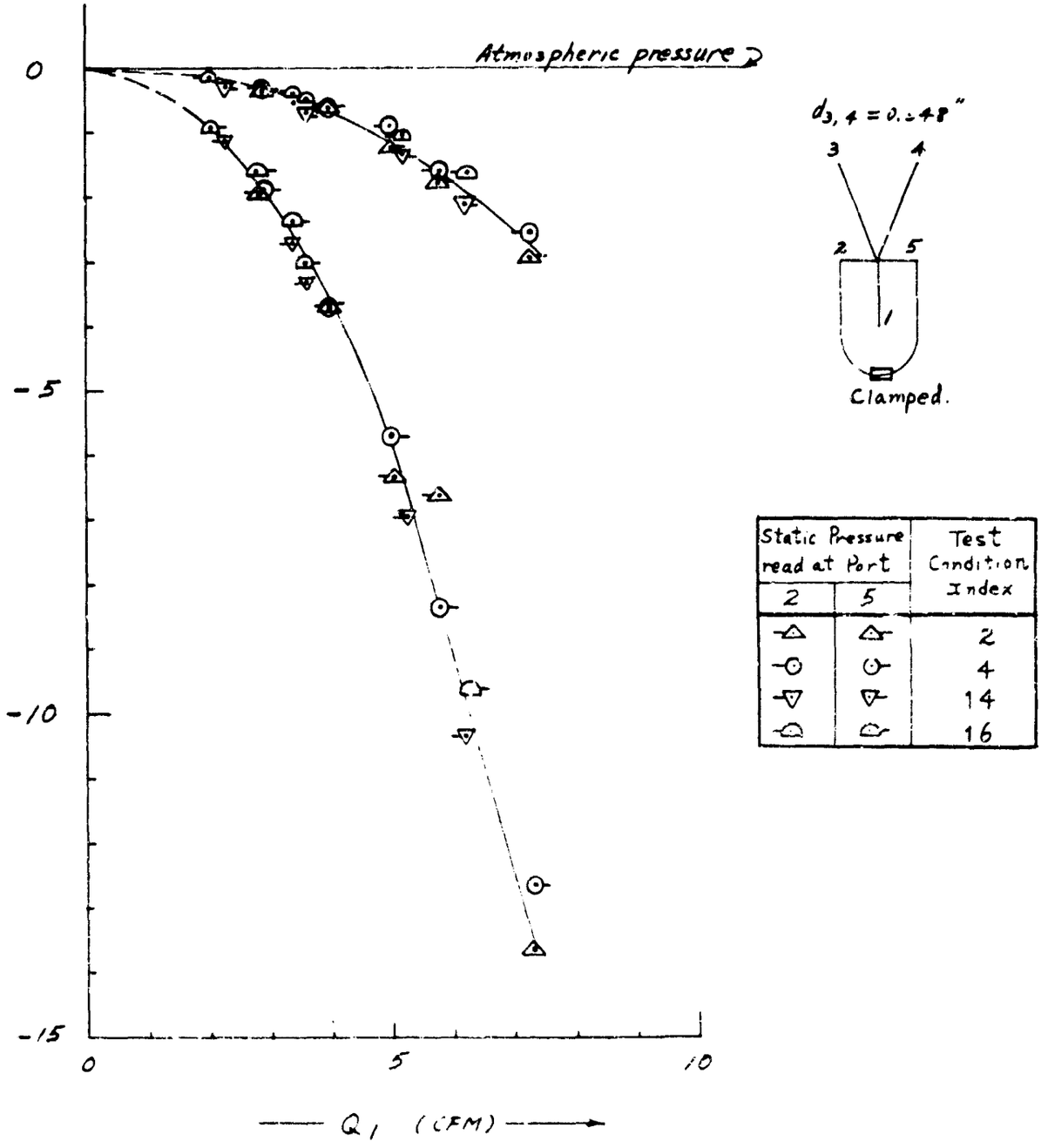

Figure A-17. Lowest induced static pressure at control ports 2 and 5.

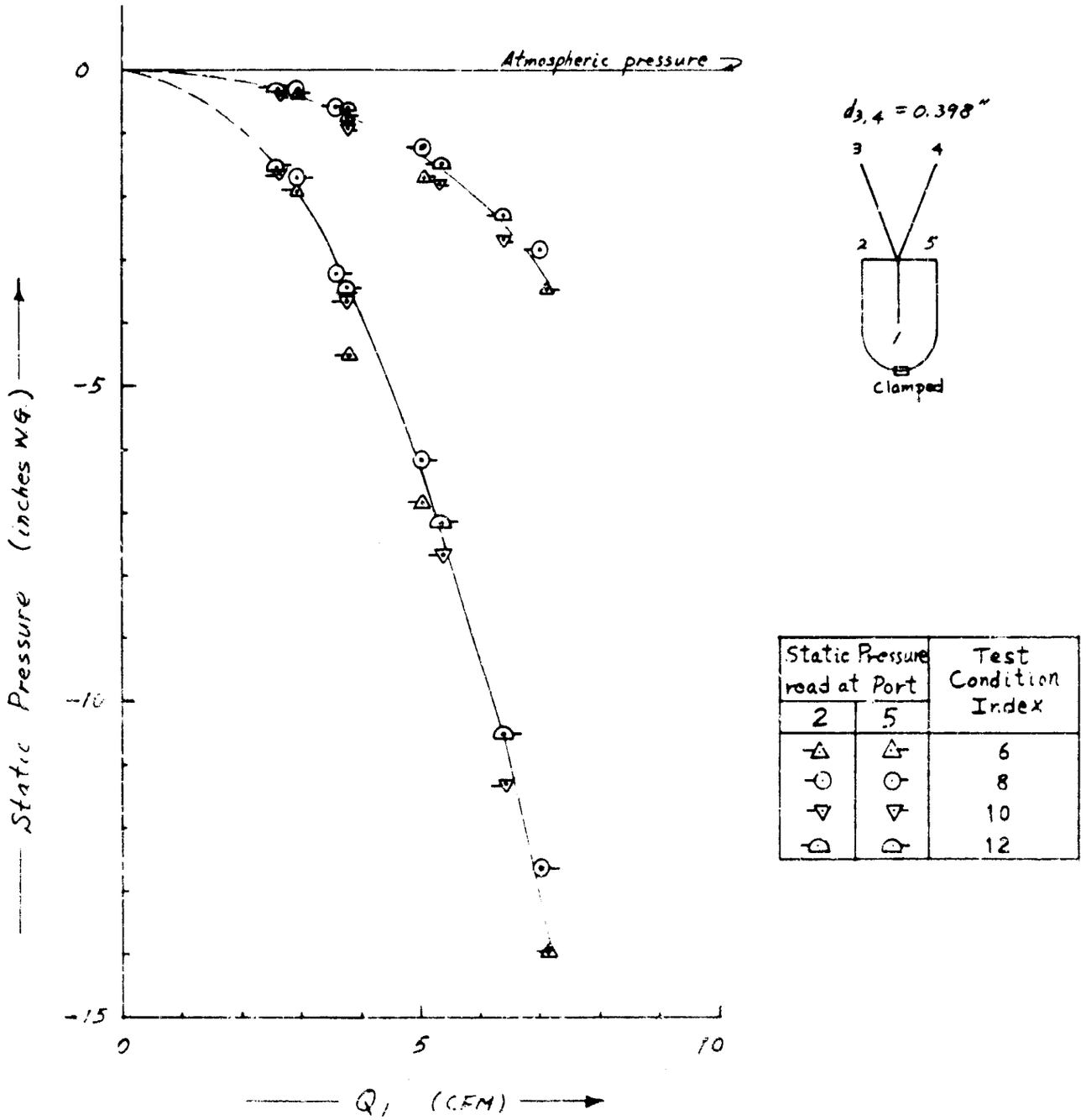

Figure A-18. Lowest induced static pressure at control ports 2 and 5.

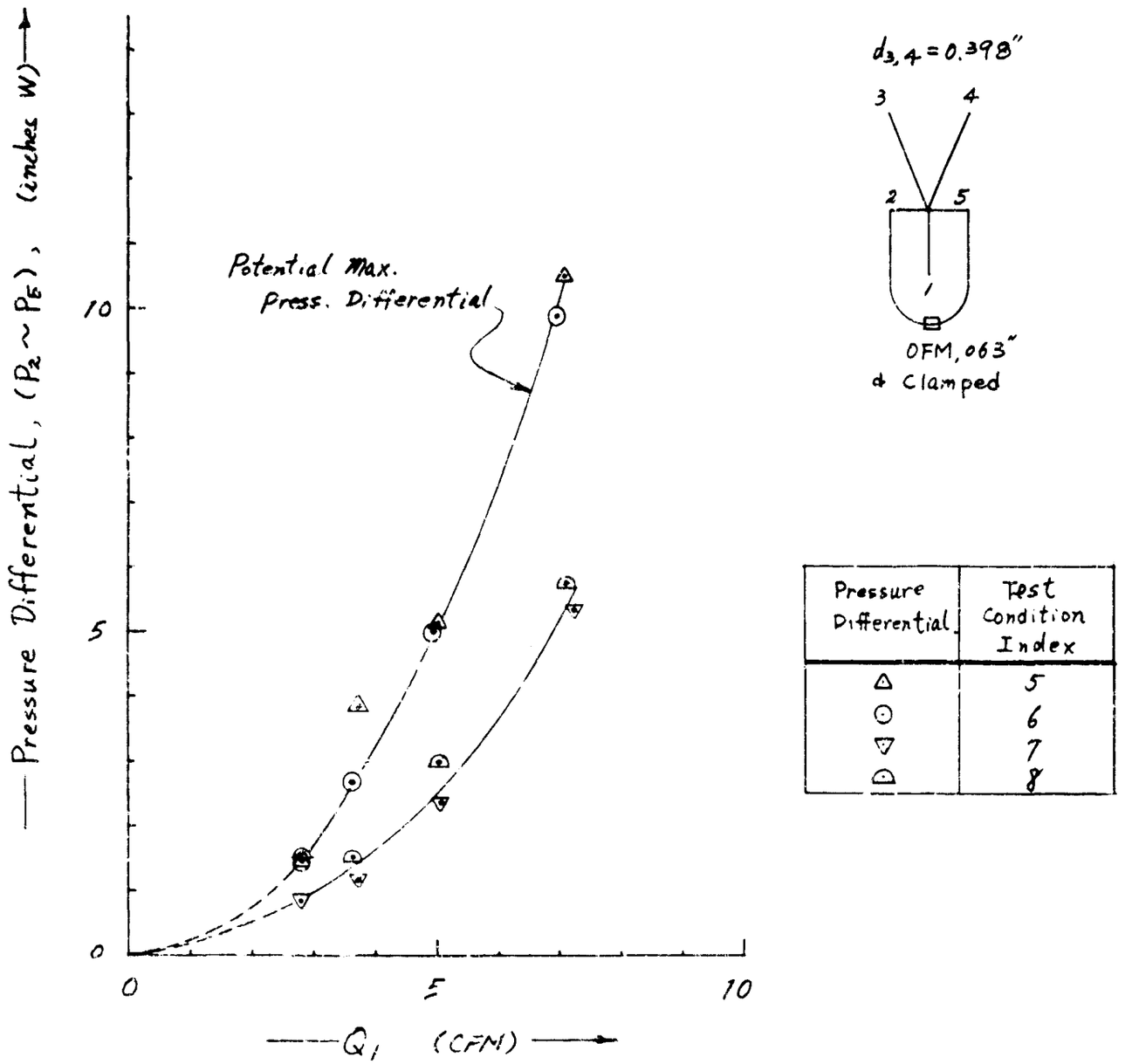

Figure A-19. Potential maximum pressure differential.

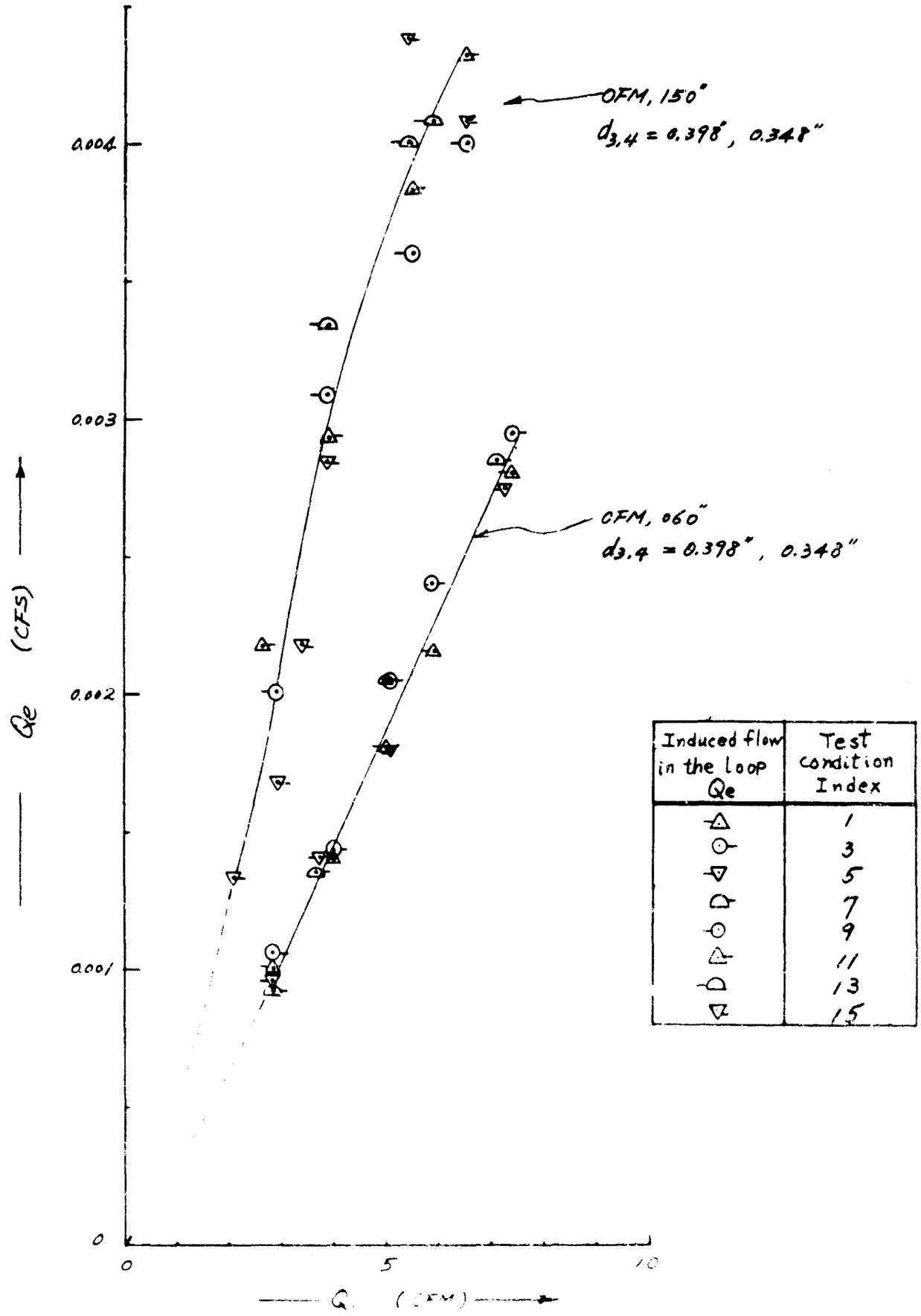

Figure A-20. Induced flow in the loop.

Table I. Sets of test conditions in the steady-state loop test.

Load in the loop	Output Load	Power jet flow rate	State of power jet	Loop condition	Test condition Index
OFM, .060"	$d_{3,4}=0.348"$	$Q_1 = 2 \sim 7.5$ CFM	3	open	1
				clamped	2
			4	open	3
				clamped	4
	$d_{3,4}=0.398"$	"	3	open	5
				clamped	6
			4	open	7
				clamped	8
OFM, .150"	$d_{3,4}=0.398"$	"	3	open	9
				clamped	10
			4	open	11
				clamped	12
	$d_{3,4}=0.348"$	"	3	open	13
				clamped	14
			4	open	15
				clamped	16

APPENDIX B.—STEADY-STATE, SUBSONIC FLOW ISOLATION BY GAP

T. F. Chen

ILLUSTRATIONS

APPENDIX B.—STEADY-STATE, SUBSONIC FLOW ISOLATION BY GAP

1. INTRODUCTION

In designing a fluid circuit one is often confronted with the complexity of analyzing the circuit as a whole. The problem is, essentially, to solve a large number of equations simultaneously. The complexity increases in accordance with the number of components in the circuit. If an efficient isolation device is available, it will permit us to break a complex circuit into a number of simple individual circuits, and thus build a complex circuit before the complex circuit theory is developed.

A simple, gap-type, isolator was investigated here. The idea used is simply that by providing a gap of suitable size between two components in the circuit; only the output flow of the driving component can efficiently jump across the gap to trigger the following component but the undesirable feedback is spilled out at the gap. Physically, a gap-type isolator consists of a gap of suitable size and a recovery port as shown in figure B-1. According to the situation in which the isolator is used, the isolator can be either an independent component or integrated with the component being isolated.

The configuration of the recovery port is important because it is one of the factors that determines the flow pattern at the isolator. Three representative types of recovery port configuration were chosen in this study. In the following discussion, an isolator is considered to consist of dimensions as given in figure B-1 (list 1).

The investigation was conducted with the attempt to provide some design data as well as to bring out the basics of the flow across a gap. The input and output of the isolator and the loads used in the test were defined. Then the results were analyzed and presented to show the relationship of input and output flow and pressure with respect to the gap size and loads.

2. DESCRIPTION OF TEST APPARATUS AND ARRANGEMENT

The test apparatus is shown schematically in figure B-2. Two pieces of brass tube with dimensions as given in the figure were held together in a larger size brass sleeve. The larger size brass sleeve was perforated to give free escape paths to ambient atmosphere. There were four static pressure taps located at points 1, 2, 3, and 4 as shown in figure B-2. They were 1.5 in. from the ends of each tube.

The input and output flows were measured with venturi flow meters as shown in figure B-3. Two flow meters were necessary for covering the test range desired. In the test, there were three loads used. The maximum load condition was obtained by blocking off completely the end of the test piece. The medium and minimum loading conditions are illustrated in figure B-4. The pressure taps on the test tube were used to measure the flow recovered at minimum loading condition.

3. DEFINITIONS

(1) P_1, P_2, P_3, and P_4 — Static pressures (gauge) measured at points 1, 2, 3, and 4 (fig. B-2).

(2) P_5 — Static pressure (gauge) calculated from P_3 and P_4 at section $5D_1$ from recovery port.

(3) Q_1, Q_2 — Volume rate of flow in the brass tubes upstream and downstream of the gap.

(4) A — Admittance of a component as defined in the following expression.

$$A = \frac{Q^2}{\Delta P} = \frac{(\text{Volume rate of flow through the component})^2}{\text{Drop in the total pressure through the component}}$$

Applying this definition, the admittance of the loads used can be expressed as following (fig. B-2).

$$A_{\text{maximum load}} = \frac{Q_5^2}{\Delta P} = 0$$

$$A_{\text{medium load}} = \frac{Q_5^2}{\left(P_5 + \frac{\rho V_2^2}{2}\right) - \frac{\rho(V_3^2 + V_4^2)}{2}}$$

$$= \frac{Q_5^2}{P_5 + \frac{\rho(V_2^2 - V_3^2 - V_4^2)}{2}} \qquad (1)$$

$$A_{\text{minimum load}} = \frac{Q_5^2}{\left(P_5 + \frac{\rho V_2^2}{2}\right) - \frac{\rho V_2^2}{2}} = \frac{Q_5^2}{P_5} \qquad (2)$$

When the end of the test tube was blocked completely, the air flowed through the gap. The admittance of the gap is calculated as:

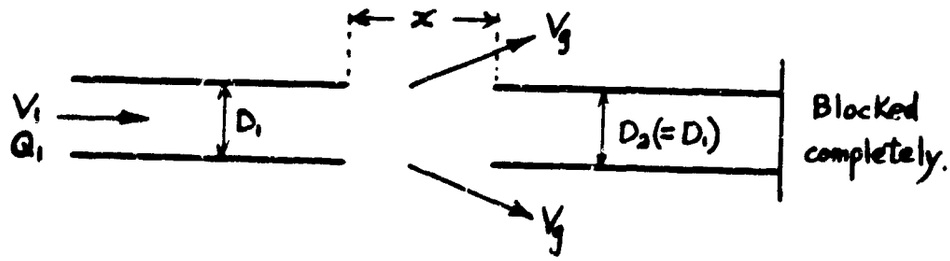

Area of gap = $\pi D_1 X$

Average velocity of air through gap = V_g

$$A_{gap} = \frac{Q_1^2}{\frac{\rho}{2}(V_1^2 - V_g^2)} \qquad (3)$$

(5) Degree of feedback — Zero degree of feedback refers to a complete isolation of flows upstream and downstream of the gap. It was calculated from

$$\text{Degree of feedback } (\%) = \frac{\Delta P_2}{\frac{\rho V_1^2}{2}} \times 100$$

$$\text{or } = \frac{(P_2)\text{ output blocked} - (P_2)\text{ output open}}{\left(\frac{\rho V_1^2}{2}\right)\text{ output open}} \times 100$$

(6) Total pressure — The sum of the dynamic pressure $\left(\frac{\rho V^2}{2}\right)$ and static pressure.

(7) Stagnation pressure — P_3 or P_4 when the end of test tube was blocked completely.

4. STEADY-STATE TEST

The variables considered in the test were:

(1) Independent variables

(a) Q_1 (or P_1, or $P_1 - P_2$)

(b) Types of recovery port configuration - Type A
Type B
Type C

(c) End condition of the test tube - open or closed

(d) Gap size, X

(e) Loads

(2) Dependent variables

(a) Q_2

(b) P_3 (or P_4)

The test was designed to obtain the following information:

(1) Relationship between degree of feedback and gap size, (X/D_1) for the three types of recovery port configuration.

(2) Flow recovery, (Q_2/Q_1) versus gap size, (X/D_1) for the three types of recovery port configuration.

(3) Stagnation pressure versus gap size.

(4) Flow recovery versus loads.

(5) Total and dynamic pressure recoveries with respect to loads.

The results of the tests are presented in the next section.

5. TEST RESULTS AND DISCUSSION

(1) The main concern in this investigation was to determine the minimum gap size which would provide zero feedback. In figures B-5, (a) and (b), the test results are presented. For convenience, the degree of feedback was expressed in terms of percent of the input dynamic pressure $(\rho V_1^2/2)$. Three curves representing each type of recovery port configuration showed quite different characteristics. For the range of (X/D_1) values shown, the degree of feedback in Type A changed significantly from a positive to a slightly negative value at $X/D_1) \simeq 0.6$. Zero degree of feedback was obtained at $(X/D_1) = 2.38$.

For Type B, the feedback effect was negative for the range $0.269 < X/D_1 < 1.67$. This means that when the end of the receiving tube was blocked, the static pressure P_2 was reduced from its value when the end was open.

For Type C, the feedback effect was always positive. Zero degree of feedback was achieved at $X/D_1 = 1.0$. The spread of points at a given X/D_1 value for one type reflects the influence of V_1 which was varied from 100 to 220 fps. (4,000 to 15,000 in terms of Reynolds number). Depending on the degree of isolation and the other requirements of each specific case of application, figures B-5(a) and (b) can be used as a guide for the design of the recovery port configuration and gap size of an isolator.

(2) The flow recovery (Q_2/Q_1) at various gap size (X/D_1) for type A, B, & C is presented in figures B-6 (a) and (b). The overall characteristics of each curve in this figure was quite flat for a considerable part of the test range of X/D_1. Within this range of X/D_1 shown, the flow recovery was always slightly higher than 0.7.

The difference among different types was not significant. Beyond the flat part of the curve a large drop in flow recovery was observed for type A and B.

Figure B-6 (a) and (b) serve to show the relationships of:

(a) Velocity recovery, since

$$\frac{V_2}{V_1} = \frac{Q_2}{Q_1} \quad \text{for same size tubing}$$

(b) Dynamic pressure recovery, since

$$\frac{\frac{\rho V_2^2}{2}}{\frac{\rho V_1^2}{2}} = \left(\frac{Q_2}{Q_1}\right)^2 \quad \text{for same size tubing}$$

(3) Stagnation pressure recovered versus X/D_1 for type A, B, & C is shown in figures B-7(a) and (b). By knowing the stagnation pressure recovered for different gap sizes and types of entrance configuration, we get a measure of the maximum total pressure recoverable as the output flow, or the admittance of the load, approaches zero.

Stagnation pressure was normalized with respect to the input dynamic pressure. The results are shown in figures B-7(a) and (b). The ratio of the maximum velocity to mean velocity for

a fully developed turbulent flow is approximately 1.2. Thus, the stagnation pressure would be about 1.44 times the input dynamic pressure ($\rho V_1^2 1/2$ if the gap sizes were within the core flow region and there were no other effects. Referring to the curves showing the stagnation pressure recovered in figures B-7(a) and (b), when the gap is very small, the stagnation pressure recovered is greater than 1.44.

The gap size plays an important role in determining the downstream (recovery tube) pressure. For large gap sizes, the downstream pressure is influenced by the atmospheric pressure in the gap. But for very small gaps, the flow pattern is such that no part of the "through" flow is subjected to atmospheric pressure; thus, the upstream pressure becomes controlling. One might say that pressure is "transmitted" downstream, and may be likened to the case of a small hole drilled in a pipe for the purpose of measuring static pressure. In the latter case, the effect of the "exposure" to the atmosphere in governing the flow inside the pipe is insignificant.

Another practical way to explain this phenomenon is shown in the following sketch.

For a large gap size:
$(\frac{x}{D_1} \simeq 3 \text{ to } 6)$

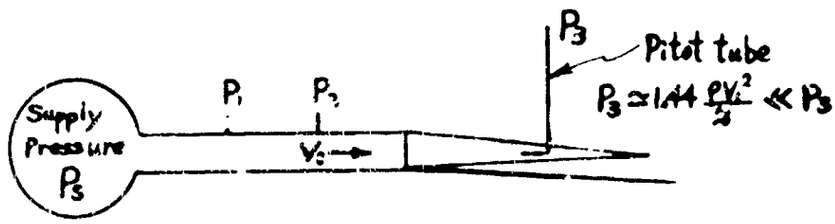

For a small gap size:
$(\frac{x}{D_1}$ approaches $0)$

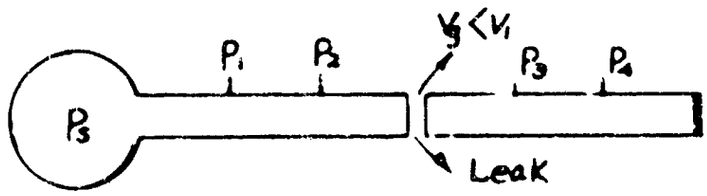

In the lower diagram, the situation approximates that of a blocked pipe and P_3 approaches P_s.

(4) In figure B-8 the flow recovery (Q_2/Q_1) is plotted against admittance of loads ($Q_2^2/\Delta P$) for $X/D_1 = 1$. In figure B-9, the total and dynamic pressure recoveries are plotted with respect to the admittance of the loads for $X/D_1 = 1$. There were three loads used in the test as described previously. The admittance values of these loads were calculated according to the definitions and experimental data shown in figures B-10, B-11, and B-12. Flow recovery increased as the admittance of the loads increased. The shaded, rectangular areas represent the spread of experimental results due to varying input pressure and recovery port configuration. As stated previously, figure B-8 serves to show both velocity and dynamic pressure recoveries with respect to loads.

(5) As the admittance of the load increased the dynamic pressure increased, but the total pressure recovered remains almost the same (fig. B-9). If there were no energy loss in the isolator the total pressure recovery line would be horizontal. Since the ratio of the maximum to average velocity in a fully developed turbulent flow is about 1.2, then this horizontal line should be at 1.44 on the ordinate as shown in figure B-9. The net energy loss is represented by the distance between the constant total energy line and the total pressure recovery line. For a given load with its admittance value known, figure B-9 shows the performance characteristics of the isolator, i.e., the efficiency, the static pressure and dynamic pressure recovery.

(6) The relationship between the input total pressure and output flow of the isolator at two load levels are shown in figures B-10, B-11, and B-12. These were used to calculate the admittance of the loads. The gap size and the type of entrance configuration were also recorded.

These results showed that the input versus output relationship depended very slightly on the type of entrance configuration and X/D_1 value in the range of test as shown in the figures.

6. CONCLUSION

Steady state, subsonic flow isolation can be achieved by mea. of a gap of proper dimension along the flow channel. In an axisymmetrical flow, an adequate isolation of flow can be achieved by providing gap size ranging from 1.0 to 2.38 depending on the recovery port configuration. The cone shape recovery port requires the smallest gap size whereas the funnel shape takes considerably larger size gap. On the basis of the flow and pressure recoveries, and the gap size necessary for complete flow isolation, the cone shape recovery port is most attractive.

The output characteristics of the isolators are also a function of the load. Admittance of a load as defined here can be used to map the output characteristics of the isolator.

7. SUGGESTIONS

(1) A similar investigation of the transient state would be highly valuable and desirable.

(2) The direct application of the information presented here to a two dimensional flow isolator needs additional investigation.

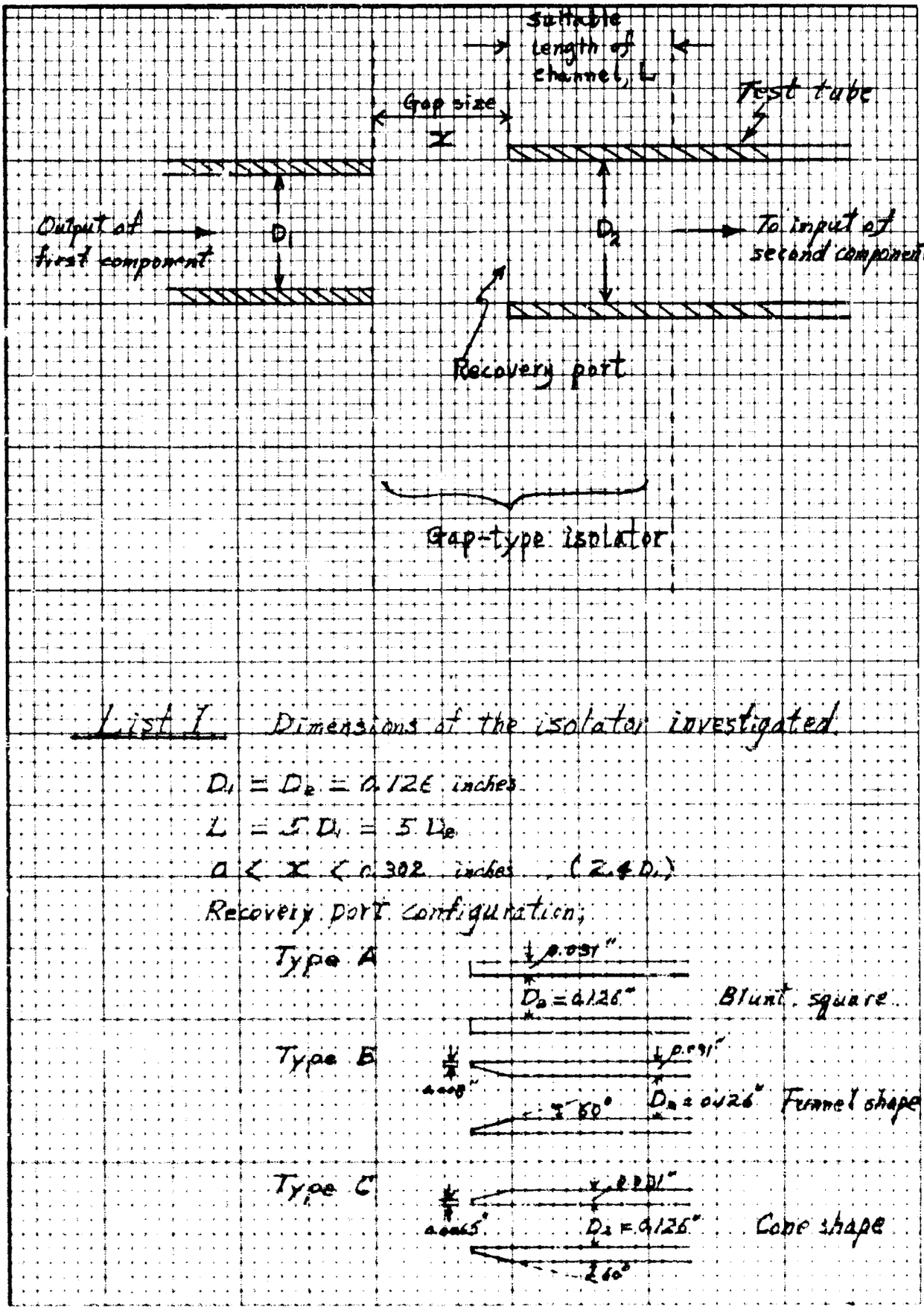

Figure B-1. Gap-type isolator.

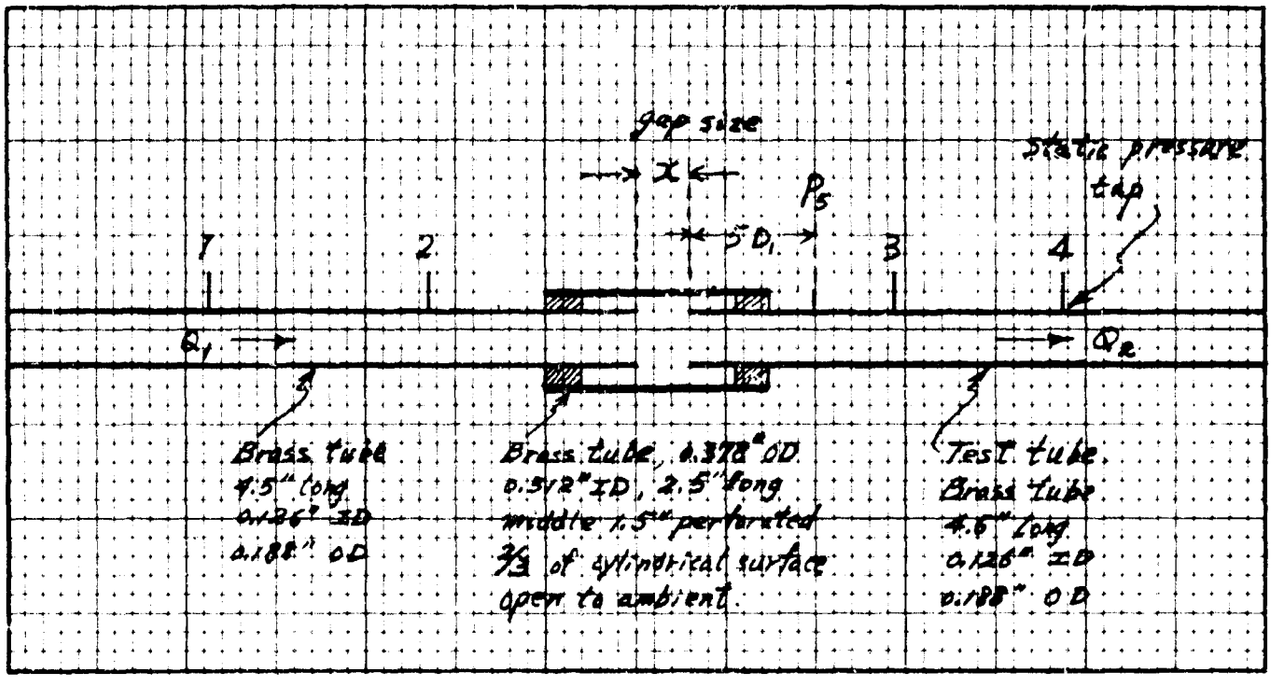

Figure B-2. Test apparatus.

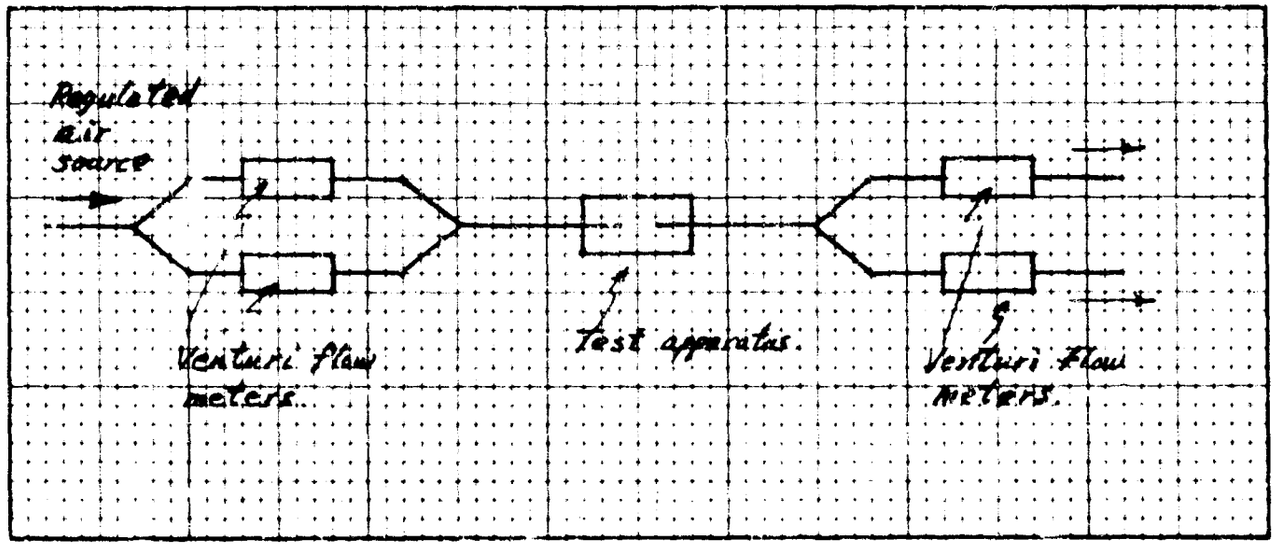

Figure B-3. Test arrangement.

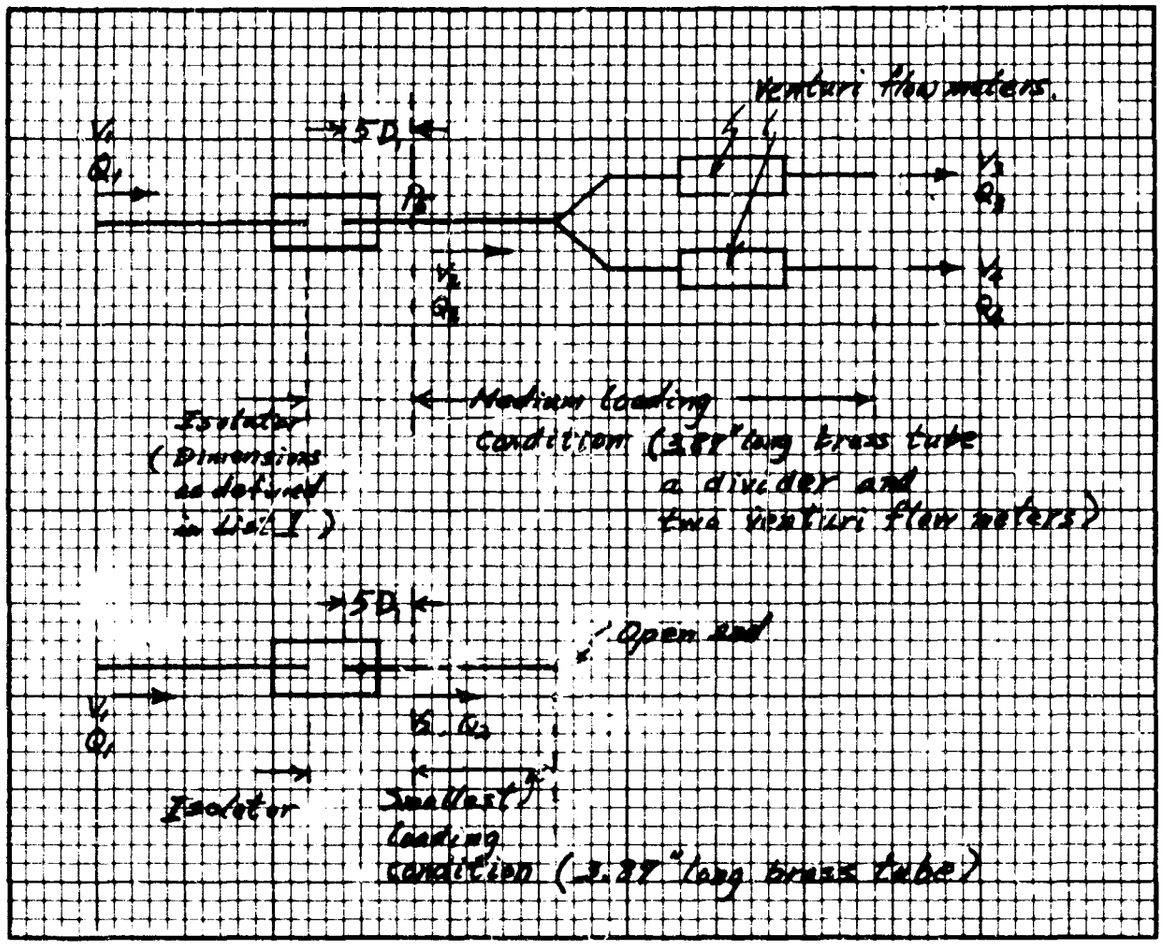

Figure B-4. Loading conditions.

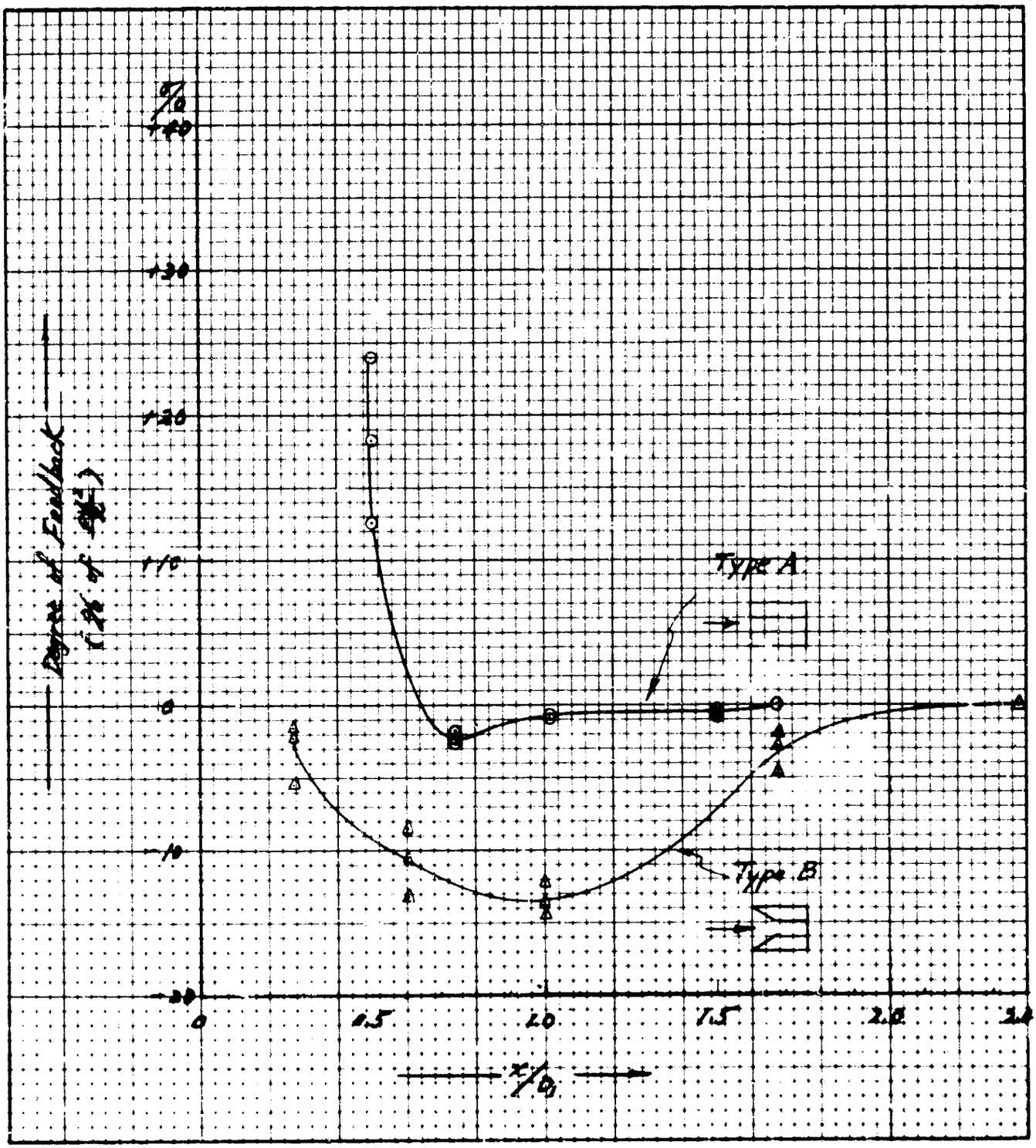

Figure B-5a. Degree of feedback at various gap sizes up to complete isolation.

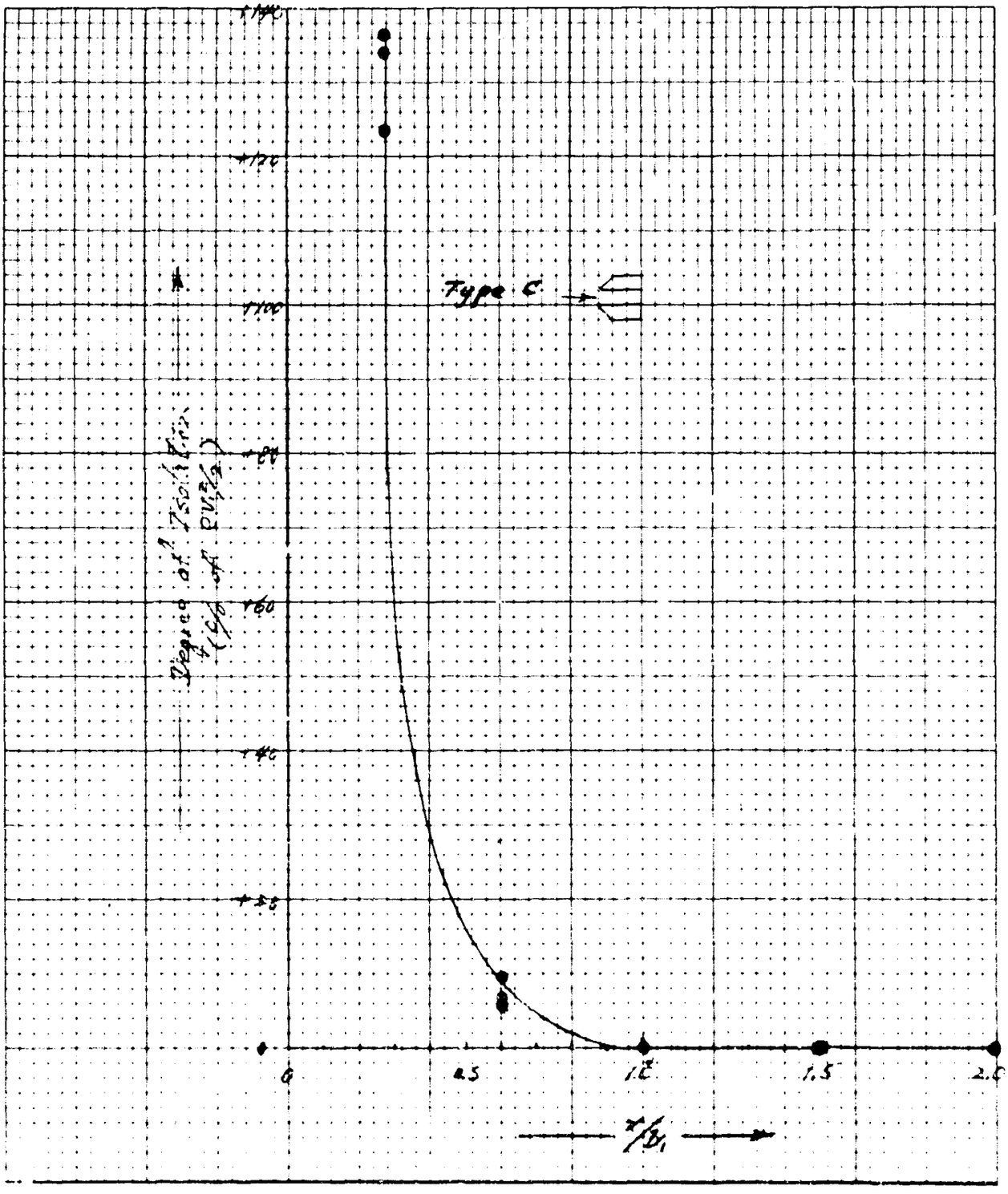

Figure B-5b. Degree of feedback at various gap sizes up to complete isolation.

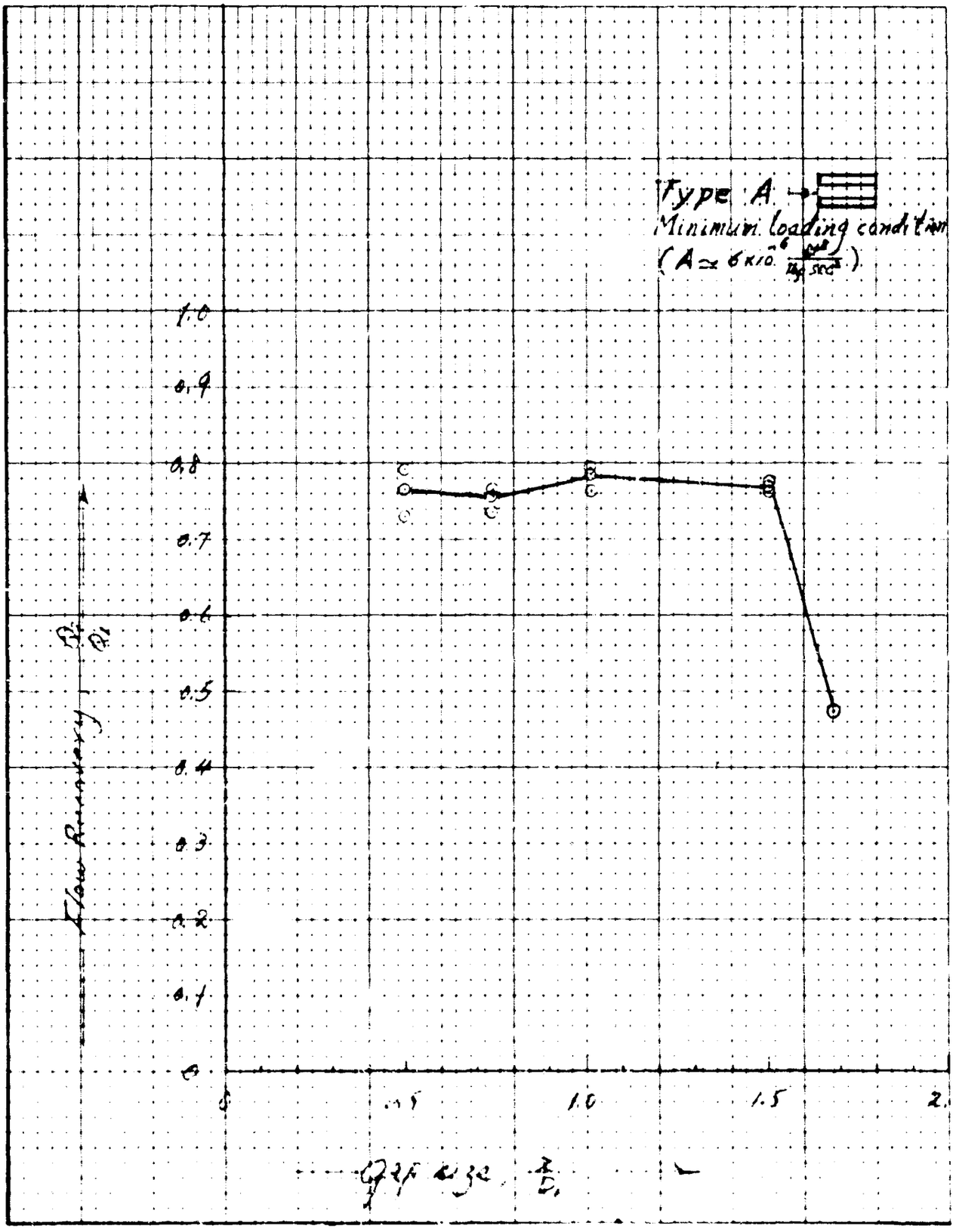

Figure B-8a. Flow recovery at various gap sizes up to complete isolation.

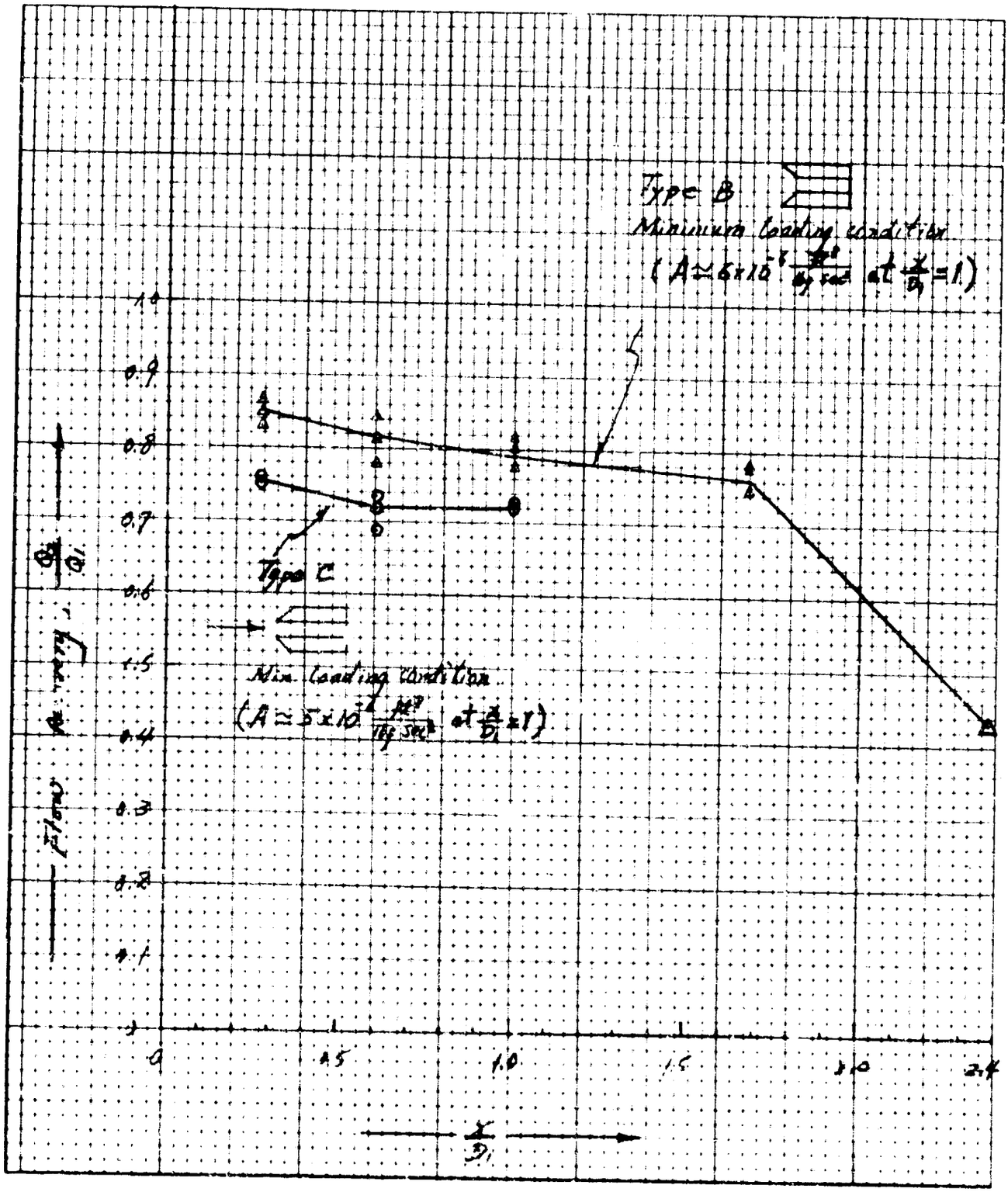

Figure B-65. Flow recovery at various gap sizes up to complete isolation.

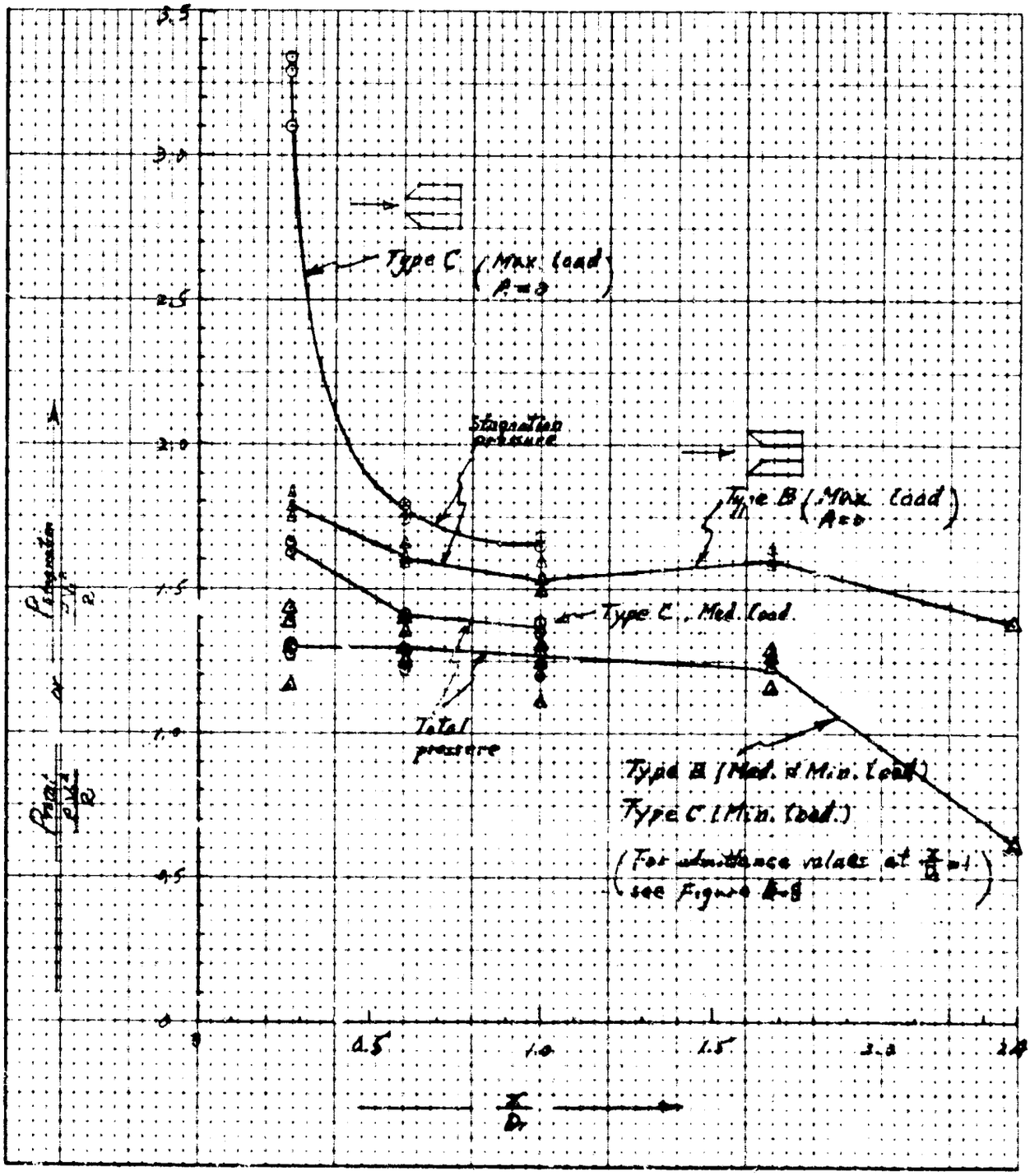

Figure 3-7a. Total and stagnation pressure recovered at various gap sizes up to complete isolation.

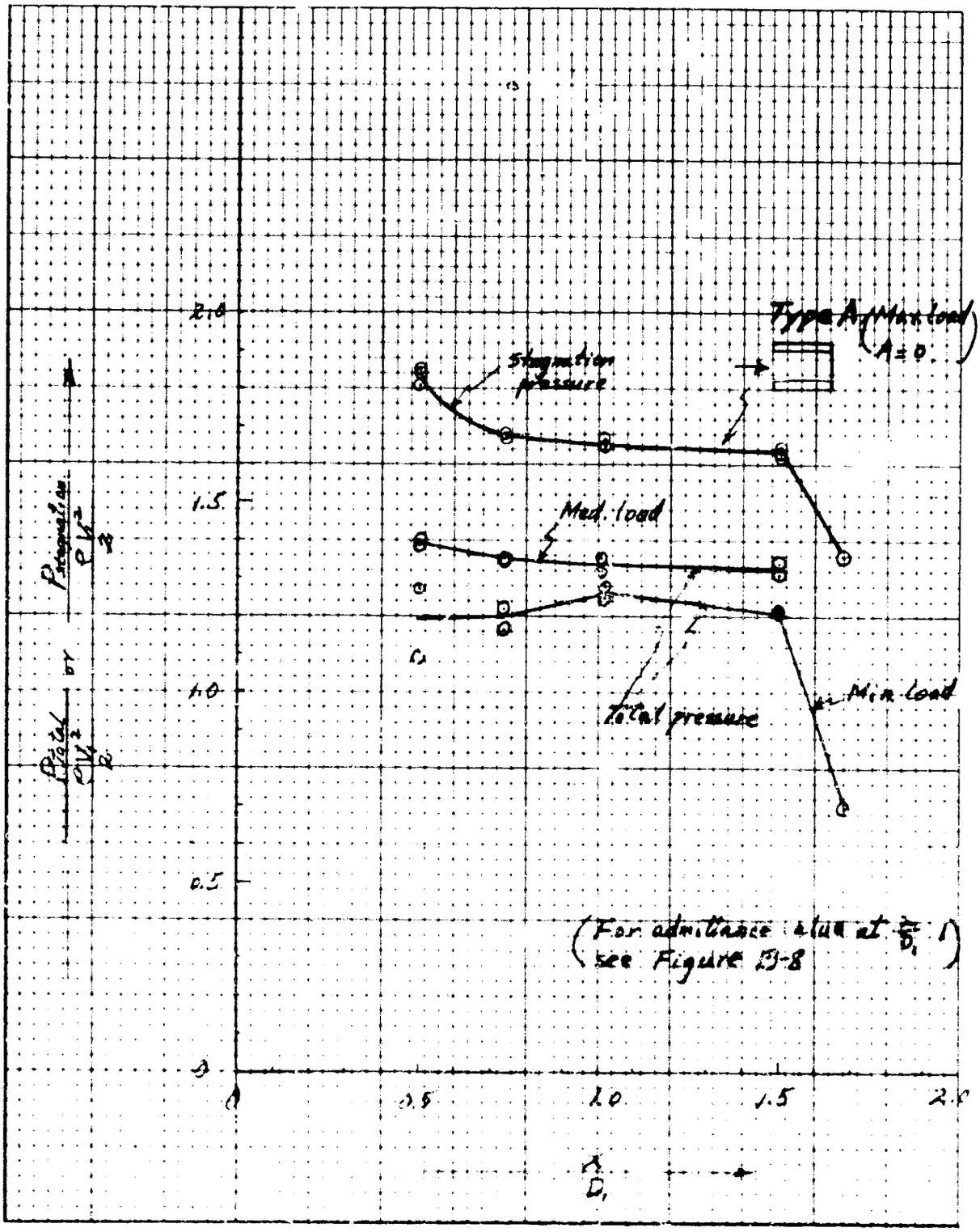

Figure B-7b. Total and stagnation pressure recovered at various gap sizes up to complete isolation.

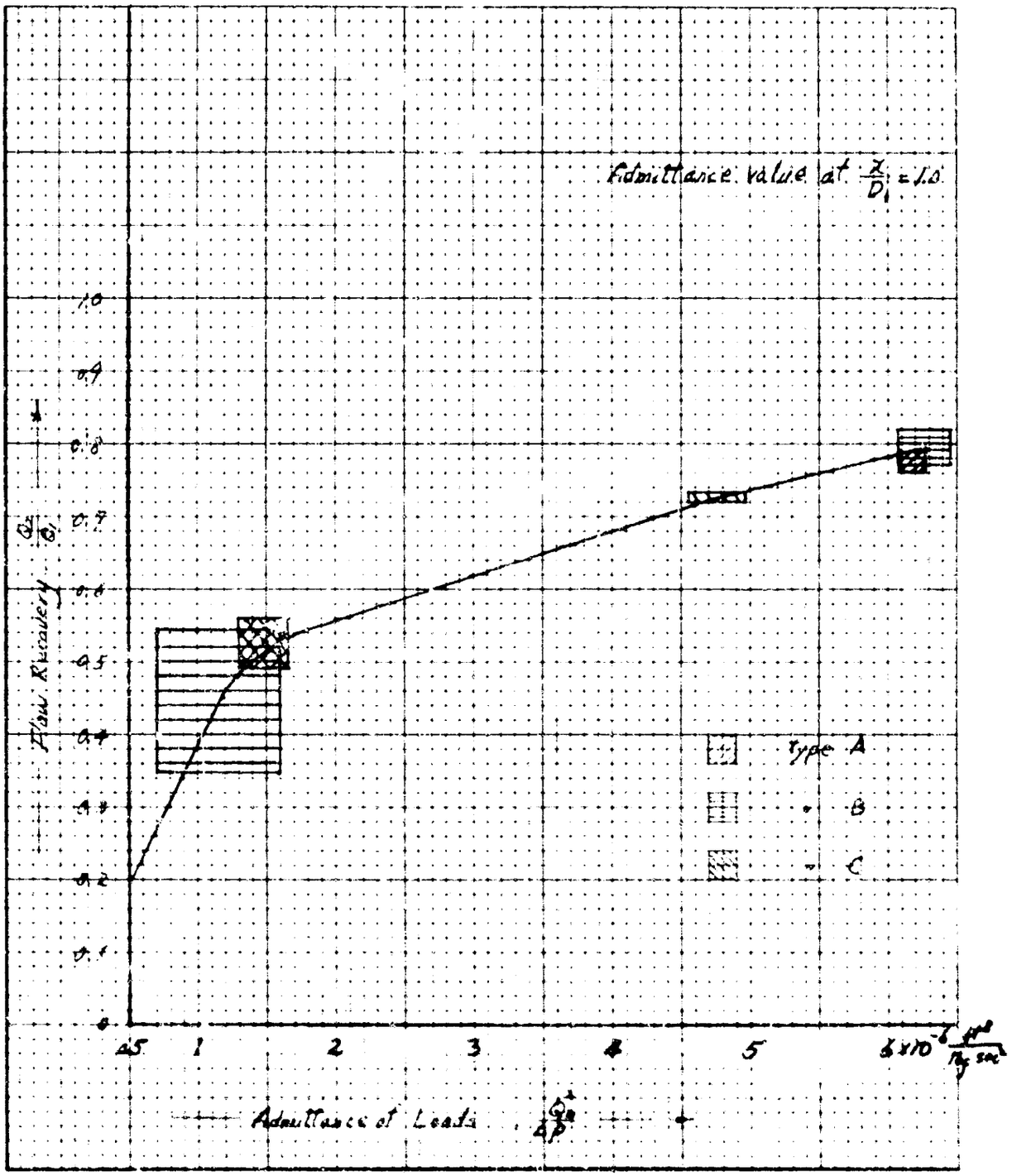

Figure B-8. Flow recovery of the isolator with respect to the admittance of loads.

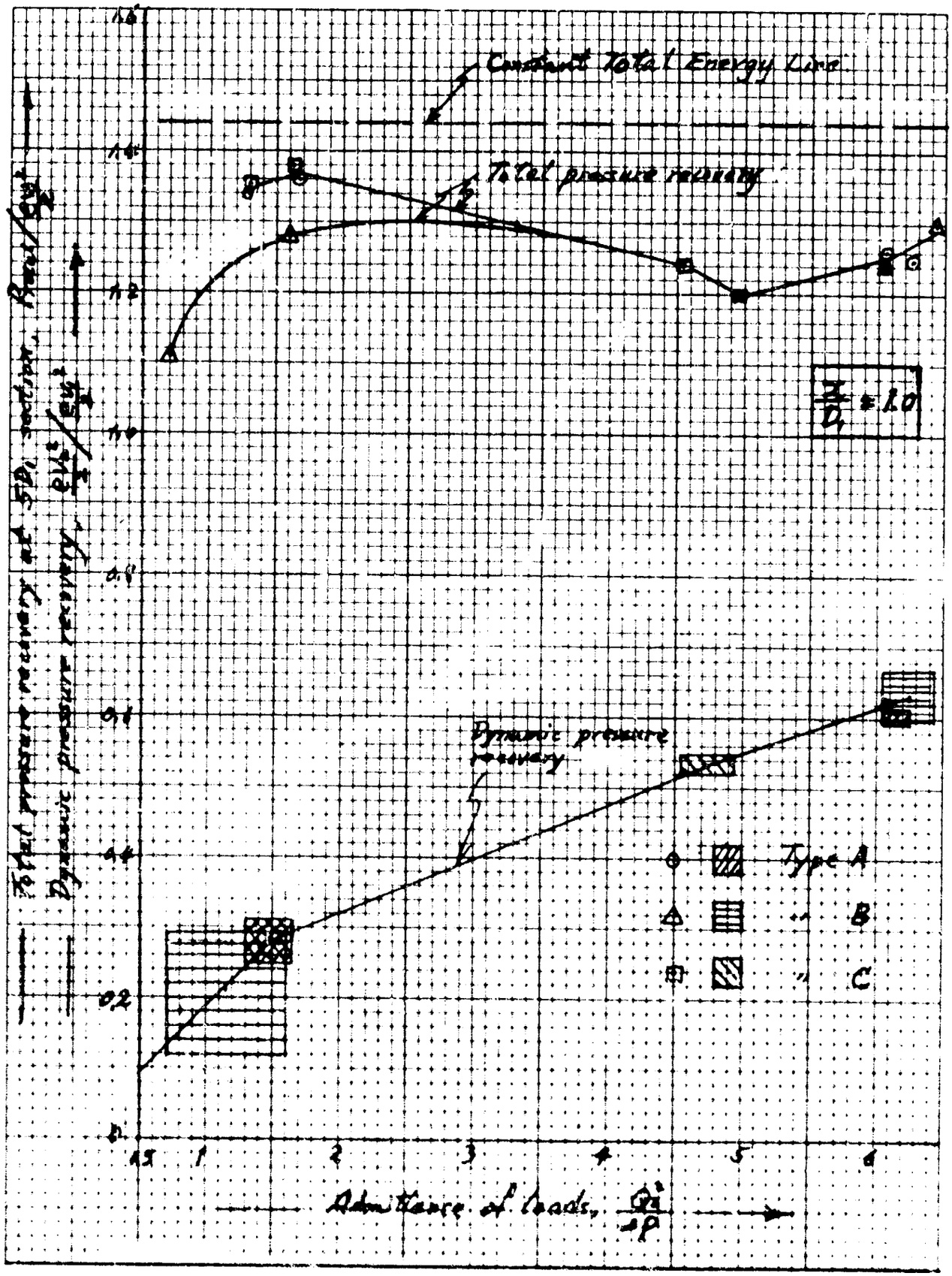

Figure B-9. Total and dynamic pressure recoveries with respect to the admittance of loads for $X/D_1 = 1$.

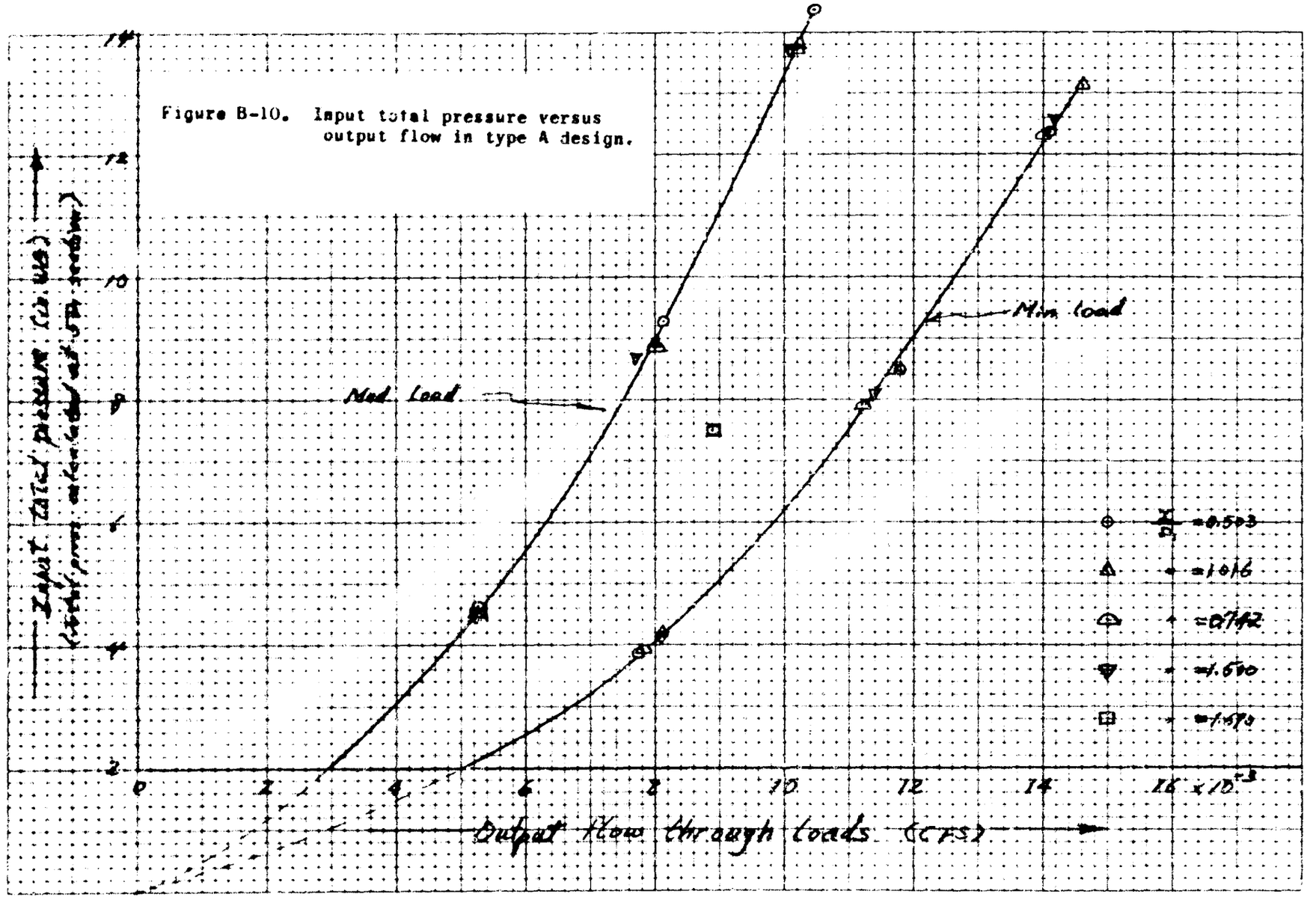

Figure B-10. Input total pressure versus output flow in type A design.

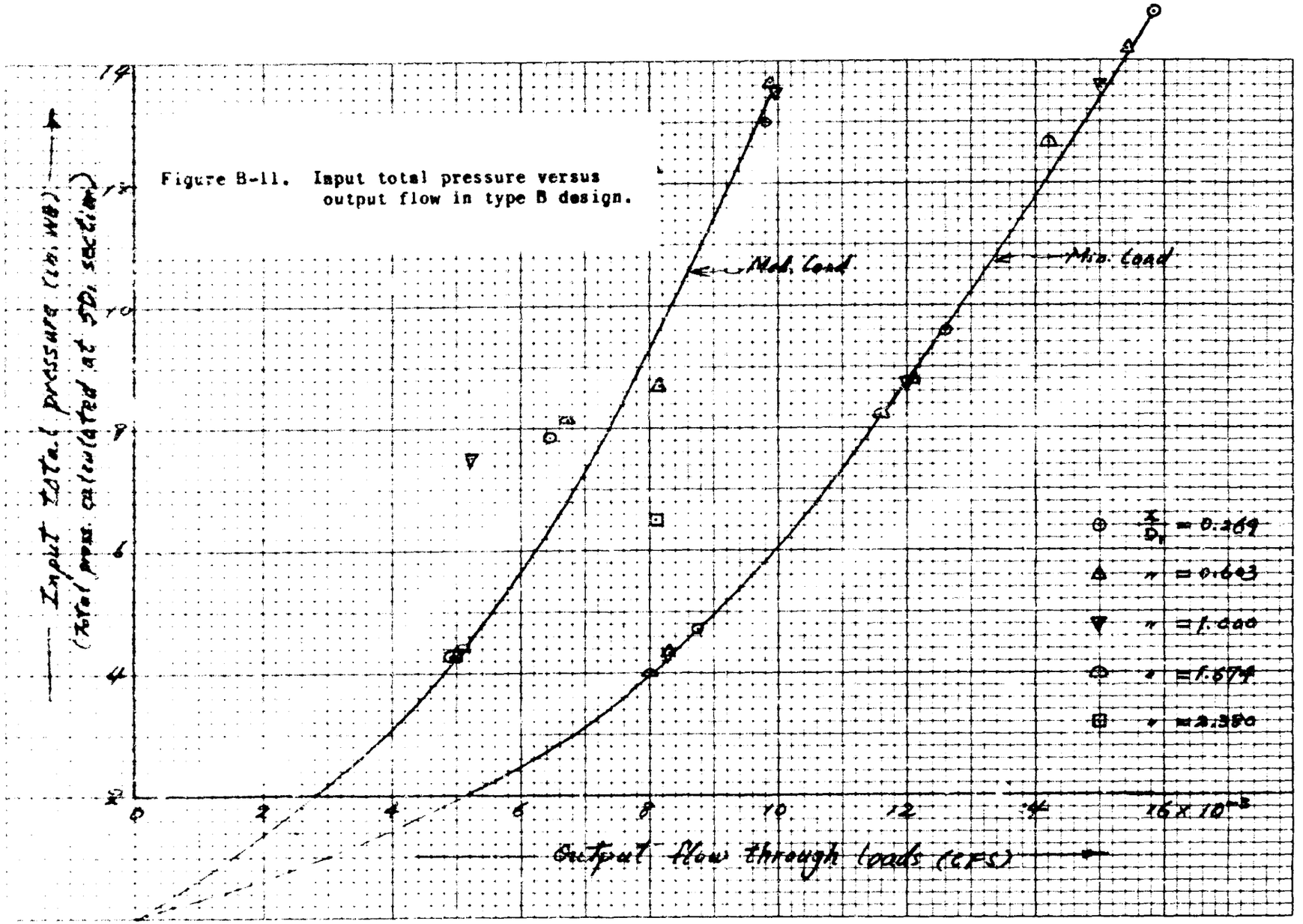

Figure B-11. Input total pressure versus output flow in type B design.

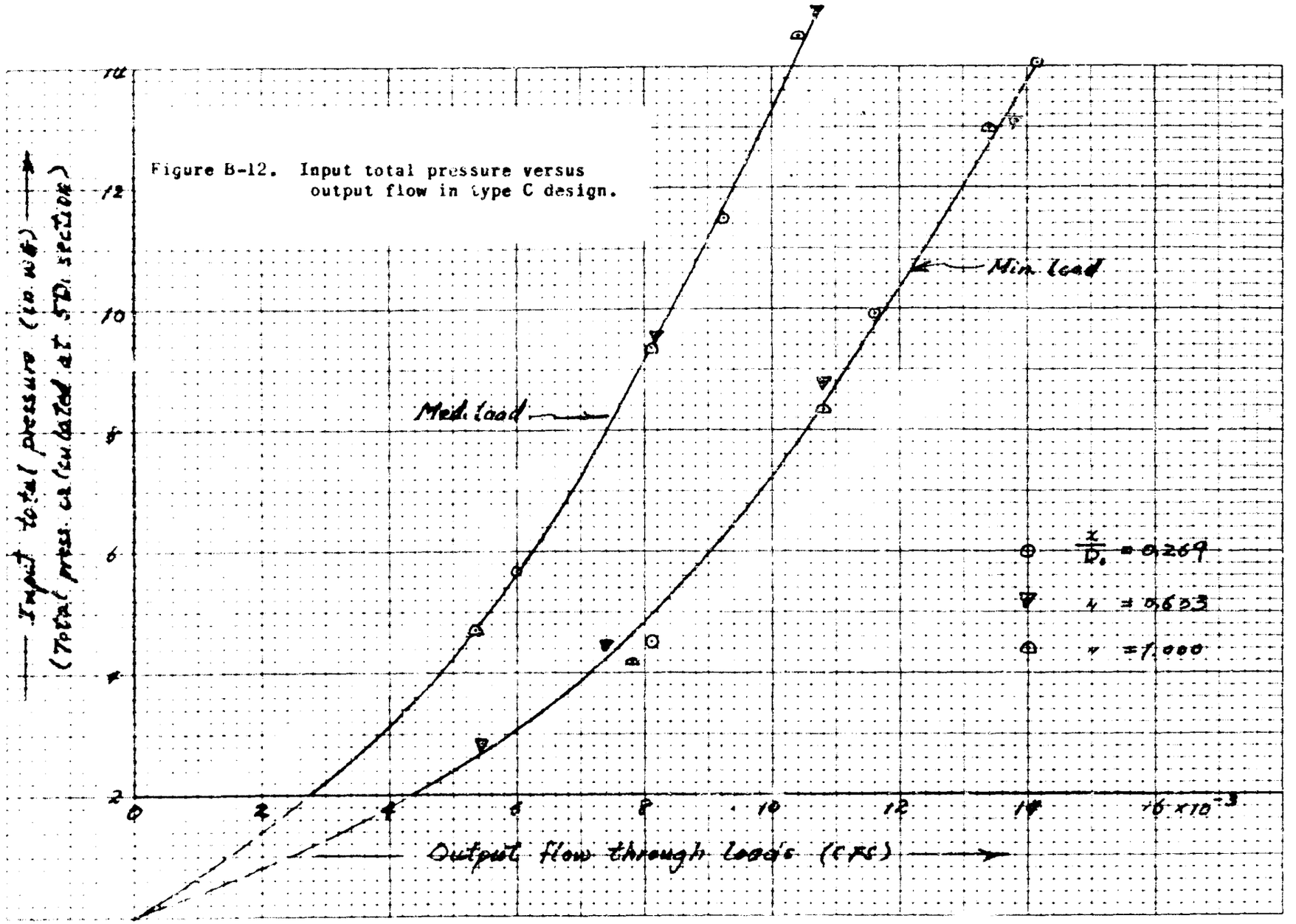

Figure B-12. Input total pressure versus output flow in type C design.

APPENDIX C.—STEADY-STATE CIRCUIT THEORY

T. D. Reader

I L L U S T R A T I O N S

APPENDIX C.—STEADY-STATE CIRCUIT THEORY

1. GENERAL DESCRIPTION OF HDL FLIP-FLOP

The design of all fluid circuits used to perform logical functions requires that under conditions of constant input each element in the circuit shall produce a constant output. Steady-state operation of a circuit involves a study analogous to steady-state direct-current theory in electronics, where even before the transient response is considered, the D.C. levels must be calculated, and suitable resistors used to ensure that all steady-state conditions are met.

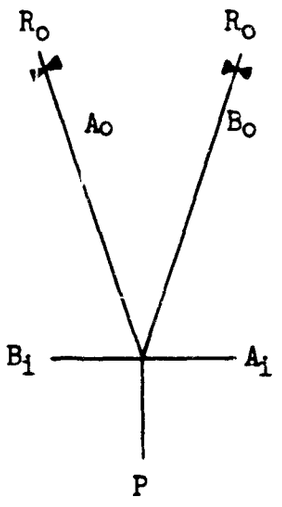

Figure C-1. Diagram showing operation of HDL flip-flop.

The HDL flip-flop was the active element in a binary counter circuit employing delay lines and AND gates. Figure C-1 shows the flip-flop with equal orifice resistances placed on its output channels A_o and B_o. A signal applied at A_i causes a flow to switch from output B_o to output A_o. Conversely, a signal applied at B_i causes an output flow to switch from output A_o to output B_o.

Experiments have shown that the sensitivity of the flip-flop depends on the output resistance loads R_o. A larger resistance, corresponding to a smaller orifice, attached to each output leg of the flip-flop results in a reduced flow from one leg and reduced entrainment by the other leg. As the resistance R_o is increased the flip-flop becomes more sensitive to a switching signal, and the pressure gain improves.

When a certain critical value of R_o is reached the flip-flop becomes unstable and oscillates even in the absence of an input signal.

2. THE EQUIVALENT AREA OF ORIFICES

A useful concept in determining the value of an orifice is the equivalent area of the orifice. This is given by A in the expression:

$$q = A\sqrt{\frac{2p}{\rho}}$$

Where:		
	q is the measured flow in	in^3/sec
	A is the equivalent area of orifice in	in^2
	p is the total pressure drop across the orifice in	$lb./in^2$
	ρ is the density of the fluid in	$lb.\ sec^2/in^4$

The equivalent area specified in this manner is independent of the fluid or the operating pressure used, and furnishes a meaningful figure of admittance for the orifice.

3. CIRCUITS CONSISTING OF ORIFICES ONLY

All steady-state fluid circuits may be reduced to:

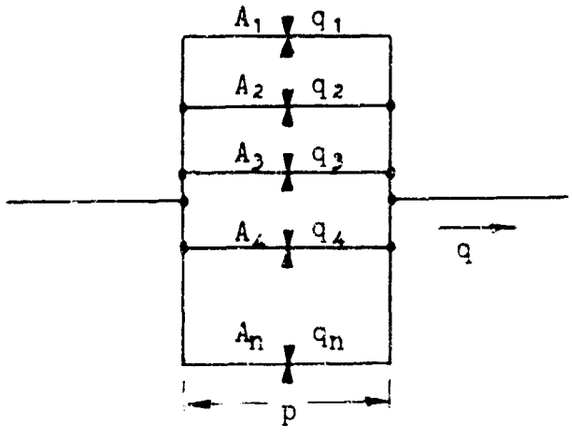

Figure C-2. Orifices connected in parallel.

Referring to figure C-2,

$$q = q_1 + q_2 + q_3 + \ldots + q_n$$

$$A\sqrt{\frac{2p}{\rho}} = A_1\sqrt{\frac{2p}{\rho}} + A_2\sqrt{\frac{2p}{\rho}} + A_3\sqrt{\frac{2p}{\rho}} + \ldots + A_n\sqrt{\frac{2p}{\rho}}$$

$$A\sqrt{\frac{2p}{\rho}} = \sqrt{\frac{2p}{\rho}}\left(A_1 + A_2 + A_3 + \ldots + A_n\right)$$

Thus, the equivalent area A for orifices A_1, A_2, $A_3 \ldots A_n$ (fig. C-3) connected in parallel is given by:

$$A_{parallel} = A_1 + A_2 + A_3 + \ldots + A_n$$

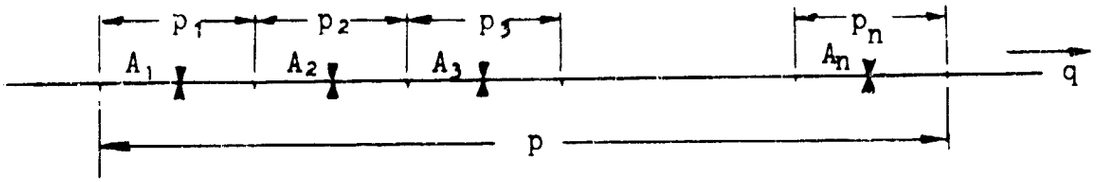

Figure C-3. Orifices connected in series.

Referring to figure C-3,

$$p = p_1 + p_2 + p_3 + \ldots + p_n \qquad (1)$$

Since,

$$q = A\sqrt{\frac{2p}{\rho}}$$

$$p = \frac{1}{A^2}\,\frac{\rho q^2}{2} \qquad (2)$$

Similarly,

$$p_1 = \frac{1}{A_1^2}\,\frac{\rho q^2}{2}$$

$$p_2 = \frac{1}{A_2^2}\,\frac{\rho q^2}{2}$$

$$p_n = \frac{1}{A_n^2}\,\frac{\rho q^2}{2} \qquad (3)$$

Substituting for pressure the expressions (2) and (3), we obtain

$$\frac{1}{A^2}\,\frac{\rho q^2}{2} = \frac{1}{A_1^2}\,\frac{\rho q^2}{2} + \frac{1}{A_2^2}\,\frac{\rho q^2}{2} + \frac{1}{A_3^2}\,\frac{\rho q^2}{2} + \ldots \frac{1}{A_n^2}\,\frac{\rho q^2}{2}$$

$$\therefore \quad \frac{1}{A^2} = \frac{1}{A_1^2} + \frac{1}{A_2^2} + \frac{1}{A_3^2} + \ldots + \frac{1}{A_n^2}$$

Thus, we have the following useful relationships for orifices connected in parallel and in series:

$$A_{parallel} = A_1 + A_2 + A_3 + \ldots + A_n$$

$$\frac{1}{(A_{series})^2} = \frac{1}{A_1^2} + \frac{1}{A_2^2} + \frac{1}{A_3^2} + \ldots + \frac{1}{A_n^2}$$

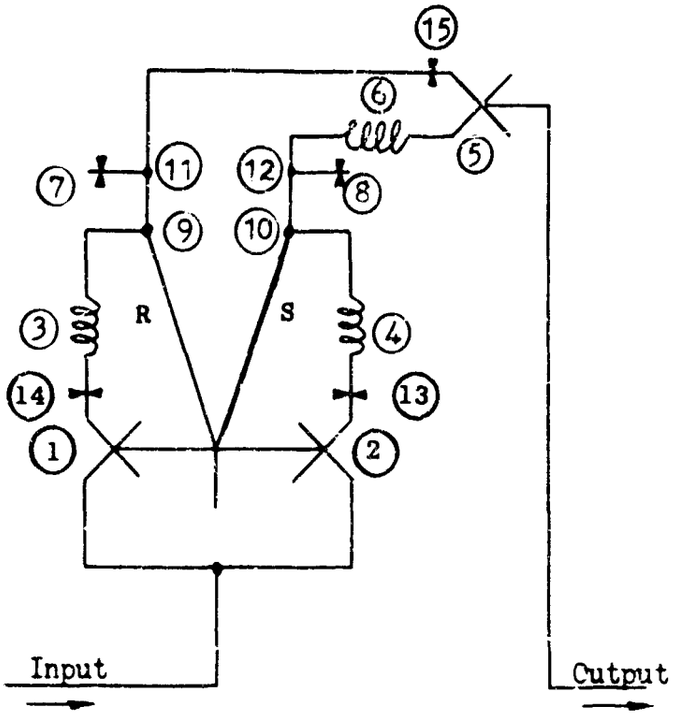

Figure C-4. Diagram of binary counter circuit.

A single stage of the three-stage binary counter circuit is shown in figure C-4.

The input line receives a signal from the pulse former of the previous stage. This pulse is gated with a level at one of the two AND gates (1) or (2) depending on the existing state of the flip-flop.

If the flip-flop is in the reset condition, such that there is flow from the left hand output, then the level at AND gate (1) will permit the input pulse to switch the flip-flop to its SET condition. At the instant the flip-flop was being set the input pulse arriving at AND gate (2) was blocked because the other input to that gate was low. However, on being set, the flip-flop starts sending a signal along delay (4) but by the time this signal reaches AND gate (2) the input pulse has gone. The flip-flop will not be reset until the next input pulse is received, at which time AND gate (2) will admit the pulse while AND gate (1) will be closed.

Delays (3) and (4) therefore serve to hold up the output signal at the AND gates (1) and (2) until the input pulse has passed.

The pulse forming AND gate (5) permits a pulse to be generated only at the instant when its inputs coincide. Since the output from the set side S of the flip-flop is held up by the delay, the inputs

to AND gate (5) will not be exactly of opposite phase. Thus, there will be a period, equal to the delay produced by (6) during which both inputs to the AND gate will be high and the AND gate will generate a pulse.

It can be seen from figure C-4 that the output from each flip-flop must be admitted by two AND gates in series in order to switch the next flip-flop. Tests have shown that the pressure recovery from an AND gate whose output is required to drive two AND gates is approximately 50 percent, while the pressure recovery from an AND gate whose output is required to switch a flip-flop is approximately 60 percent. Thus the control pressure at the input to each flip-flop can be expected to be of the order $0.5 \times 0.6 \times 100$ percent , or 30 percent of the available output pressure.

4. SELECTION OF EQUIVALENT AREA TO BE USED ON NOL FLIP-FLOP FOR RELIABLE OPERATION

Tests carried out on nine flip-flops of power nozzle width 0.030 in. showed that a pressure gain of better than 6:1 could be obtained from five of them, when an orifice of equivalent area equal to 0.00414 sq in. was used. It was felt that since the required gain for marginal operation was a little over 3:1, a gain of 6:1 would result in reliable operation. An equivalent area equal to 0.00414 in. was therefore selected for the output load of each side of the flip-flop, and the bleeds (7) and (8), shown in figure C-4 were calculated to provide this effective orifice area when taken in conjunction with the remainder of the circuit.

The equivalent areas of all delay lines, flow dividers and AND gates were obtained by experiment, and are shown in the following table:

Table I. Calculation of the Orifice Diameters in the Counter Circuit.

Element (see figure C-4)	Equivalent Area
AND gates (1) (2) (5)	1.484×10^{-3} in.^{2}
Delay (6)	3.93×10^{-3} in.^{2}
Delays (3) (4)	4.92×10^{-3} in.^{2}
Flow Dividers (9) (10)	8.34×10^{-3} in.^{2} at each output
Bleeds T's (11) (12)	13.1×10^{-3} in.^{2} straight through 9.1×10^{-3} in.^{2} right angle turn

The values of the equivalent orifice areas for the different elements on the set output S of the flip-flop are shown in figure C-5.

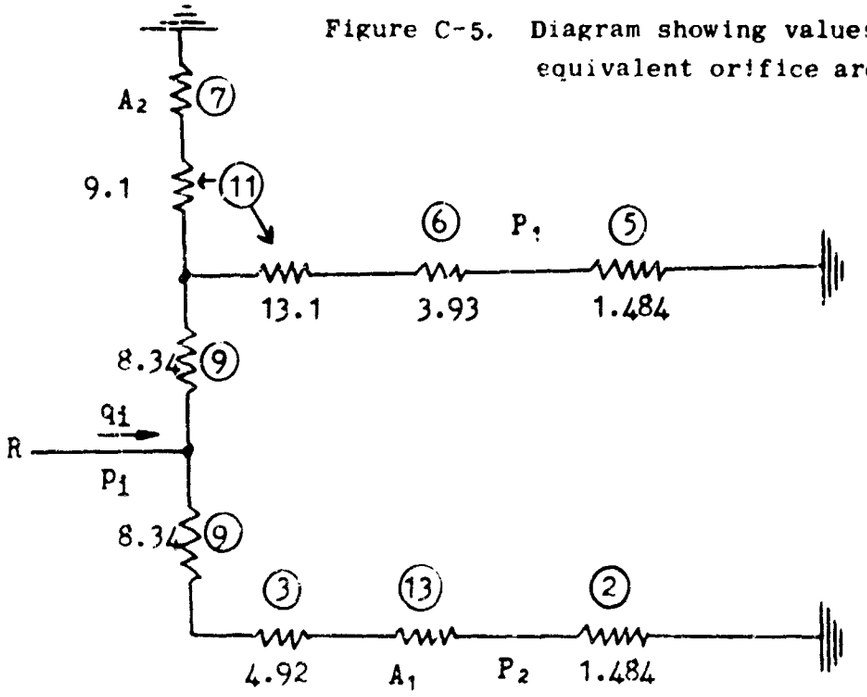

Figure C-5. Diagram showing values of equivalent orifice areas.

Note: All areas are multiplied by 10^{-3}

The resistance A_1 is calculated to give a pressure drop such that the two inputs to AND gate (2), figure C-4, are equal when high. To calculate A_1 it is necessary to satisfy the condition that the input pressure to AND gate (2). Figure C-4 is equal to the output pressure from AND gate (5).

Since the output pressure from AND gate (5) is 50 percent of the input pressure we may calculate A_1 and A_2 in the network shown in figure C-5 by satisfying the following two conditions simultaneously:

(1) The pressure p_2 is 50 percent of the pressure p_1.

(2) The network has an admittance equal to that of an orifice of equivalent area 4.14×10^{-3} sq in.

Figure C-5 may be simplified as shown in figure C-6.

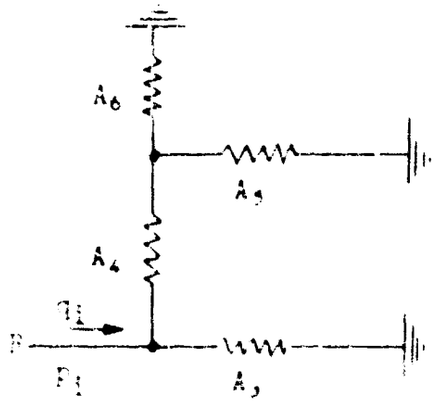

Figure C-6. Simplified diagram of figure C-5.

Where:

$$\frac{1}{A_3^2} = \frac{1}{8.34^2} + \frac{1}{4.92^2} + \frac{1}{A_1^2} + \frac{1}{1.484^2}$$

$$A_4 = 8.34$$

$$\frac{1}{A_5^2} = \frac{1}{13.1^2} + \frac{1}{3.93^2} + \frac{1}{1.484^2}$$

$$\therefore \quad A_5 = 1.381$$

$$\frac{1}{A_6^2} = \frac{1}{9.1^2} + \frac{1}{A_2^2}$$

where A_3 and A_6 become the two unknowns.

A_3 and A_6 may now be determined from the equations:

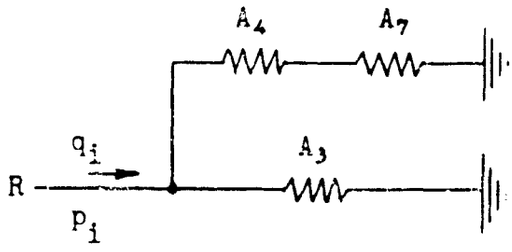

$$A_7 = A_5 + A_6$$

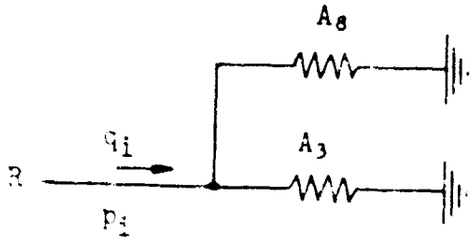

$$\frac{1}{A_8^2} = \frac{1}{A_4^2} + \frac{1}{A_7^2}$$

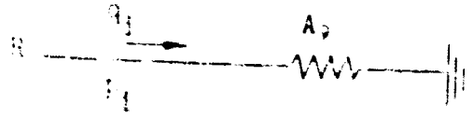

$$A_2 = A_8 + A_3 = 4.14$$

Solving these equations we obtain:

$A_1 = 1.89 \times 10^{-3}$ sq in.

$A_2 = 2.002 \times 10^{-3}$ sq in.

Referring again to figure C-4, the two pressure levels at the inputs of AND gate (5) were to be made equal when high. It was therefore necessary to place an orifice at (14) such that its equivalent area was equal to that of the delay tubing (6).

Having obtained the equivalent areas of the orfices to be placed at positions (7), (8), (13), (14), and (15), results of tests carried out on orifices of different sizes were used to derive the actual orifice diameters. These diameters are shown in the following table:

Orifice Position	Orifice Diameter (in)
Bleed (7)	0.061
Bleed (8)	0.061
Restrictor (13)	0.057
Restrictor (14)	0.057
Restrictor (15)	0.079

A 3-stage counter was then built using the dimensions for bleeds and restrictors shown in table I. The counter operated as predicted, thus confirming the method of obtaining the values for bleeds and restrictors described above.

APPENDIX D.—SWITCHING TESTS

T. F. Chen

ILLUSTRATIONS

Figure

APPENDIX D.—SWITCHING TESTS

1. INTRODUCTION

An equivalent electronic circuit can be drawn for the pneumatic counter circuit under investigation, so that electronic circuit analysis can be adapted conveniently to predict the performance of the pneumatic counter circuit. The flip-flop is considered as a "black Box" in this approach; only the input and output relationships are required, regardless of the exact switching mechanism within this black box. It is toward this end that the following switching test was designed and carried out.

2. DESIGN OF THE SWITCHING TEST ON THE 0.030 IN. SIZE (0.030 IN. X 0.090 IN. POWER NOZZLE)

The switching test consists of two major parts; the test arrangements for each part are shown schematically in figures D-1 and D-2. In each figure, the black box is shown to contain a flip-flop and an extra length of tubing for interconnection. The gap between the control jet nozzle and entrance to the black box was kept constant at 0.737 in. This gap is to be considered as a parameter in describing the input to the black box, since the signal received at the entrance to the black box varies with respect to the gap size. (See Apx B, Isolator Study.) Thus, the total pressure of control jet P_c, the angular speed of the rotating disc ω and the gap size would be sufficient to characterize the input signal.

The first part of this report describes the test results in which the minimum total pressure of the control jet P_c necessary to switch the power jet (not repeatedly but only once) is characterized by the parameters ω (wheel speed) and τ (pulse width). Since the test arrangement as shown in figure D-1 provides a train of pulses rather than a single pulse, it was impossible to avoid the interaction of the successive pulses in the train in this "single-switching test." In order to be consistent through the test, a pulse train which switched the power jet within 5 seconds after the application of the pulse train was considered as the minimum total pressure of control jet necessary. This consideration is not necessary in the dynamic switching test in which the power jet was switched back and forth continuously. The power jet flow was kept constant throughout the entire tests. It was calculated from a convenient power jet average velocity of 250 fps. The output pulse form was of no concern in the single switching test, therefore, it was not measured.

In the second part of this report, the result of the dynamic switching test is presented. In addition to the test arrangement as shown in figure D-1, oscillocopes, hot-wire probes and pressure pickup were used. Figure D-2 shows the entire test arrangement.

2.1 Description of Single Switching Test

The variables considered in the test were:

(1) Independent Variables

(a) Power Jet Flow Q_1 (or P_1)	Test was done for $Q_1 = 4.67 \times 10^{-3}$ CFS (V_1 = 250 fps) only.
(b) Load on the flip-flop outputs	Test was done with no load and with 0.084 in. orifice at flip-flop outputs.
(c) Pulse width, τ	Pulse width was varied by both the angular velocity of the disc ω and the length of the slots θ (the angle that the radial lines connecting the center of disc and edges of slot makes). Test was done with ω ranging from 0 to 65 revolutions per second, and θ for 10, 20, and 45 degrees.

(2) Dependent Variables

(a) Minimum total pressure of control jet P_c

The test was designed to obtain the minimum total pressure of control jet P_c to switch the power jet in a fixed length of time (in 5 seconds here) at various θ and ω (or τ) values.

2.2 Results of Single Switching Test

In figure D-3 the minimum total pressure of control jet P_c is plotted against the angular velocity of the disc ω for three different discs with 10-, 20-, and 45-degree slots. Increase in ω required higher value of P_c. Also shorter slot required higher P_c.

Figure D-4 was reduced from figure D-3. Reading from figure D-3 the values of P_c at ω values of 10, 30, and 50 revolutions per second and plotting the relationship between P_c and τ, we find that the points fall on a single curve as shown in figure D-4.

When the flip-flop was loaded with 0.084 in. orifices at the outputs, the minimum total pressure P_c required to switch the power jet was reduced slightly except at small values of τ. This is shown in figure D-5 in which P_c versus τ for both loaded and unloaded conditions are plotted for comparison.

2.3 Description of Dynamic Switching Test

The variables considered in the test were:

(1) Independent Variables

(a) Power jet flow Q_1 (or P_1)	Test was done for $Q_1 = 4.67 \times 10^{-3}$ CFS (V_1 =250 fps)only.
(b) Load on the flip-flop outputs	Test was done with no load and with 0.084 in. orifices at flip-flop outputs.
(c) Pulse width, τ	Pulse width was varied by varying the wheel speed of the 10-degree disc.

(2) Dependent Variables

(a) Minimum total pressure of control jet P_c.

(b) Characteristics of the output signals of the black box.

The transient part of the output signal can be described by its delay time, rise time, and the shape of the leading edge.

The steady state part of the output signal is described by its amplitude.

The test arrangement is shown in figure D-2. The traces on the oscilloscopes were recorded with a Polaroid camera so that all dependent variables described above could be determined from these photographs.

2.4 Results of Dynamic Switching Test

Three sets of photographs were taken at values of τ equal to 0.89, 4.00, and 7.45 msec. In the 4.00-msec set, the flip-flop outputs were loaded with 0.084-in. orifices to see the change in the output characteristics. Also, the hot-wire probes were placed upstream and downstream of the orifice load. In short, we have three sets of photographs obtained under the following test conditions:

Set 1 τ = 0.89 msec, unloaded

Set 2 τ = 4.00 msec, unloaded, and loaded (hot wire placed upstream and downstream of orifice load).

Set 3 τ = 7.45 msec, unloaded

In each set we have taken three photographs showing:

(1) The power jet being switched back and forth cleanly,

(2) A complete cycle of the traces, and

(3) The magnified transient portion of the traces.

The first two photographs were taken for the purpose of supporting the third photograph in order to be sure that each set of photographs was taken under the same dynamic test conditions. The measurements can be taken solely from the third photograph, and therefore only the third photographs in each set are presented in the following pages.

3. CONCLUSION

The input and output relationships described in the previous photographs showed quite different characteristics depending on the input signal to the black box as well as the point of measurement of the output from the black box. The photographs serve to indicate the general types of variation of the input and output relationships; the corresponding electronic circuit may be drawn to give these characteristics.

As the need for more extensive data arises the test scheme described in this report can be used to provide this information.

1st Set

τ = 0.89 msec, unloaded

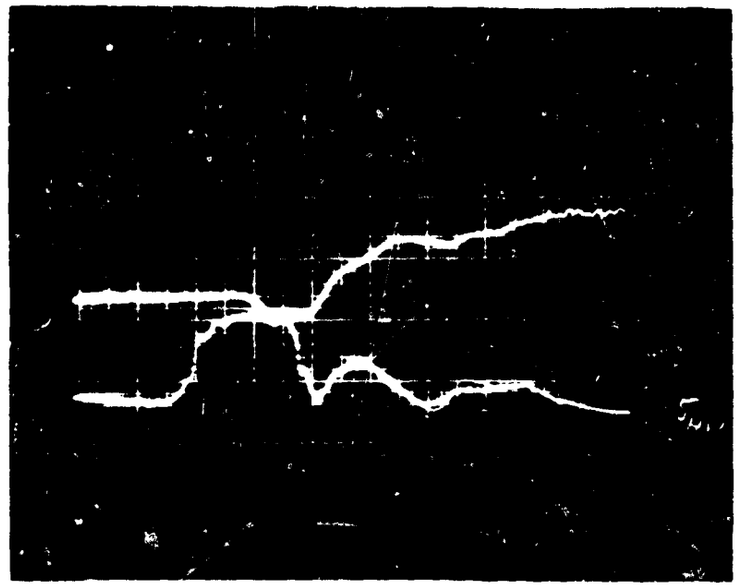

Upper trace: Output 3, Time scale 0.5 msec/cm
Ampt. scale 0.2 v/cm

Lower trace: Input 5 Time scale 0.5 msec/cm
Ampt scale 2.0 v/cm

Power jet flow Q_1 = 0.00467 CFS (V_1 = 250 fps).

10-deg disc, rotating at ω = 31.2 rps.

Peak value of input velocity reduced from hot-wire probe at 5 (lower trace) was 108 fps.

Minimum total pressure of control jet = 29.15 in. WG.

2nd Set

τ = 4.00 msec, loaded, hot-wire at downstream of orifice.

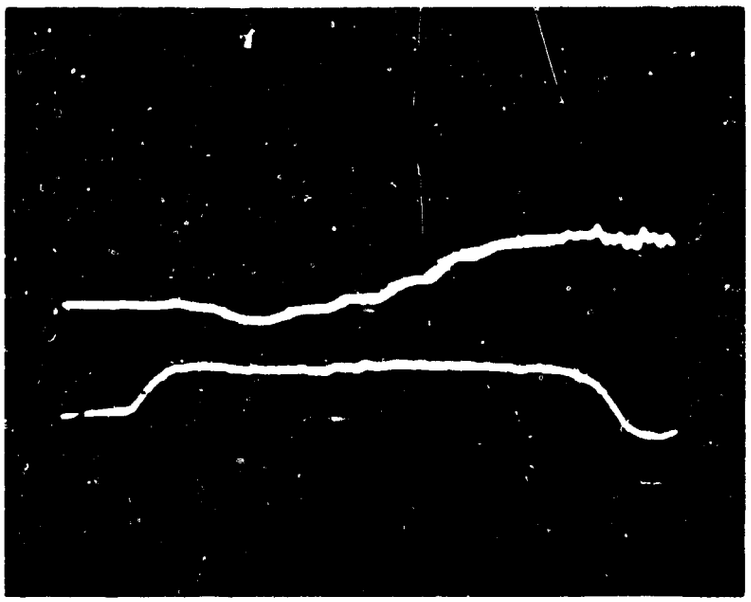

Upper trace: Output 3, Time scale 0.5 msec/cm
Ampt scale 0.5 v/cm

Lower trace: Input 5, Time scale 0.5 msec/cm
Ampt scale 2.0 v/cm

Power jet flow Q_1 = 0.00467 CFS (V_1 = 250 fps).

10-deg disc, rotating at ω = 6.55 rps.

Peak value of input velocity reduced from hot-wire probe at 5 (lower) was 37 fps.

Minimum total pressure of control jet = 10.7 in. WG.

2nd Set

τ = 4.00 msec, loaded, hot-wire at downstrean of orifice

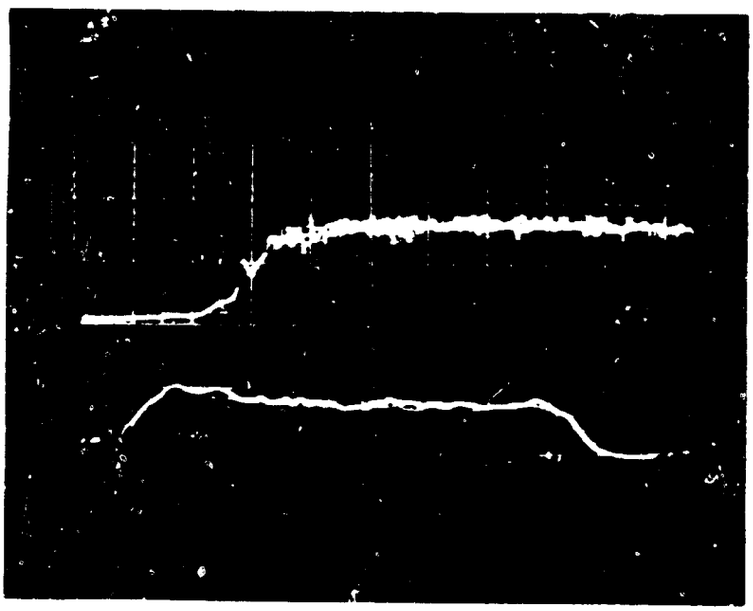

Upper trace: Output 3, Time scale 0.5 msec/cm
Ampt scale 0.2 v/cm

Lower trace: Input 5, Time scale 0.5 msec/cm
Ampt scale 0.1 v/cm

Power jet flow Q_1 = 0.00467 CFS (V_1 = 250 fps).

10-deg disc, rotating at ω = 6.95 rps.

Peak value of input velocity reduced from hot-wire probe at 5 (lower trace) was 37 fps.

Minimum total pressure of control jet = 11.1 in. WG.

2nd Set

τ = 4.00 msec, loaded, hot-wire at upstream of orifice

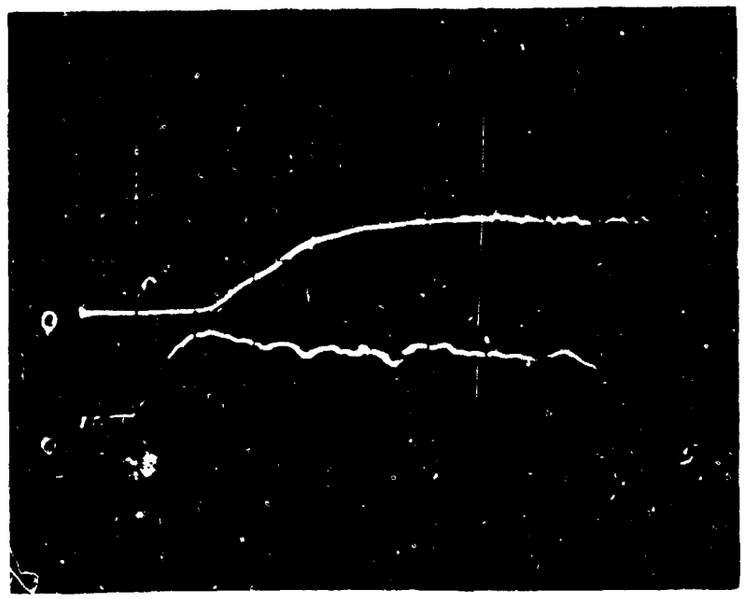

Upper trace: Output 3, Time scale 0.5 msec/cm
Ampt scale 0.2 v/cm

Lower trace: Input 5, Time scale 0.5 msec/cm
Ampt scale 0.1 v/cm

Power jet flow Q_1 = 0.00467 CFS (V_1 = 250 fps).

10-deg disc, rotating at ω = 6.95 rps.

Peak value of input velocity reduced from hot-wire probe at 5 (lower trace) was 55 fps.

Minimum total pressure of control jet = 11.1 in. WG.

3rd Set

τ = 7.45 msec, unloaded

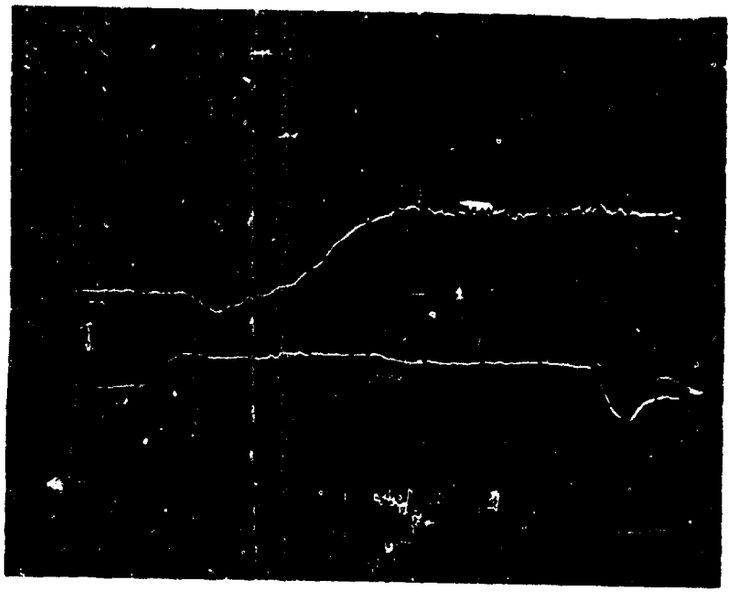

Upper trace: Output 3, Time scale 1.0 msec/cm
Ampt scale 0.2 v/cm

Lower trace: Input 5, Time scale 1.0 msec/cm
Ampt scale 2.0 v/cm

Power jet flow Q_1 = 0.00467 CFS (V_1 = 250 fps).

10-deg disc, rotating at ω = 3.73 rps.
at 5 (lower trace) was 37 fps.

Minimum total pressure of control jet = 7.5 in. WG.

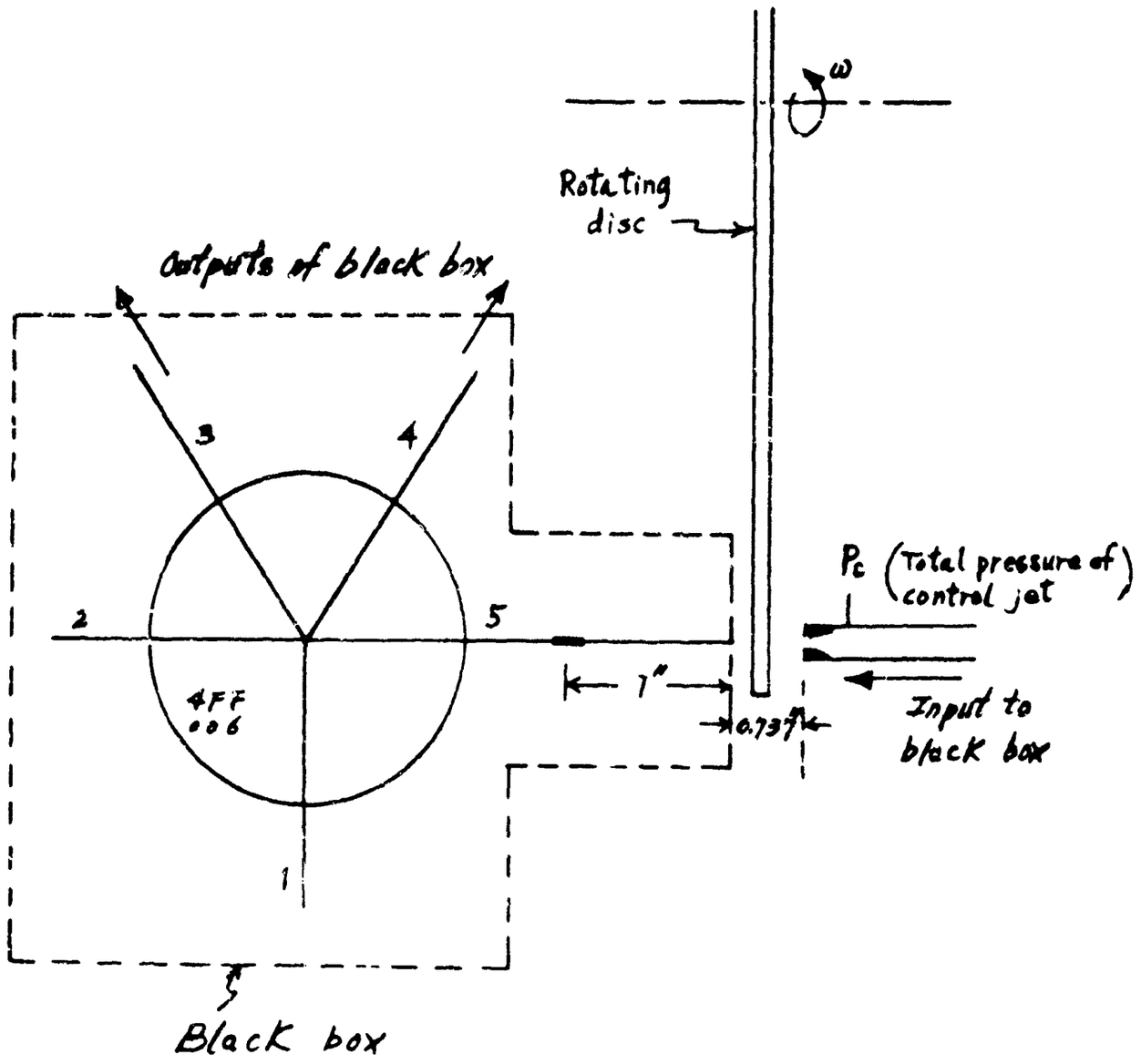

Figure D-1. Arrangement used for the single-switching test.

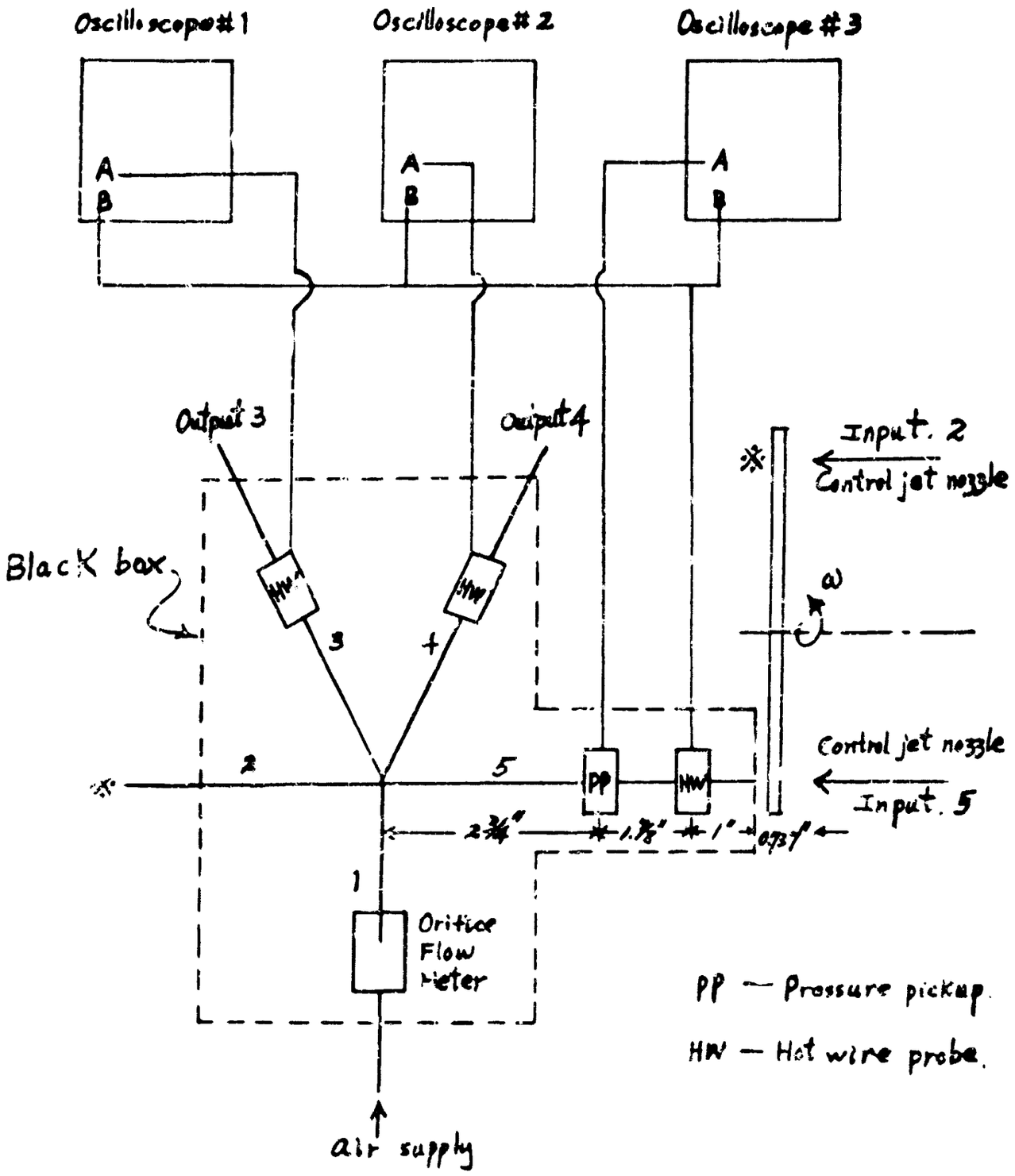

Figure D-2. Arrangement for the dynamic switching test.

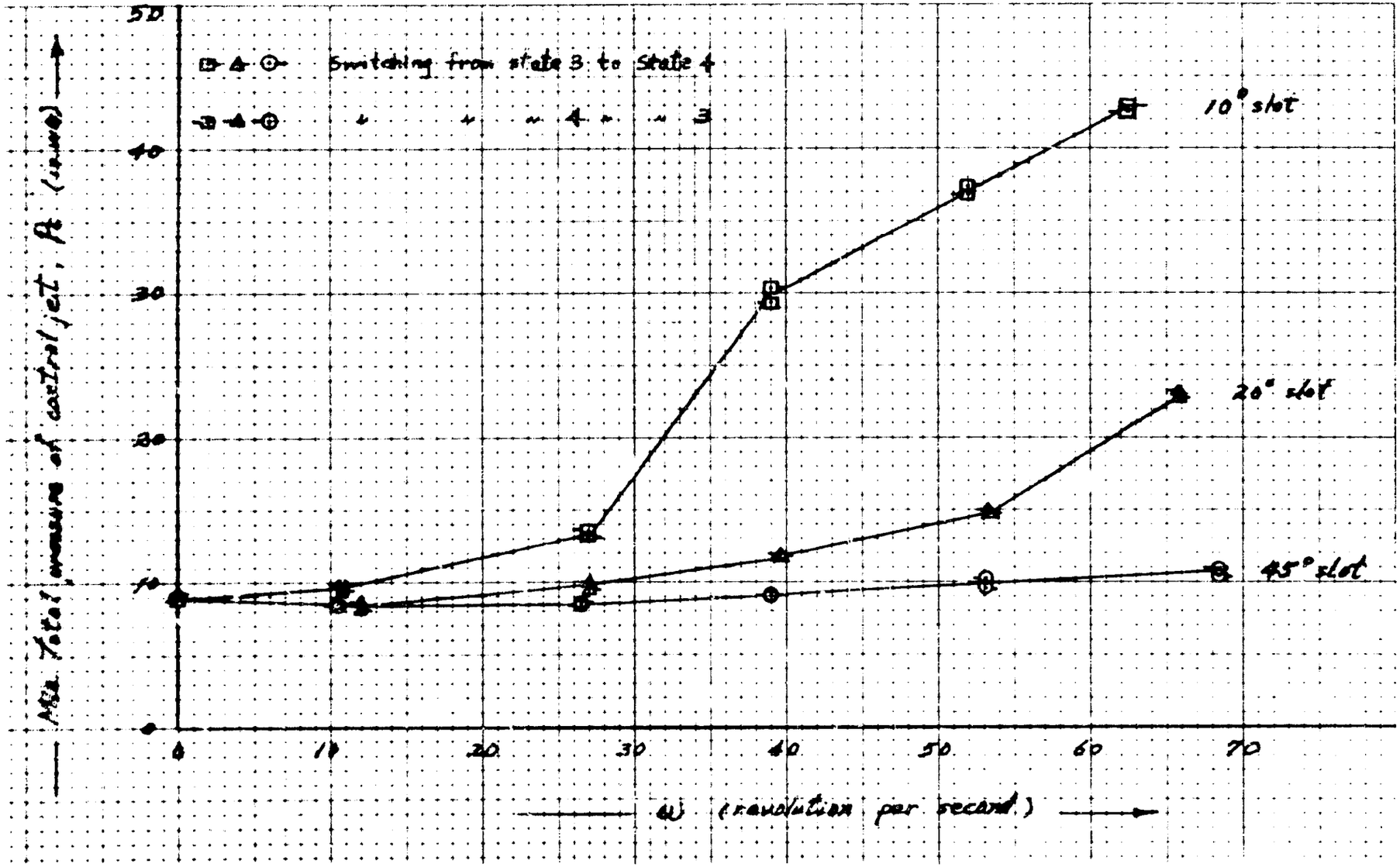
Switching from state 3 to state 4
" " " 4 " " 3
10° slot
20° slot
45° slot
50
40
30
20
10
0
10
20
30
40
50
60
70
Ma, Total pressure of control jet, ft (psia)
ω (revolution per second)

Figure D-3

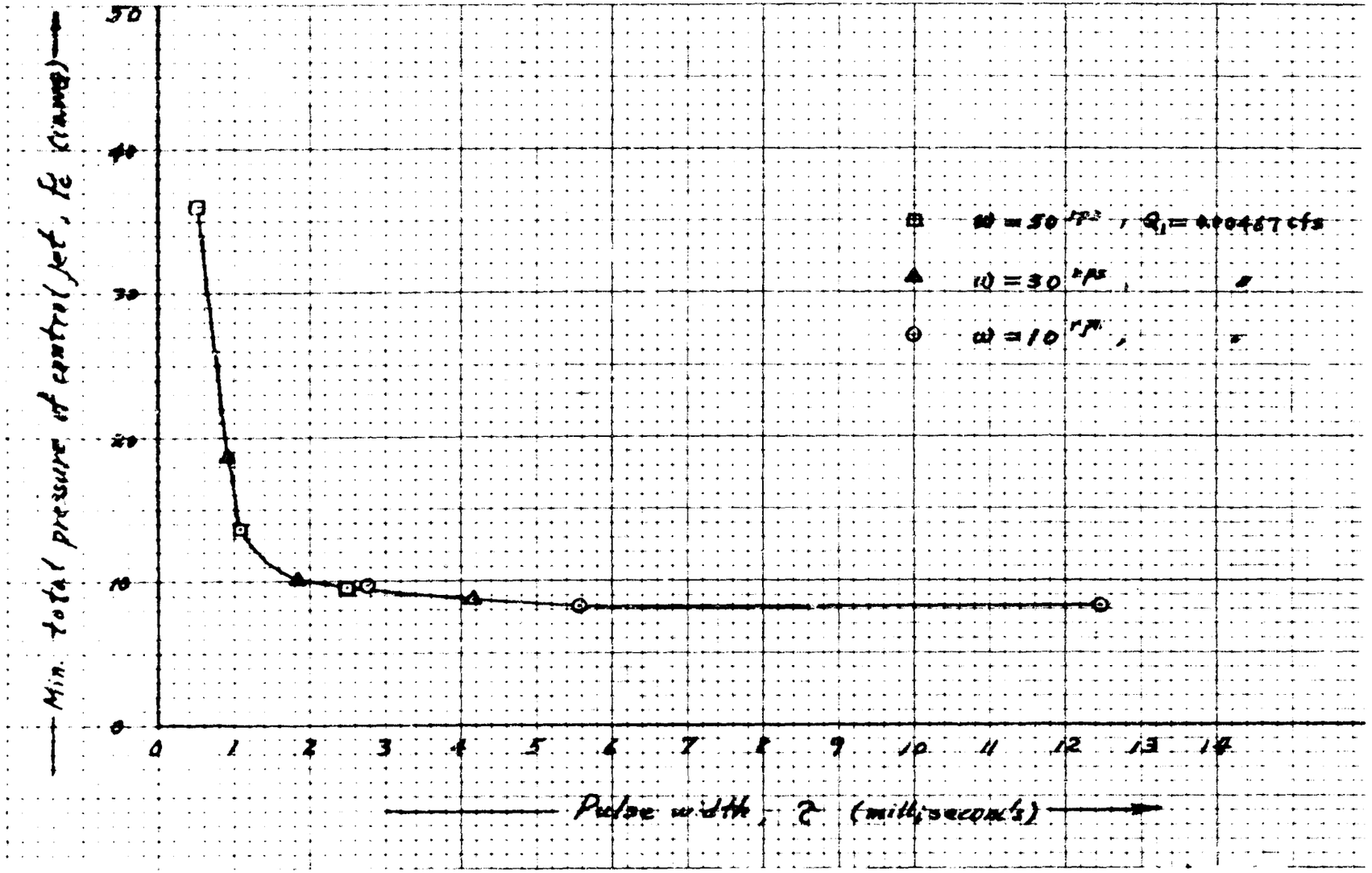
Min. total pressure at control jet, P_c (psia)
50
40
30
20
10
0
0
1
2
3
4
5
6
7
8
9
10
11
12
13
14
Pulse width, τ (milliseconds)
$\omega = 50$ rps, $Q_j = 0.00467$ cfs
$\omega = 30$ rps,
$\omega = 10$ rps,

Figure D-4

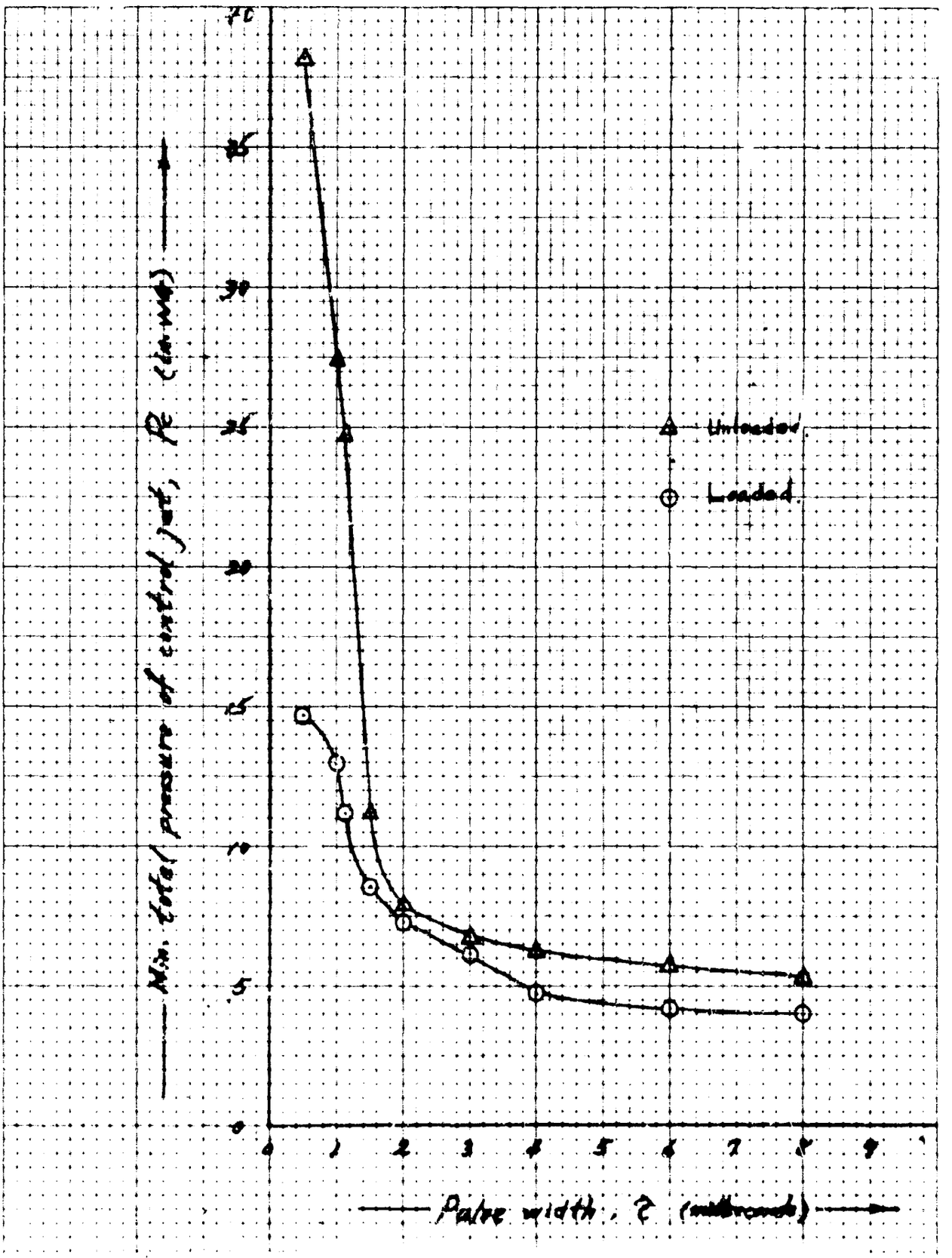

Figure D-5

APPENDIX E.—FLUID CIRCUIT THEORY

T. D. Reader

I L L U S T R A T I O N S

1. SUMMARY

After the development of a satisfactory DC circuit theory for fluid devices, the next logical step is the development of a workable AC fluid circuit theory.

This analysis shows that fluid circuit theory may be treated using the same general approach as electronic circuit theory, provided certain frequency requirements are met. Essentially the approach is to idealize the circuit into linear and nonlinear elements whose response is invariant with respect to frequency, together with linear inductive and capacitive elements. The nonlinear elements are then idealized into piecewise linear elements, and an analytic solution is applied over the linear regions, such that all boundary conditions are satisfied.

2. UNIVAC UNITS AND TERMS

FORCE

It is proposed to use the POUND WEIGHT as the standard unit of force, since this is the unit most commonly used in mechanical engineering.

LENGTH

The manufacturing industry in this country uses the INCH as the standard unit of length, and since our pneumatic devices will eventually be specified in in. for production purposes, it is proposed to use the INCH as the standard of length. This unit is commonly used with the engineering unit of force, the pound.

TIME

The SECOND will be used as the unit of time, since this is almost universally recognized as the standard unit.

The following table shows the units we shall use:

Term	Unit	Name	Abbreviations
Pressure (gauge)	$\frac{lbf}{in.^2}$	psi	p
Flow	$\frac{in.^3}{sec}$	cis	Q
Inductance	$\frac{psi}{(cis/sec)}$	—	
Resistance (linear)	$\frac{psi}{cis}$		
Capacitance	$\frac{cis}{(psi/sec)}$		

3. THE FLUID-ELECTRICAL ANALOG

In deriving the electrical analogs of inductance, resistance, and capacitance it will normally be assumed that flow Q is equivalent to electric current i, and pressure p is equivalent to voltage e. With these assumptions we may formulate the following pairs of relationship:

	ELECTRICAL	PNEUMATIC
Inductance L	$e = L \frac{di}{dt}$	$p = L \frac{dQ}{dt}$
Resistance R	$e = R\, i$	$p = R\, Q$
Capacitance C	$e = \frac{1}{c} \int i\, dt$	$p = \frac{1}{c} \int Q\, dt$

4. FLUID CIRCUIT THEORY

A pneumatic circuit normally consists of a number of active and passive elements with interconnections.

Although most pneumatic elements have essentially nonlinear performance characteristics, there are certain conditions under which the characteristics of some passive elements become close to linear.

When the required conditions prevail we may design circuits consisting of linear pneumatic elements which have characteristics equivalent to the electrical terms: INDUCTANCE, RESISTANCE, and CAPACITANCE.

Fortunately the conditions for linear performance are compatible with the requirements of low power and miniaturization. We shall examine these conditions for the three types of element separately, since some elements require more restrictive conditions than others.

4.1 Inductance L

By definition, we may state the inductance L of a pneumatic line as follows:

$$L = \frac{p}{(\frac{dQ}{dt})}$$

where p is the pressure difference at the ends of the line resulting from a rate of change of flow $\frac{dQ}{dt}$ in the line.

Since air is compressible, the assumption that Newton's Law may be applied to the whole mass of air in a pipe is not strictly valid. However, if the acoustic wave length is long compared with the length of the pipe, and if the changes in pressure are small (say less than one tenth) compared with the absolute pressure, then the assumption of incompressibility may be applied as follows:

Let:

Cross-sectional area of pipe	= A	in.
Length of pipe	= ℓ	in.
Pressure at outlet of pipe	= p_o	lbf/in.^{2}
Pressure at entrance of pipe	= p_1	lbf/in.^{2}
Density of air at pressure p_o	= ρ	lbf/sec^2/in.^{4}
Velocity of air in pipe	= V	in./sec
Flow of air in pipe	= Q	in.^{3}/sec

Then from Newton's Second Law of Motion:

$$A(p_1 - p_o) = \rho(A\ell)\frac{dV}{dt} \quad \text{assuming } \rho_o = \rho$$

$$\therefore \quad p_1 - p = \rho\ell\frac{d}{dt}\left(\frac{Q}{A}\right)$$

$$\therefore \quad \frac{p_1 - p_o}{\left(\frac{dQ}{dt}\right)} = \frac{\rho\ell}{A} \qquad \text{---------- (1)}$$

Equation (1) expresses the pressure difference at the ends of the pipe resulting from unit rate of change of flow. We shall, therefore, define the inductance of a pipe as

$$L = \frac{\rho\ell}{A} \qquad \frac{\text{lbf sec}^2}{\text{in.}^5}$$

4.2 Resistance R

By definition we may state the resistance R of a pneumatic element as follows:

$$R = \frac{\xi}{Q} \qquad \text{---------- (2)}$$

where ρ is the pressure difference across the element resulting from a constant flow Q through the element.

For the resistance of an element as defined by equation (2) to be constant there must be no loss of energy due to turbulence.

An element which satisfies the conditions required for laminar flow will have a constant resistance since the only losses will be those caused by viscosity. Such an element may be designed by stacking thin-walled capillary tubing parallel to the direction of flow of the air:

Let:

Length of each capillary tube	=	l_1	in.
Internal diameter of each capillary tube	=	D	in.
Number of capillary tubes in passage	=	N	
Viscosity of air	=	μ	lbf sec/in.^{2}
Ratio of total area of cross section of tube passages to area of main passage	=	K	

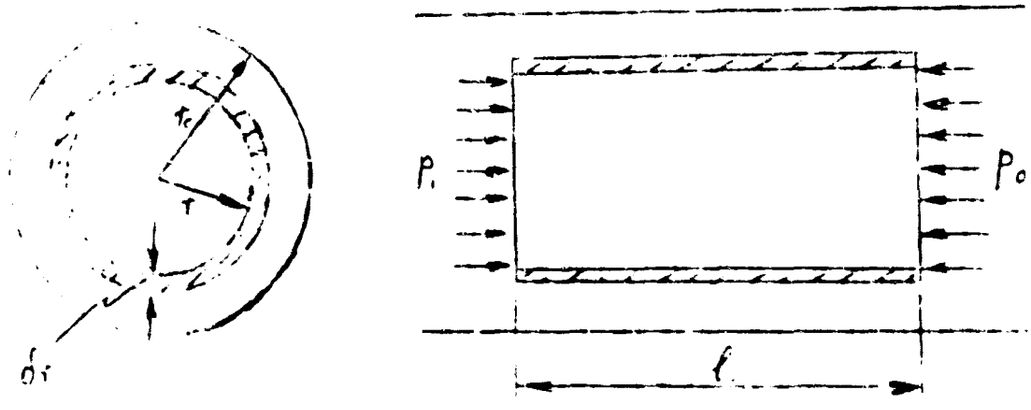

Consider the elemental thin cylinder of radius r and thickness δr.

Let the velocity of the air at radius r be v then the velocity gradient at this radius is $\frac{dv}{dr}$.

Equating the forces due to the pressure difference $(p_1 - p_o)$ acting on the ends of the solid cylinder or radius r to the force imparted to the curved surface of the solid cylinder by virtue of the viscous shear stress in the enveloping thin cylinder we have:

$$\left\{\begin{array}{l}\text{Force due to pressure difference between ends of solid cylinder of radius r.}\end{array}\right\} + \left\{\begin{array}{l}\text{Force due to viscous shear stress in thin cylinder of radius r.}\end{array}\right\} = 0$$

$$\therefore \quad (p_1 - p_o)\,\pi r^2 + \mu \frac{dv}{dr}\, 2\pi r l_1 = 0$$

$$\therefore \quad \frac{dv}{dr} = - \frac{(p_1 - p_o)\, r}{2\mu l_1}$$

$$\therefore \quad v = - \frac{p_1 - p_o}{2\mu l_1} \int r\,dr + A$$

$$\therefore \quad v = \frac{-(p_1 - p_o)}{2\mu l_1} \quad \frac{r^2}{2} + A$$

when $r = r_o$ $v = 0$ since the velocity of a fluid at a stationary wall must always be zero.

$$\therefore \quad A = \frac{p_1 - p_o}{2\mu l_1} \quad \frac{r_o^2}{2}$$

thus:

$$v = \frac{p_1 - p_o}{4\mu l_1} \quad (r_o^2 - r_1^2) \text{ in./sec.}$$

Let the flow through the tube be q $\text{in.}^3/\text{sec}$, and let the flow due to the elemental cylinder be δq.

then $\delta q = v\,(2\pi r)\,\delta r$ $\text{in.}^3/\text{sec}$.

$$\therefore \quad q = \int_o^{r_o} 2\pi v r\,dr$$

$$= \frac{(p_1 - p_o)\,\pi}{2\mu l_1} \int_o^{r_o} (r_o^2 r - r^3)\, dr$$

$$\therefore\ q = \frac{(p_1 - p_o)\,\pi\, r_o^4}{8\mu l_1} \quad \text{in.}^3/\text{sec.}$$

Since there are N tubes

$$Q = Nq$$

$\therefore$ we may express the total flow through the resistance element as:

$$Q = \frac{N(p_1 - p_o)\,\pi\, D^4}{128\mu l_1}$$

Therefore,

$$\frac{(p_1 - p_o)}{Q} = \frac{128\mu l_1}{N\pi D^4} \qquad (2)$$

Equation (2) expresses the pressure difference between the ends of the capillary tubes resulting from unit flow.

We shall therefore define the resistance of a stack of capillary tubes as:

$$R = \frac{128\mu_1}{N\pi D^4} \qquad \frac{\text{lb sec}}{\text{in.}^5}$$

provided the following two conditions are met:

Reynolds Number condition

$$\rho\, \frac{Q\ (\text{max})\ D}{KA\ \mu} < 2000$$

Compatibility condition:

$$\frac{\pi D^2 N}{4} = KA$$

where $K < .75$

4.3 CAPACITANCE C

By definition we may state the capacitance C of a container as follows:

$$C = \frac{Q}{(\frac{dp}{dt})}$$

where Q is the flow into the container, resulting from a rate of change of pressure $\frac{dp}{dt}$ at the opening of the container.

For a container to have capacitance we depend upon the fact that air is compressible.

Let

Volume of container = V $in.^3$

Absolute pressure of air at any instant = P $\frac{lb}{in.^2}$

Assuming that the air is compressed into the volume V adiabatically we have:

$$PV^{1.4} = C$$

$$\text{Bulk modulus of air} = \frac{\text{change in pressure}}{\text{change in volume}}$$

per unit volume.

$$\frac{\text{change in pressure}}{\text{change in volume}} = \frac{dP}{dV} = \frac{-1.4\ C}{V^{2.4}}$$

$$= -1.4\ \frac{P}{V}$$

since the volume V is unity, the bulk modulus is 1.4 P $lb/in.^2$.

If the changes in pressure $P_1 - P_o$ are small compared with the absolute pressure P_o, we may assume that the bulk modulus is a constant

$$K = 1.4\ P_o\ lb/in^2$$

Thus, a volume V of air when subjected to a rate of change of pressure dP/dt will change to a volume V + δV after a time δt, thus:

$$V + \delta V = V + \frac{1}{1.4\ P_o}\ V\ \left(\frac{dP}{dt}\right)\ \delta t$$

Now

$$\frac{\delta V}{\delta t_{(t \to o)}} = \frac{dV}{dt} = Q$$

Thus,

$$\frac{Q}{\left(\frac{dP}{dt}\right)} = \frac{1}{1.4\ P_o}\ V \qquad (3)$$

Equation (3) expresses the flow resulting from unit rate of change of pressure at the entrance to a container. We shall, therefore, define the capacitance of a container as:

$$C = \frac{1}{1.4\ P_o}\ V \quad \frac{in.^5}{lbf}$$

Thus, we have defined inductance, resistance and capacitance for passive pneumatic elements operating under conditions which permit the use of linear approximations. Under these conditions the values of the inductance, resistance and capacitance of the three types of element may be expressed as follows:

INDUCTANCE	L	$K_L \frac{\ell}{A}$	$\frac{lbf\ sec^2}{in.^5}$
RESISTANCE	R	$K_R \frac{\ell}{ND^4}$	$\frac{lbf\ sec}{in.^5}$
CAPACITANCE	C	$K_C\ V$	$\frac{in.^5}{lbf}$

The values of K_L, K_R, and K_C have been calculated for air at 20°C and 14.7 lb/sq in. as follows:

$$K_L = 1.13 \times 10^{-7} \quad \frac{lbf\ sec^2}{in.^4}$$

$$K_R = 1.07 \times 10^{-7} \quad \frac{lbf\ sec}{in.^2}$$

$$K_C = 4.85 \times 10^{-2} \quad \frac{in.^2}{lbf}$$

5. ELECTRICAL ANALOG OF FLUID CIRCUITS

Inductance Element L—This element may be replaced by an electrical inductance with no further change in the circuit except when the acoustic wave length is of the same order as the pipe lengths under consideration.

Resistance Element R—This element may be replaced by an electrical resistance with no further change in the circuit.

Capacitance Element C—This element must be replaced by an electrical capacitor to ground as indicated below.

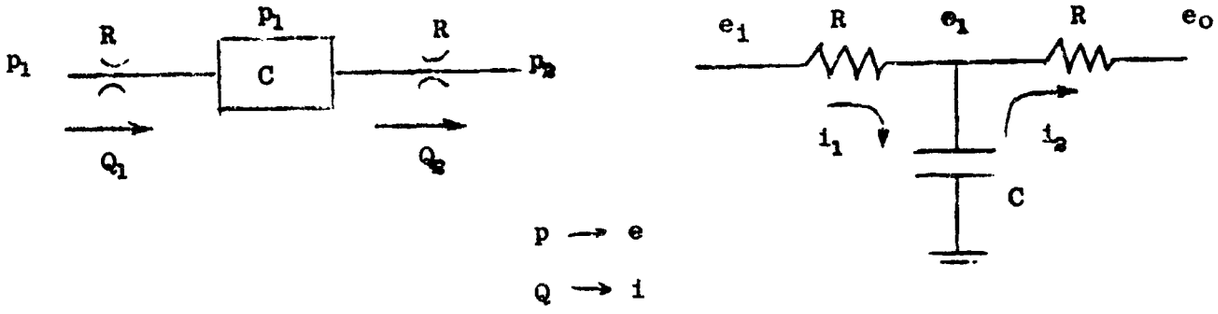

Pneumatic Circuit

Equivalent electrical circuit

6. CIRCUIT ANALYSIS

We shall apply the voltage-pressure analog to show how the transfer function for a simple pneumatic LRC network may be obtained by reference to the equivalent electrical network.

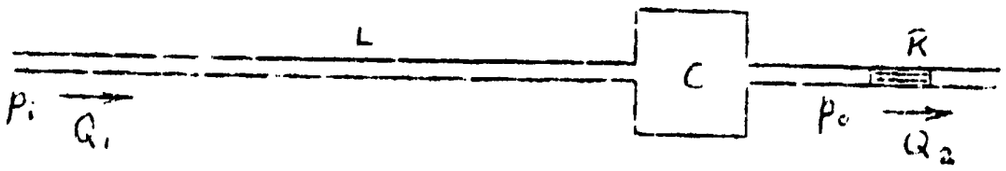

Actual pneumatic circuit

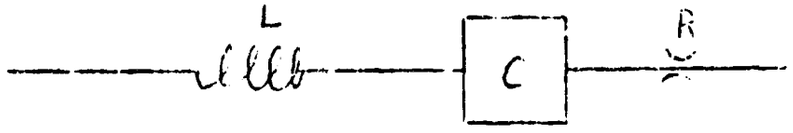

Idealized pneumatic circuit

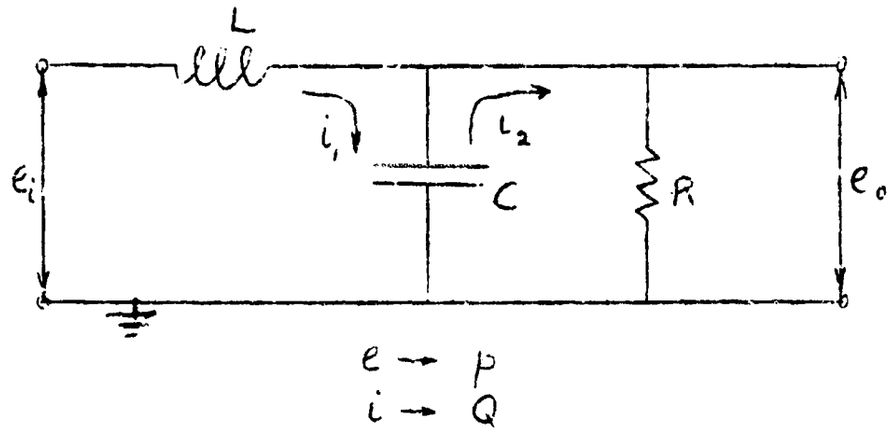

Equivalent electrical circuit

The circuit equations may now be solved using Laplace transforms:

$$E_i = I_1\left(SL + \frac{1}{SC}\right) - I_2\left(\frac{1}{SC}\right)$$

$$0 = -I_1\left(\frac{1}{SC}\right) + I_2\left(R + \frac{1}{SC}\right) \qquad (1)$$

$$E_0 = I_2R$$

These equations may be rewritten:

$$\begin{bmatrix} a_1 & b_1 & c_1 & 0 \\ 0 & b_2 & c_2 & 0 \\ 0 & 0 & c_3 & d_3 \end{bmatrix} \begin{bmatrix} E_i \\ I_1 \\ I_2 \\ E_0 \end{bmatrix} = 0$$

where

$a_1 = -1$; $b_1 = SL + \frac{1}{SC}$; $C_1 = -\frac{1}{SC}$

$b_2 = -\frac{1}{SC}$; $C_2 = R + \frac{1}{SC}$

$c_3 = -1$; $d_3 = R$

OR

$$\begin{bmatrix} I_1 \\ I_2 \\ E_0 \end{bmatrix} = \begin{bmatrix} e_1 & 0 & g_1 & 0 \\ 0 & f_2 & 0 & 0 \\ 0 & 0 & g_2 & 0 \end{bmatrix} \begin{bmatrix} E_i \\ I_1 \\ I_2 \\ E_0 \end{bmatrix} \qquad (2)$$

where $e_1 = -\frac{a_1}{b_1}$ $\qquad g_1 = -\frac{c_1}{b_1}$

$f_2 = -\frac{b_2}{c_2}$ $\qquad g_2 = -\frac{c_3}{d_3}$

The signal flow graph corresponding to equations (2) is as follows:

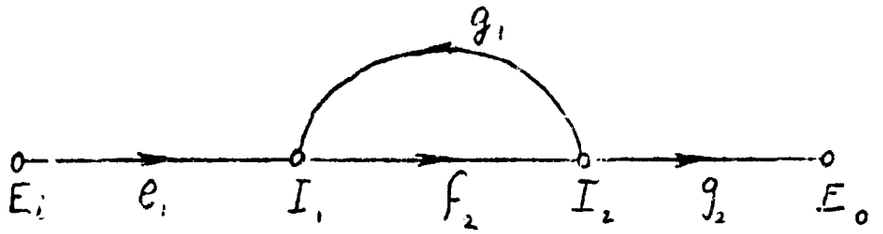

and the graph transmittance is

$$\frac{E_0}{E_i} = \frac{e_1 f_2 g_2}{1 - f_2 g_1} \qquad (3)$$

Making the appropriate substitutions for e_1 f_2 g_1 g_2 in terms of L R and C, we obtain the transfer function for the circuit.

It should be noted that the inverse Laplace transform of E_o corresponds to the pressure p_o in psi expressed as a function of time when a step input p_i is applied.

If the output flow is required then we use the graph transmittance:

$$\frac{I_o}{E_i} = \frac{e_1 f_2}{1 - f_2 g_1} \quad \text{in place of (3)}$$

If a constant current input is applied in the form of a step function, then we may make either of the following two assumptions:

(1) The inductance L is negligible

In this case the signal flow graph reduces to:

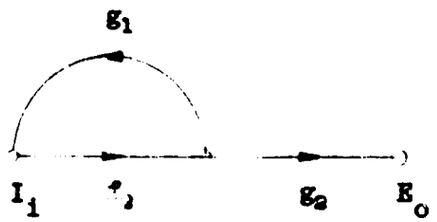

and the graph transmittance becomes:

$$\frac{E_o}{I_i} = \frac{f_2 g_2}{1 - f_2 g_1}$$

(2) The inductance L has associated with it a small but not negligible capacitance C_1.

To solve this problem we must first redraw the equivalent electrical network. If capacitance C_1 is small compared with C it will be a reasonable approximation to assume the following equivalent electrical network, where C_1 is the lumped capacitance of the line L.

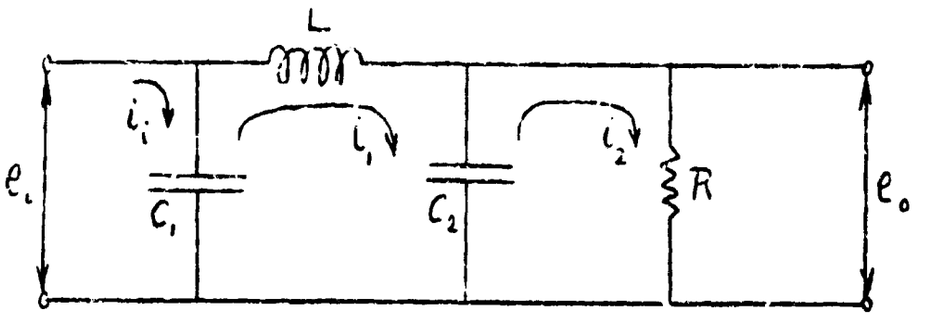

$$E_1 = I_i \left(\frac{1}{SC_1}\right)$$

$$0 = I_i \left(\frac{1}{SC_1}\right) + I_1 \left(SL + \frac{1}{SC} + \frac{1}{SC_1}\right) - I_2 \left(\frac{1}{SC}\right)$$

$$0 = -I_1 \left(\frac{1}{SC_1}\right) + I_2 \left(R + \frac{1}{SC}\right)$$

$$E_o = I_2 R$$

Since E_1 is not required we may eliminate the first equation. The remaining three equations may now be written in the form:

$$\begin{bmatrix} a_1 & b_1 & c_1 & 0 \\ 0 & b_2 & c_2 & 0 \\ 0 & 0 & c_3 & d_3 \end{bmatrix} \begin{bmatrix} I_i \\ I_1 \\ I_2 \\ E_o \end{bmatrix} = 0$$

OR

$$\begin{bmatrix} I_1 \\ I_2 \\ E_o \end{bmatrix} = \begin{bmatrix} e_1 & 0 & g_1 & 0 \\ 0 & f_2 & 0 & 0 \\ 0 & 0 & g_3 & 0 \end{bmatrix} \begin{bmatrix} I_i \\ I_1 \\ I_2 \\ E_o \end{bmatrix} \qquad (4)$$

The signal flow graph corresponding to equations (4) is as follows:

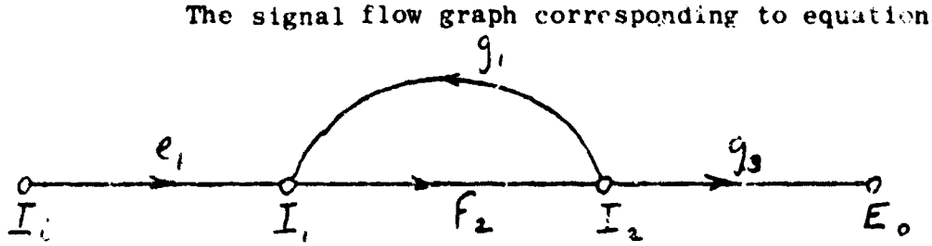

and the graph transmittance is

$$\frac{E_o}{I_i} = \frac{e_1 f_2 g_3}{1 - f_2 g_1} \tag{5}$$

It will be noted that the forms of (5) and (3) are identical, however, the branch transmittances e_1 and g_1 will be observed to be different for the two transfer functions.

7. LINEAR APPROXIMATIONS FOR THE ORIFICE RESISTANCE ELEMENT

The pressure loss across an orifice is due to the dissipation of the kinetic energy gain as the air is accelerated from plane A to plane B, as indicated in figure E-1.

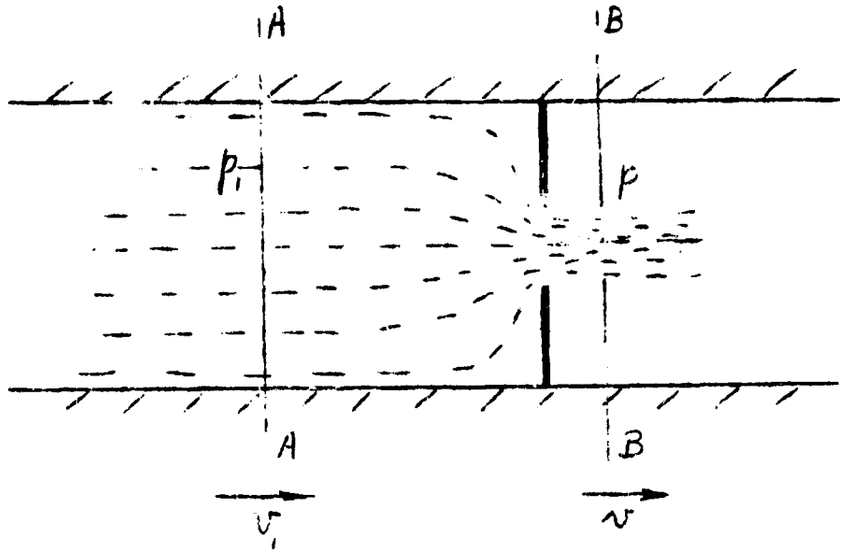

Figure E-1

Since the loss of energy due to turbulence is negligible between these two planes, we may apply Bernoulli's equation as follows:

$$\frac{p_1}{\rho} + \frac{v_1^2}{2} = \frac{p_o}{\rho} + \frac{v_o^2}{2}$$

where the density ρ is assumed constant.

Velocities v_1 and v_o are related by the continuity equation:

$$v_1 \frac{\pi D_1^2}{4} = C_c v_o \frac{\pi D_o^2}{4}$$

where C_c is the contraction coefficient for the orifice, D_1 and D_o are the diameters of the pipe and the orifice, respectively.

Thus

$$\frac{v_o^2}{2}\left[1 - C_c^2\left(\frac{D_o}{D_1}\right)^4\right] = \frac{p_1 - p_o}{\rho}$$

$$\therefore \quad v_o = \sqrt{\frac{2(p_1 - p_o)}{\rho\left(1 - C_c^2\left[\frac{D_o}{D_1}\right]^4\right)}}$$

This result gives the ideal velocity at the vena contracta. Multiplying by the velocity coefficient C_v we obtain the actual velocity v_o'

$$v_o' = C_v \sqrt{\frac{2(p_1 - p_o)}{\rho\left(1 - C_c^2\left\{\frac{D_o}{D_1}\right\}^4\right)}}$$

The product $v_o' C_c A_o$, where A_o is the area of the orifice, gives the actual flow Q thus:

$$Q = C_v C_c A_o \sqrt{\frac{2(p_1 - p_o)}{\rho\left\{1 - C_c^2\left(\frac{D_o}{D_1}\right)^4\right\}}}$$

When the orifice diameter is small compared with the inner diameter of the pipe we may neglect the term $C_c^2\left(\frac{D_o}{D_1}\right)^4$ and the expression for flow may then be reduced to:

$$Q = C_d A_o \sqrt{\frac{2(p_1 - p_o)}{\rho}} \qquad (6)$$

where $C_d = C_v C_c$ the coefficient of discharge.

Equation (6) may therefore be expressed in the form

$$p_1 - p_o = K_o \frac{Q^2}{D^4} \quad \text{psi}$$

For air at 70°C and 14.7 psi the value of K_o is found to be

$$0.146 \times 10^{-6} \quad \frac{\text{lbf sec}^2}{\text{in.}^4}$$

Thus, for an orifice resistance we have:

$$\frac{p_1 - p_o}{Q^2} = \frac{0.146 \times 10^{-6}}{D^4} \quad \frac{\text{lbf sec}^2}{\text{in.}^8}$$

We may define the orifice resistance coefficient K as follows:

$$K = \frac{p}{Q^2} \quad \frac{\text{psi}}{(\text{cis})^2}$$

where p is the pressure drop across the orifice resulting from a flow Q.

Since the relationship between Q and p for an orifice is non-linear we shall approximate to a piecewise linear circuit as shown in figure E-2.

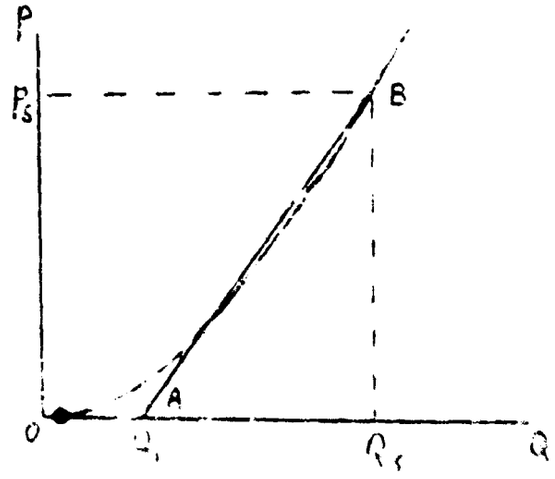

Figure E-2

Let the estimated maximum flow through the orifice when operating in a circuit be Q_s, and let the corresponding pressure drop across the orifice be p_s.

Figure E-2 shows the relationship between p and Q for an orifice. We may reduce the parabola OB to two linear portions OA and AB such that the area under the parabola is equal to the area under the linearized approximation to the parabola as given by the line OAB.

Since $p = KQ^2$ the area under the parabola between the limits 0 and Q_s is:

$$\int_0^{Q_s} p \, dQ$$

$$= \int_0^{Q_s} KQ^2 \, dQ$$

$$= \frac{1}{3} \quad p_s Q_s$$

This area must be made equal to the area of triangle ABC

$$\therefore \quad \frac{1}{3} \quad p_s Q_s = \frac{1}{2} \quad (Q_s - Q_1) \, p_s$$

$$\therefore \quad Q_1 = \frac{1}{3} \quad Q_s$$

We may now obtain the equation for the line AB as follows:

The equation of the line AB will be of the form:

$$p = QR + B$$

where

R and B are constants.

when

$$p = 0 \quad Q = \frac{1}{3} \, Q_s$$

when

$$p = p_s \quad Q = Q_s$$

Thus, we may solve the two simultaneous equations:

$$p_s = Q_s R + B \qquad (1)$$

$$0 = \frac{1}{3} \, Q_s R + B \qquad (2)$$

to obtain the constants R and B.

Subtracting (2) from (1)

$$p_s = \frac{2}{3} \; Q_s R$$

$$R = \frac{3p_s}{2Q_s}$$

Substituting for R in 2;

$$R = -\frac{1}{3} \; Q_s \; \frac{3p_s}{2Q_s}$$

$$= -\frac{1}{2} \; p_s$$

Thus, for the portion of the linear approximation between $\frac{1}{3} Q_s$ and Q_s, we have:

$$p = \left(\frac{3}{2} \; \frac{p_s}{Q_s} \right) Q \; - \frac{1}{2} \; p_s$$

The complete linearized expression for pressure as a function of flow may be expressed as:

$$p = \left[0 \right]_{Q=0}^{\frac{1}{3}Q_s} + \left[\frac{3}{2} \; \frac{p_s}{Q_s} \; Q - \frac{1}{2} \; p_s \right]_{Q=\frac{1}{3}Q_s}^{Q_s}$$

An equivalent piecewise linear approximate circuit is shown in figure E-3.

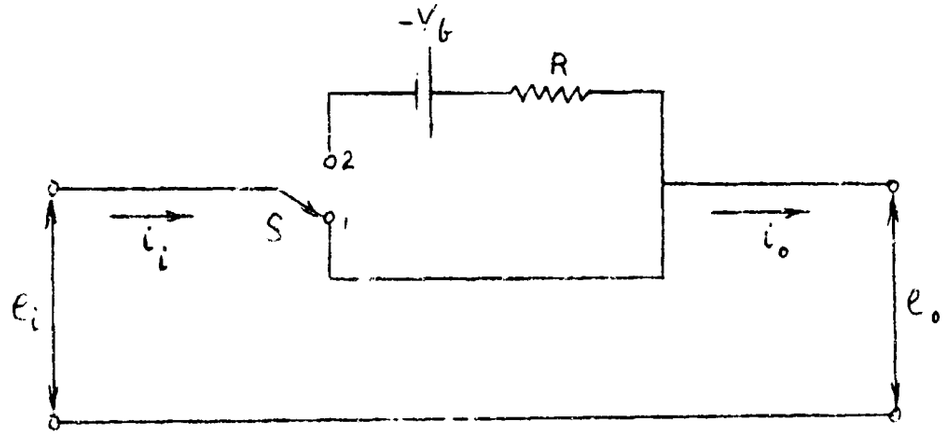

Figure E-3

The switch S is set to switch from pole 1 to pole 2 whenever the input current i_1 exceeds $\frac{1}{3}\ i_s$, where i_s is the current required to switch the driven device in the analog circuit.

Also $R = \frac{3}{2}\ \frac{p_s}{Q_s}$ $\qquad Q_s \longleftrightarrow i_s$

and

$$V_b = -\frac{1}{2}\ p_s \qquad p_s \longleftrightarrow e_s$$

where p_s is the pressure drop across the orifice caused by a flow Q_s.

Thus, the circuit shown in figure E-3 is the voltage-pressure analog electrical circuit corresponding to an orifice operating under conditions of flow Q such that $0 < Q < Q_s$, where Q_s is the orifice flow required to perform a switching function in the circuit.

APPENDIX F.—TRANSIENT CIRCUIT CALCULATIONS

T. D. Reader

I L L U S T R A T I O N S

APPENDIX F.—TRANSIENT CIRCUIT CALCULATIONS—Illustrations Cont'd

APPENDIX F.—TRANSIENT CIRCUIT CALCULATIONS

T. D. Reader

1. TRANSIENT STATE CIRCUIT THEORY

The approach to the solution of the problem of dynamic performance for fluid logic circuits is essentially as follows:

(1) The fluid circuits are idealized into linear and nonlinear elements such that while the linear elements can be capacitive, inductive, or resistive, the nonlinear elements are either resistive only, or are pure switches which close after a specified delay.

(2) The equivalent electronic circuit is drawn based on measurements taken from tests on the actual fluid elements.

(3) The resistance elements are then linearized by calculating the equivalent linear resistance satisfying the steady-state condition.

(4) An analytic solution is applied to the idealized circuit using linear network analysis and synthesis.

2. EQUIVALENT CIRCUIT FOR THE HDL FLIP-FLOP

The idealized equivalent electrical circuit shown in figure F-1 was assumed for one output leg of the flip-flop.

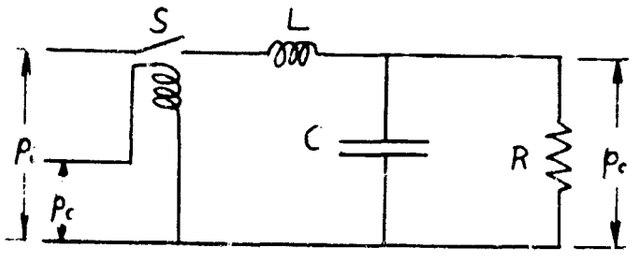

Figure F-1

The switch S is assumed to close at the instant when the control pressure p_c reaches the pressure required to switch the flip-flop.

With the output load R known, values of L and C were obtained from a synthesis of the network. The procedure was to obtain the experimental response of the flip-flop to a control pulse, and then to determine by calculation the values of L and C for which the response of the circuit shown in figure F-1 most closely approximated the actual flip-flop response.

3. SYNTHESIS OF AN EQUIVALENT L-R-C CIRCUIT FOR THE FLIP-FLOP

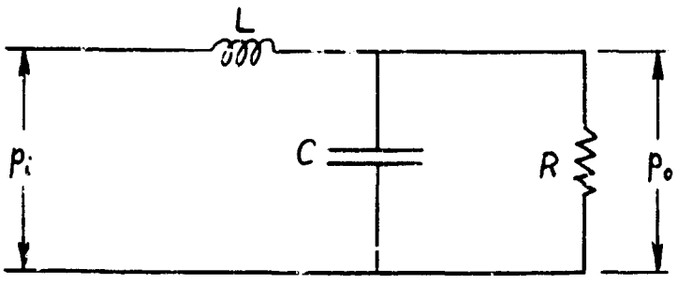

Figure F-2

The transfer function for the circuit shown in figure F-2 was obtained by the method of Laplace transforms, and is given by:

$$\frac{P_o(s)}{P_i(s)} = \frac{R}{RLCs^2 + Ls + R} \tag{1}$$

If $P_i(s)$ is the step function $p_i(\frac{1}{s})$ then the output p_o may by expressed as a function of time in terms of LRC and p_i as follows:

$$\frac{p_o}{p_i} = 1 - e^{-\frac{1}{2RC}t}\left\{\cos\sqrt{\frac{1}{LC} - \left(\frac{1}{2RC}\right)^2}\,t + \frac{\frac{1}{2RC}}{\sqrt{\frac{1}{LC} - \left(\frac{1}{2RC}\right)^2}}\sin\sqrt{\frac{1}{LC} - \left(\frac{1}{2RC}\right)^2}\,t\right\} \tag{2}$$

Where p_i is a step input at $t = 0$

This expression may be simplified by making the substitutions:

$$K = \frac{1}{2RC} \tag{3}$$

and

$$\omega = \sqrt{\frac{1}{LC} - \left(\frac{1}{2RC}\right)} \tag{4}$$

The output p_o may now be expressed as a function of time in terms of the values K, ω and p_i as follows:

$$\frac{p_o}{p_i} = 1 - e^{-Kt}\left\{\cos\omega t + \frac{K}{\omega}\sin\omega t\right\} \qquad (5)$$

A typical response to a control signal given to the HDL flip-flop is shown in figure F-3. Values of K and ω were obtained by a method of successive approximation, and the calculated curve is shown superimposed on the experimental curve.

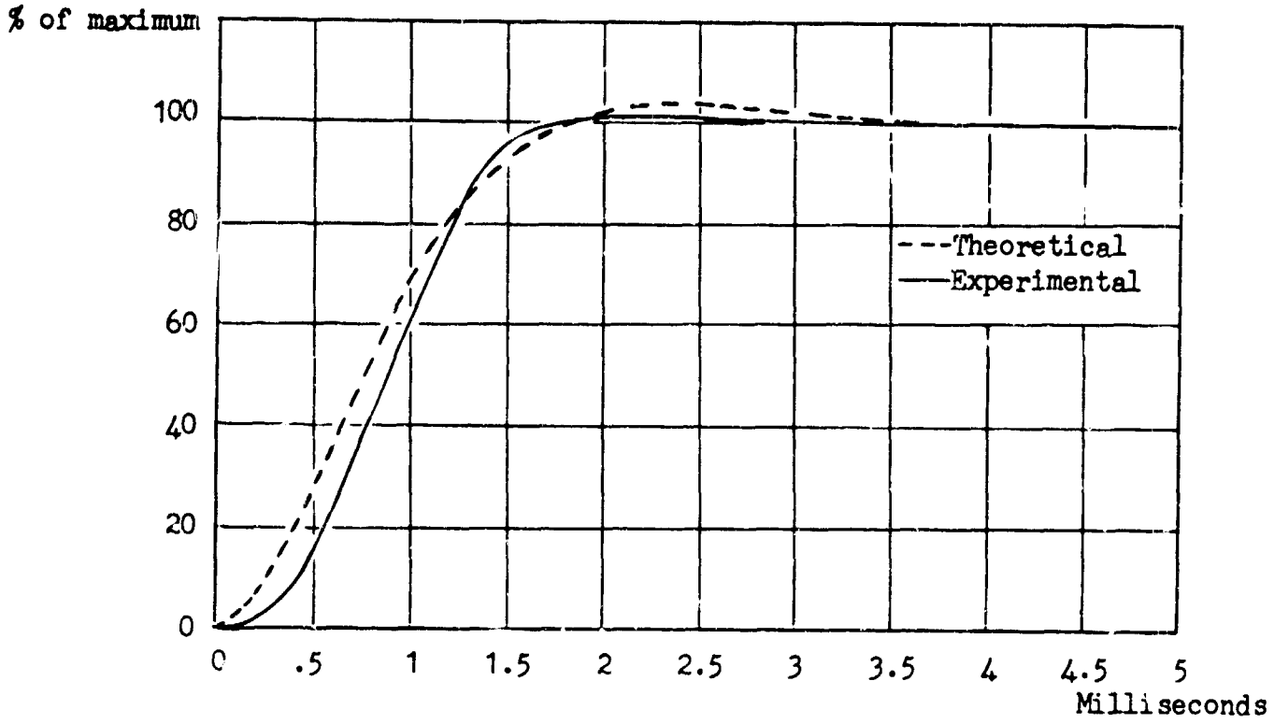

Figure F-3

It can be seen that agreement between the two curves is sufficiently good to permit the use of the equivalent circuit in calculations involving the response of a flip-flop.

The analytical expression which agreed most closely with the experimental results was:

$$\frac{p_o}{p_i} = 1 - e^{-1,457t}(\cos 1,317t + 1.11 \sin 1,317t) \qquad (6)$$

where

t is in seconds.

4. EXPERIMENTAL CONFIRMATION OF THEORY

In order to verify that the circuit theory derived in this report is valid over a useful range of operating frequencies it was decided to set up a binary counter stage so that it was free to oscillate at its natural frequency.

The actual circuit used is shown in figure F-4.

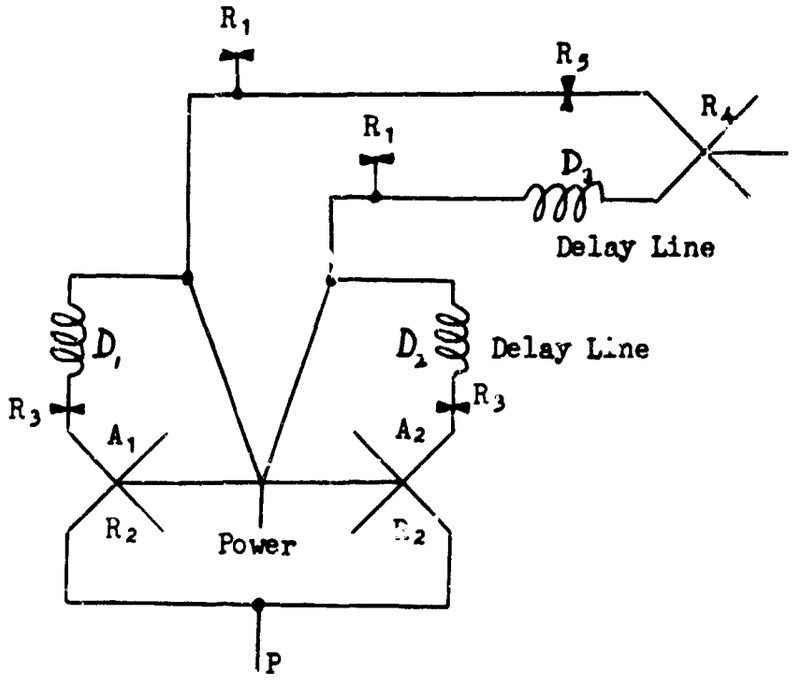

Figure F-4

Input P was maintained at a constant signal level, so that the feedback from the delay lines D_1 and D_2 could be transmitted by the AND gates A_1 and A_2 thus causing the flip-flop to multivibrate.

The values of L and C in the circuit shown in figure F-2 were first obtained then the remainder of the circuit was incorporated into a complete electrical analog of the counter element. The circuit which represents the load on the left hand output is shown in figure F-5(a), and the equivalent electrical circuit is shown in figure F-5(b). The delay line tubes of the fluid circuit have been simulated by means of the LC ladder network shown

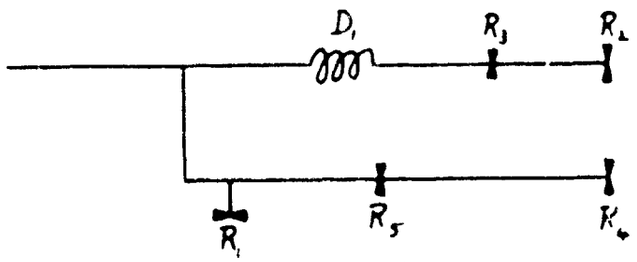

Figure F-5(a)

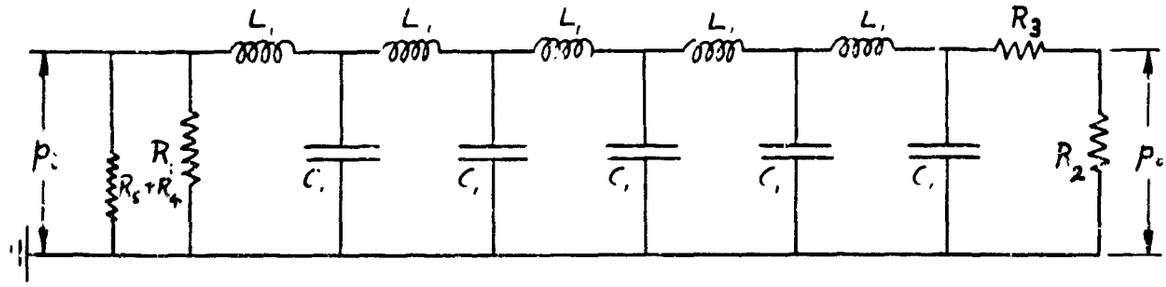

Figure F-5(b)

The circuit which represents the load on the right-hand output is shown in figure F-6(a) and the equivalent electrical circuit is shown in figure F-6(b).

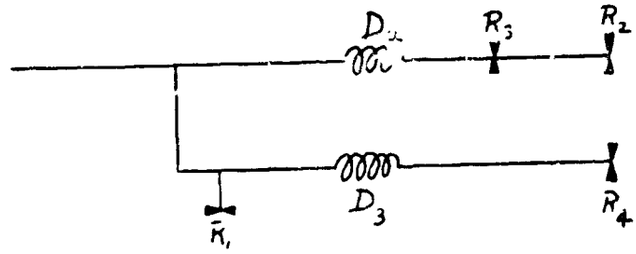

Figure F-6(a)

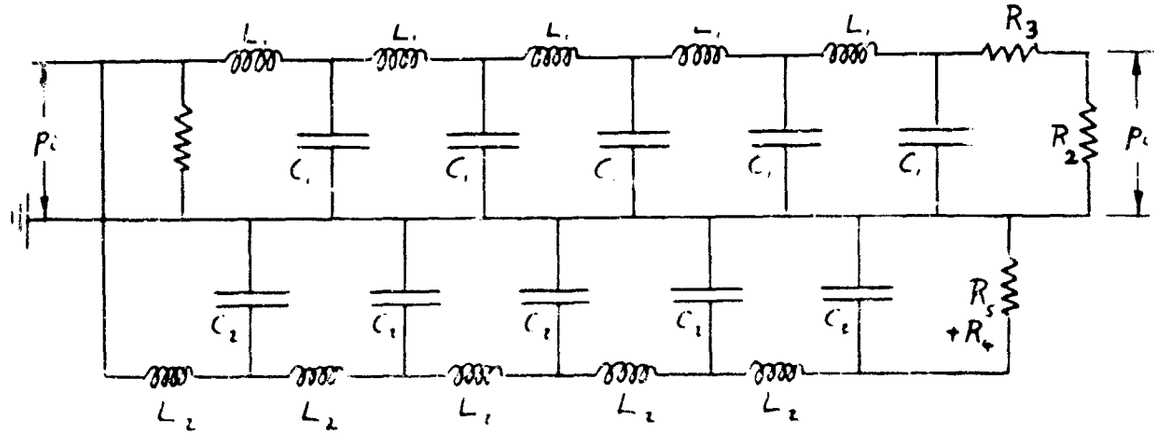

Figure F-6(b)

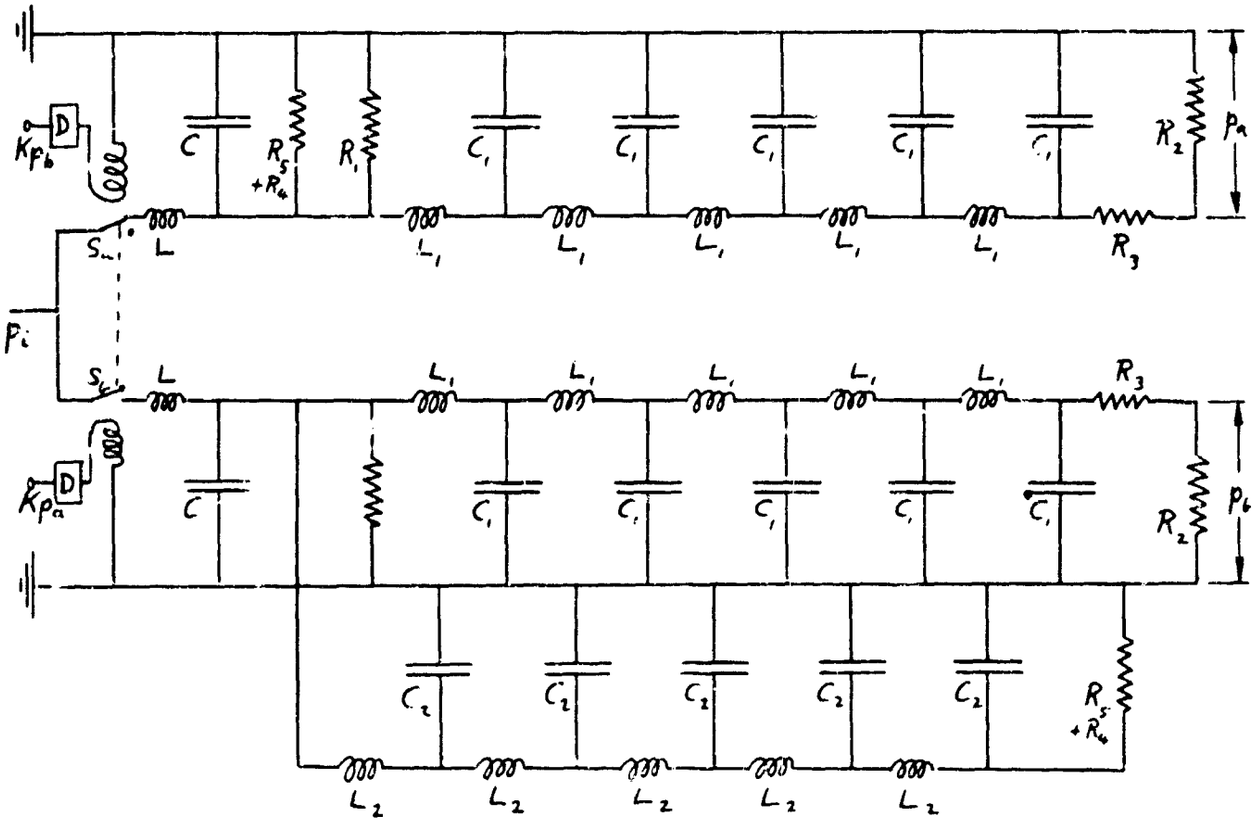

Figure F-7

The complete flip-flop oscillator can be represented by means of the electrical circuit shown in figure F-7.

The input delays D represent a delay in the switching action of the flip-flop. This delay is determined by the strength of the input signal.

5. DETERMINATION OF EQUIVALENT CIRCUIT PARAMETERS

Values of L and C were obtained from a series of tests carried out to determine the response of the flip-flop under different loading conditions. The values of the remaining components in the circuit were obtained by direct measurement and calculation.

6. MODE OF OPERATION OF THE CIRCUIT

Referring to figure F-7, let us assume that switch S_a has just closed. Then the effective supply pressure p_i will cause an increasing flow in the circuit, corresponding to the load attached to the

output leg A of the flip-flop shown in figure F-4. When the pressure drop p_a across the resistor R_a reaches a value such that the input signal Kp_a can close the switch S_b and simultaneously open switch S_a, the flip-flop will switch, and the output pb will begin to rise while the output p_a will begin to fall. Similarly when the output pb reaches the required switching value the flip-flop will again change state. In this way the flip-flop circuit will operate as an oscillator.

7. MATHEMATICAL SOLUTION

The Laplace transform for the combined flip-flop and load is given by:

$$\frac{p_o(s)}{p_i(s)} = \frac{R_a R e^{-(T + \sqrt{L_d C_d})s}}{(R_a + R_a)(LRCs^2 + Ls + R)} \qquad (7)$$

where

T is the switching delay time

L_d is the lumped inductance of the feedback delay line

C_d is the lumped capacitance of the feedback delay line

From (7) the output from the delay line may be expressed as a function of the circuit parameters and the input function by means of the transformed expression:

$$P_o(s) = \frac{P_i(s) R_a e^{-(T + \sqrt{L_d C_d})s}}{(R_a + R_a)\ (RLCs^2 + LS + R)} \qquad (8)$$

In deriving the transformed expression corresponding to the flip-flop output, it was assumed that the input $P_i(s)$ was the step function $p_i\ (1/s)$. Thus, the output of the delay line may now be expressed in terms of the input signal p_i as follows:

$$P_b(s) = \frac{p_i R_a R e^{-(T + \sqrt{L_d C_d})s}}{s(R_a + R_a)(RLCs^2 + Ls + R)} \qquad (9)$$

Taking the Inverse Laplace Transform of both sides of expression (9) we obtain an expression from which the half-cycle time may be calculated:

$$p_b = \frac{p_1 R_2 u(\tau)}{R_2 + R_3}\left[1 - e^{-\frac{1}{2RC}\tau}\left\{\cos\sqrt{\frac{1}{LC} - \left(\frac{1}{2RC}\right)^2}\,\tau + \frac{\frac{1}{2RC}}{\sqrt{\frac{1}{LC} - \left(\frac{1}{2RC}\right)^2}}\sin\sqrt{\frac{1}{LC} - \left(\frac{1}{2RC}\right)^2}\,\tau\right\}\right] \quad (10)$$

Where

$$\tau = t - T - \sqrt{L_d C_d} \quad (11)$$

It now remains only to determine the values of the parameters in expressions (10) and (11) in order to specify completely the output pressure p_b as a function of time t measured from the instant the input signal pressure Kp_a reaches the value required to switch the flip-flop.

8. DETERMINATION OF CIRCUIT PARAMETERS

8.1 Linear Resistances

In determining the diameters of the bleeds and restrictors (appx C) use was made of the concept of an equivalent orifice area A defined as follows:

$$q = A\sqrt{\frac{2p}{\rho}}$$

where

q is the measured flow in	$in.^3/sec$
A is the equivalent area of orifice in	$in.^2$
p is the total pressure drop across the orifice	$lb./in.^2$
ρ is the density of the fluid in	$lb\ sec^2/in.^4$

In order to use the Laplace transform it is necessary to idealize an orifice as a linear resistance. The principle function of resistive elements, whether linear or quadratic, is to satisfy

the steady-state requirements for stability and gain. Under transient conditions, the inductive and capacitive elements are of primary importance, because of their phase shift effects.

Since the steady-state conditions must be met it is necessary to simulate an orifice by means of an equivalent linear resistance across which the pressure drop is the same as for the orifice when the steady-state flow is maintained. Let this flow be q_1 and let the resulting pressure drop across an orifice of equivalent area A be p_1.

Then using expression (12):

$$q_1 = A\sqrt{\frac{2p_1}{\rho}} \tag{13}$$

A linear resistance R will satisfy expression (13) provided

$$R = \frac{p_1}{q_1} \tag{14}$$

The resistance R may alternatively be expressed as a function of the pressure drop p_1 and the equivalent orifice area A by substituting in (14) the value of q_1 given in (13):

$$R = \frac{1}{A}\sqrt{\frac{\rho p_1}{2}} \tag{15}$$

Expression (15) shows that the effective linear resistance depends not only on the equivalent area of the orifice but also on the steady-state pressure drop across it.

8.2 Feedback Delay Lines

The inductance L_d and capacitance C_d for the feedback delay lines were obtained from their dimensions using the following theoretically derived formulae (Appendix E):

$$\text{Inductance } L = K_L\frac{\ell}{A} \quad \frac{\text{lb sec}^2}{\text{in.}^5} \tag{16}$$

$$\text{Capacitance } C = K_C V \quad \frac{\text{in.}^5}{\text{lb}} \tag{17}$$

where

ℓ is the length of the feedback delay line

A is its cross-sectional area

V is its internal volume

Values of the constants K_L and K_C for air at 20°C and 14.7 lb/sq in. are:

$$K_L = 1.13 \times 10^{-7} \quad \frac{\text{lb sec}^2}{\text{in.}^4}$$

$$K_C = 4.85 \times 10^{-2} \quad \frac{\text{in.}^2}{\text{lb}}$$

The dimensions of the feedback delay lines were:

Length	96 inches
Internal diameter	0.173 inches

Using expressions (16) and (17), the following values were obtained:

$$L_d = 4.65 \times 10^{-4} \quad \frac{\text{lb sec}^2}{\text{in.}^5} \qquad (18)$$

$$C_d = .109 \quad \frac{\text{in.}^5}{\text{lb}} \qquad (19)$$

8.3 Switching Delay Time

This time was measured by means of hot-wire anemometers. A signal equal to the calculated input pressure was applied at the control port of the flip-flop and the lead time was measured by comparing the input and output signals displayed on a dual-trace oscilloscope.

8.4 Equivalent Inductance and Capacitance of Flip-Flop

The values of K and ω in expression (5) were found to be:

K = 1,457 radians/sec

ω = 1,317 radians/sec

The output resistance R for the equivalent electrical circuit shown in figure F-1 was obtained from expression (15) and the values of L and C for the flip-flop were then calculated by substituting for K, ω, and R:

Equivalent area of output orifice = 4.14×10^{-3} in.^{2}

Pressure drop across orifice = 7.5 in. of water

Equivalent Linear Resistance

$$R = \frac{.04514 \sqrt{7.5 \times 10^{-3}}}{4.14 \times 10^{-3}}$$

$$= .0298 \ \frac{\text{lb sec}}{\text{in}^5}$$

Substituting for K, ω, and R in expressions (3) and (4), we obtain:

$$L = 2.24 \times 10^{-5} \qquad \frac{\text{lb sec}^2}{\text{in.}^5}$$

$$C = 1.15 \times 10^{-2} \qquad \frac{\text{in.}^5}{\text{lb}}$$

9. DETERMINATION OF OSCILLATOR FREQUENCY

9.1 By Direct Calculation

The values of the parameters in equations (10) and (11), obtained by the methods described above are:

$$R_2 = 12.32 \times 10^{-3} \qquad \frac{\text{lb sec}}{\text{in.}^5}$$

$$R_3 = 5.74 \times 10^{-3} \qquad \frac{\text{lb sec}}{\text{in}^5}$$

$$R = 29.8 \times 10^{-3} \qquad \frac{\text{lb sec}}{\text{in.}^5}$$

$$L = 2.24 \times 10^{-6} \qquad \frac{\text{lb sec}^2}{\text{in}^5}$$

$$C = 1.15 \times 10^{-2} \qquad \frac{\text{in.}^6}{\text{lb}}$$

$$T = 4.2 \times 10^{-3} \qquad \text{sec}$$

$$L_d = 4.62 \times 10^{-4} \quad \frac{\text{lb sec}^2}{\text{in.}^5}$$

$$C_d = 1.09 \times 10^{-1} \quad \frac{\text{in.}^5}{\text{lb}}$$

These values when inserted into expression (10) give the pressure p at the input to AND gates A_1 and A_2. The output pressure from this gate is Kp where K is the recovery ratio. Tests carried out on AND gates have shown that the value of K is 0.6. Thus the value of p at which the flip-flop will switch is given by the expression:

$$.6p = p_s \tag{20}$$

where

p_s is the pressure required to switch the flip-flop.

Switching tests have shown that the pressure required to switch the flip-flop, when loaded with a circuit of equivalent orifice area equal to 0.00414 sq in. was 0.17 times the available steady-state output pressure p_1. Thus the time t for the flip-flop to switch, measured from the instant the input signal Kp reaches the value required to switch the flip-flop, is determined by the condition:

$$0.17p_1 = 0.6p \tag{21}$$

hence,

$$p = 0.28p_1 \tag{22}$$

Since all the circuit parameters in expressions (10) and (11) are known, we may obtain the half-cycle time t_1 by substituting the right hand side of expression (22) in place of p in expression (10) and solving the expressions (10) and (11) for τ_1 and t_1:

$$0.28p_1 = 0.685p_1 \left[1-e^{-1457\tau_1}(\cos 1{,}317\tau_1 - 1.11 \sin 1{,}317\tau_1)\right] \tag{23}$$

$$\tau_1 = t_1 - .01126 \tag{24}$$

Hence

$$\tau_1 = 0.00063 \text{ sec}$$

$$\tau_1 = 0.01189 \text{ sec}$$

Thus the calculated cycle time is 23.8 msec. The calculated frequency of the oscillator is therefore 42 cps.

9.2 By Building and Testing the Equivalent Electrical Analog

The electrical networks shown in figures F-5(b) and F-6(b) may be built as a single circuit in which the ladder network representing the delay line of the pulse former is switched in or out depending on which side of the fluid oscillator is being simulated.

Figure F-8 shows a circuit diagram of the electrical analog used to study the fluid oscillator.

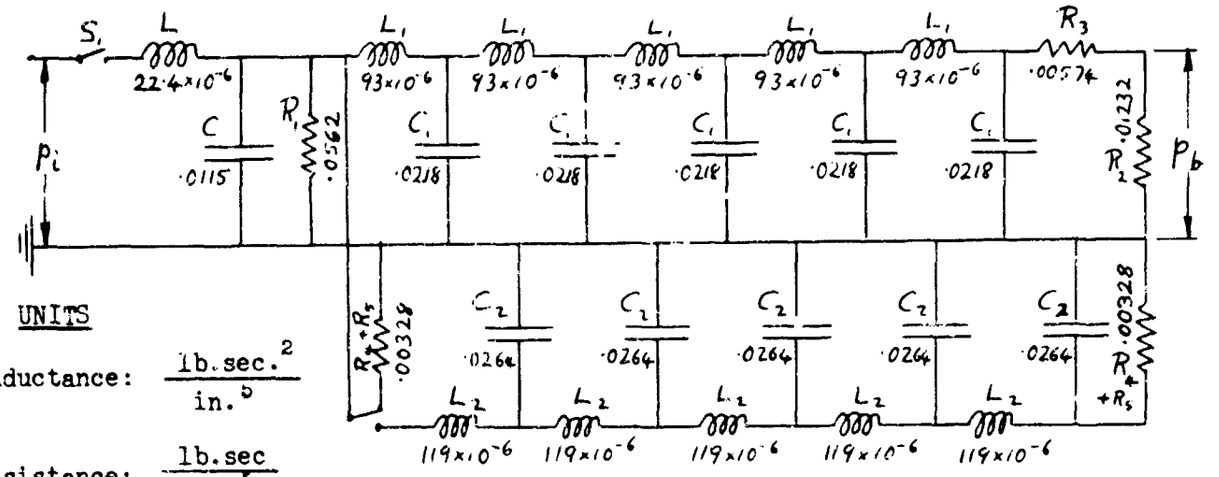

Figure F-8

In this circuit the input delays represented in figure E-7 have been omitted since these were obtained directly from tests carried out on the flip-flop. Two ladder networks each consisting of five inductors and five capacitors were used to simulate the delay lines in the fluid circuit. The total inductance and capacitance of each ladder network was made equal to that of the corresponding delay line. Thus the total inductance of the feedback delay line is $5L_1$ and the total capacitance is $5C_1$. Similarly the total inductance of the pulse forming delay line is $5L_2$ and the total capacitance is $5C_2$.

The calculated values of the parameters used in the analog circuit are shown in figure F-8.

Scaling Factors

Because the numerical values of the electrical elements shown in figure F-8 were in general outside the range of the available electrical components it was necessary to use two types of scaling:

(i) Amplitude Scaling

Consider the differential equation for a simple LRC series circuit:

$$L \frac{di}{dt} + Ri + \frac{1}{C} \int i dt = f(t) \tag{25}$$

Both sides of equation (25) may be multiplied by a constant K_s giving:

$$(K_s L) \frac{di}{dt} + (K_s R) i + \left(\frac{K_s}{C} \int i dt - K_s f(t) \right) \tag{26}$$

Thus to amplitude scale the circuit parameters it is simply necessary to make the substitutions:

$$L_s = K_s L \tag{27}$$

$$R_s = K_s R \tag{28}$$

$$C_s = \frac{C}{K_s} \tag{29}$$

where L_s, R_s and C_s are the amplitude scaled values corresponding to the original parameters.

(ii) Time Scaling

Equation (25) may be expressed in terms of a time τ whose units are different from those of time t.

$$\text{Let } t = K_t \tau \tag{30}$$

then using the right hand side of expression (30) in place of t in equation (25) we obtain:

$$L \frac{di}{d(K_t \tau)} + Ri + \frac{1}{C} \int i d(K_t \tau) = f(K_t \tau) \tag{31}$$

$$\therefore \left(\frac{L}{K_t} \right) \frac{di}{d\tau} + Ri + \left(\frac{K_t}{C} \right) \int i d\tau = K_t f(\tau) \tag{32}$$

Equation (32) shows that time scaling may be accomplished by performing the following transformations on the circuit parameters:

$$L_t = \frac{L}{K_t} \tag{33}$$

$$R_t = R \tag{34}$$

$$C_t = \frac{C}{K_t} \tag{35}$$

where L_t, R_t, and C_t are the time scaled values corresponding to the original parameters.

By combining amplitude scaling with time scaling a convenient range of values for all circuit parameters used in the analog circuit may generally be obtained.

Let the real values of inductance resistance and capacitance corresponding to the equivalent electrical circuit be L_r, R_r, and C_r, and let the actual values used in the analog circuit be L_a, R_a and C_a; then the values of the parameters in the analog circuit may be obtained by combining expressions (27), (28), and (29) with expressions (33), (34), and (35), giving:

$$L_a = \frac{K_s}{K_t} L_r \tag{36}$$

$$R_a = K_s R_r \tag{37}$$

$$C_a = \frac{1}{K_s K_t} C_r \tag{38}$$

It was found by trial that convenient values for the analog circuit could be obtained by using the scaling factors:

$$K_s = 10^6$$

$$K_t = 10^3$$

A circuit diagram giving the actual values of inductance resistance and capacitance in electrical units is shown in figure F-9.

Figure F-10 and F-11 show oscilloscope recordings of the output e_o measured from the instant the switch S_1 was closed. Figure F-10 shows the response with the switch S_2 in the position shown in figure F-9. This output corresponds to the side of the

flip-flop not connected to the pulse forming delay line. Figure F-11 shows the response with the switch S_2 in the opposite state to that shown. The effect of the additional ladder network, which corresponds to the pulse forming delay line, is seen to be small.

Since an input potential of 10 volts represents p_1, the time taken for the output potential to reach 2.8 v corresponds to the time taken for the flip-flop input to reach the required switching level of $0.28p_1$. This time is seen to be approximately 9 μsec.

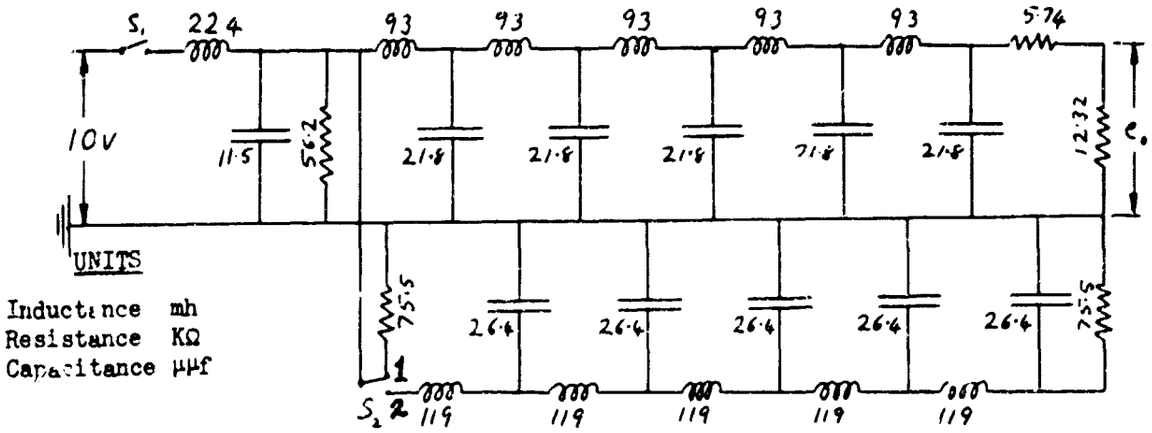

Figure F-9

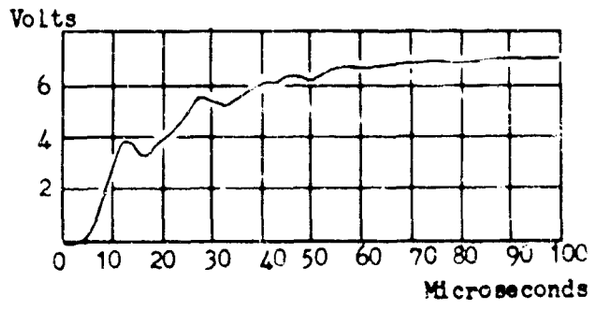

Figure F-10

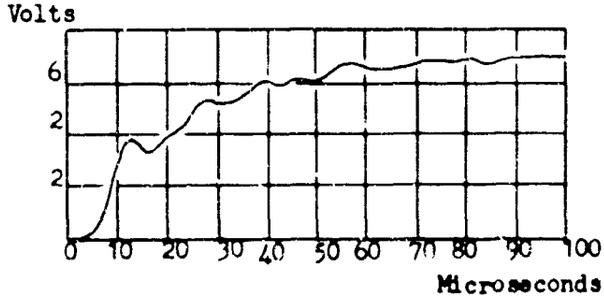

Figure F-11

A time scaling factor of 10^3 means that the electrical circuit is one thousand times faster than the fluid circuit, thus

the real time for the fluid system is nine msec. To this time must be added the switching delay time of the flip-flop, thus the cycle time T is given by:

$$T = 2(9 + 4.2)$$

$$= 26.4$$

The frequency predicted by the analog circuit is therefore 38 cps.

9.3 By Direct Measurement

A hot-wire anemometer was placed at one output of the flop-flop in the oscillator circuit and a cycle time of 25 msec was measured by means of an oscilloscope. The actual frequency is therefore 40 cps.

10. COMPARISON OF RESULTS

Both the mathematical and the electrical analog of the fluid circuit gave cycle times which were within 6 percent of the measured value. It may therefore be deduced that either method would be useful in predicting the performance of new circuits.

APPENDIX G.—THREE-STAGE BINARY COUNTER USING ISOLATION FLIP-FLOP

T. F. Chen

PAGE NO.

I L L U S T R A T I O N S

APPENDIX G.—THREE-STAGE BINARY COUNTER USING ISOLATION FLIP-FLOP

1. DESCRIPTION OF ISOLATION FLIP-FLOP

An application of the experience gained in the investigation of the steady-state, subsonic flow isolation by gap (appendix B) has resulted in a flip-flop with built in isolation. For simplicity, it is referred to as "isolation flip-flop" in the following discussion.

The HDL flip-flop (as described in figure A-1) has been modified in the fashion shown in figure G-1.*

Since the low pressure bubble formed between the power jet and the wall is essential in a stable flip-flop performance, the first step in modifying the HDL flip-flop was to determine the wall length necessary to form the low pressure bubble. It was determined experimentally that 12W is sufficient for this purpose. The second step in the modification was to determine the type of recovery port and the gap size. From the points of view of compact and easiness in reproduction, the cone shape recovery port with some bluntness of 0.005-in. at the tips of the recovery port was selected. Using cone shape recovery port it was found that a gap size of 1D, provides perfect isolation in axisymmetrical flow; see figures B-1 and B-5(b).

A larger gap size of 3W was used to account for the difference between the two dimensional flow and the axisymmetrical flow. Also four vent holes, as shown in figure G-1, are there to simulate the axisymmetric flow as closely as possible.

Modification as shown in figure G-1 was done on an epoxy cast of the HDL flip-flop. After satisfactory test result was obtained, both the device plate and its cover plate were used to reproduce a group of eight similar flip-flops by means of rubber mold. A 100-percent yield was obtained in the first group of eight with respect to bistability over the entire load range, including blocked outputs. This indicates a complete isolation, or zero feedback effects from external circuit loads. For the range of P_s from about 5 in. of water to well over 30 in. of water, the performance characteristics of these flip-flops was similar within ±5 percent. With blocked outputs, the pressure recovery is about 55 percent of the supply pressure. Figures G-2 and G-3 show the steady-state characteristics of the isolation flip-flop.

Some dynamic characteristics have been investigated. Used as the flip-flop in a circuit similar to the AND gate binary counter circuit as shown below, it oscillates at its natural frequency while driving two more similar stages. It has operated at 250 cps.

*Figures for appendix G appear on pp 165 to 172.

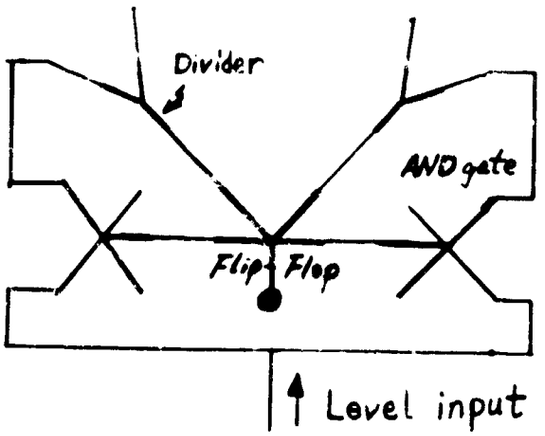

By using the shortest physically possible feedback leads in the arrangement shown below it has operated at 420 cps.

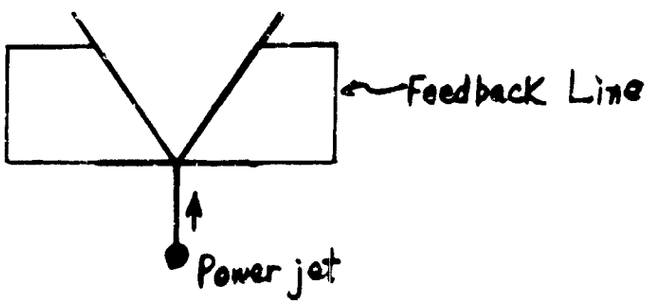

It can be safely assumed that with design refinements and miniaturization, a 1000 cycles per second unit would be quite feasible.

2. DESCRIPTION OF BINARY COUNTER CIRCUIT

To demonstrate the advantages of using the isolation flip-flops in the design and construction of a fluid circuit, it was decided to build a binary counter with unmatched components in a compact single plane. Some dimensions of the components used are shown in the table below:

Component	Nozzle size (W) (in.)	Channel Dept (t) (in.)	Aspect Ratio (t/W)
Isolation Flip-Flop	0.030	0.090	3:1
AND gate	0.020	0.120	6:1
Divider	0.015	0.120	8:1

Note: The final integrated counter stage has a uniform channel depth of 0.050 in. The nozzle width of the components remains the same as shown above. The dimensions of the whole device plate are 8.1 x 2.7 x 0.15 in. See also the attached photograph in figure G-4.

By connecting counter planes a multistage binary counter can be constructed easily.

A binary counter design as shown in figure G-5 was selected. This binary counter consists of two flip-flops, one inverter, four AND gates and six dividers, however, it does not have any delay element.

The operational features of this binary counter need considerable explanation. When there is no pulse coming into the inverter, the state of the two flip-flops in each counter stage is determined by the state of the second flip-flop FF2 (see figure G-5). That means the second flip-flop is in the set state the first flip-flop must be in the same set state.

The phase relationship of the outputs of the three-stage binary counter with respect to the pulse train is shown in figure G-6. In constructing this figure, it is assumed that the pulses are perfectly square and that the second flip-flops of each stage are at "R_2" state initially. In following through the figure, it becomes immediately clear that the first flip-flops of each stage change its state at the trailing edges of the triggering signal, whereas the second flip-flops of each stage change its state at the leading edges of the triggering signal. The frequencies of the outputs of the first, second and third stage are in the ratio of 4:2:1. Any one of the four outputs of each stage can be used to trigger the following stage, however, only the complementary outputs of the triggering outputs are in phase with one another. In figure G-5, the outputs L_1 of each stage are shown as the triggering outputs; therefore, the complementary outputs R_1 of each stage are in phase with one another, as can be seen in figure G-6.

3. METHOD OF FABRICATION OF COUNTER PLANES

In fabricating the counter planes, several kinds of components were necessary. The isolation flip-flop was obtained by modifying the HDL flip-flop as described earlier. The inverter was obtained by modifying the isolation flip-flop in such a way that one of the two output channels has less isolation compared to the other. This was accomplished by leaving one of the two output channels unmodified. The AND gate and the divider are standard UNIVAC elements, having been developed earlier.

It is quite obvious that in fabricating the counter plane a counter subunit as shown in the following diagram, can be built first.

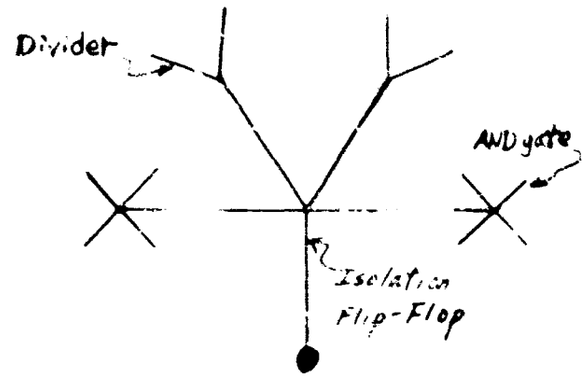

Binding three subunits together in a plane and cutting the necessary interconnection channels on both sides of the plane, an integrated binary counter plane can be built easily. The vent holes on one output channel of the first subunit can be blocked up so that it performs the function of an inverter. If a single control input is preferred, the AND gate on the opposite side of the unvented output channel can be modified to achieve this purpose.

In fabrication, the essential portion of the epoxy case unit of an isolation flip-flop, two AND gates and two dividers were prepared to build a master counter subunit. They were inserted in a compact fashion in a plexiglass plate. Then the interconnection channels were cut on the plexiglass. See attached photograph. A rubber mold of this master counter subunit was made in order to reproduce the necessary number of subunits to build a complete counter plane. The same method was used to fabricate the master counter plane and its rubber mold. Thus, a set of three epoxy cast binary counter planes was fabricated. When finishing each counter plane scotch tape was placed on the faces of the plane and the necessary vents were cut.

After each counter plane has been tested successfully, then they were cascaded one on top of the other. A three-stage binary counter has been fabricated and submitted as a part of the results obtained in this contract.

4. OPERATION OF THE THREE-STAGE BINARY COUNTER USING THE ISOLATION FLIP-FLOPS

Limited test data has been obtained on the operation of the binary counter planes using the isolation flip-flops due to the limited amount of time left in the contract period.

Using a mechanical signal generator each counter plane has operated satisfactorily up to 180 pulses per second without missing. The binary counter operated satisfactorily between 10- and 30-in. WG supply pressure; 10-in. WG is the minimum operating supply pressure; however, the counter was not tested beyond 30 in. WG. It is safe to assume that the maximum operating supply pressure is well beyond 30 in. WG.

A wide range of operation is possible with this binary counter. Figure G-7 shows the relationship of the maximum counting rate, f_{max} with respect to the supply pressure, P_s and the total pressure of the control jet, P_c. For a given value of supply pressure P_s, the maximum counting rate f_{max} increases with increasing total pressure of the control jet, P_c. On the other hand, if the available total pressure of the control jet P_c is fixed, the maximum counting rate could be either increased or decreased as the supply pressure

is increased, depending on the level of available control pressure as shown in figure G-7.

Figure G-8 shows the relationship of the minimum total pressure of control jet $(p_c)_{min}$ with respect to the pulse width τ. The pulse width was calculated from the slot angle of the rotating discs and the angular velocity of the rotation. As compared with figure D-4, which shows the switching characteristics of the original HDL flip-flop, it is noticed that the minimum total pressure of control jet is reduced considerably.

The counter is not sensitive to noise. Time did not permit a complete quantitative analysis of the influence of noise levels, however, operation is unaffected by natural air turbulence, or by the mechanical vibration of the pulse generator.

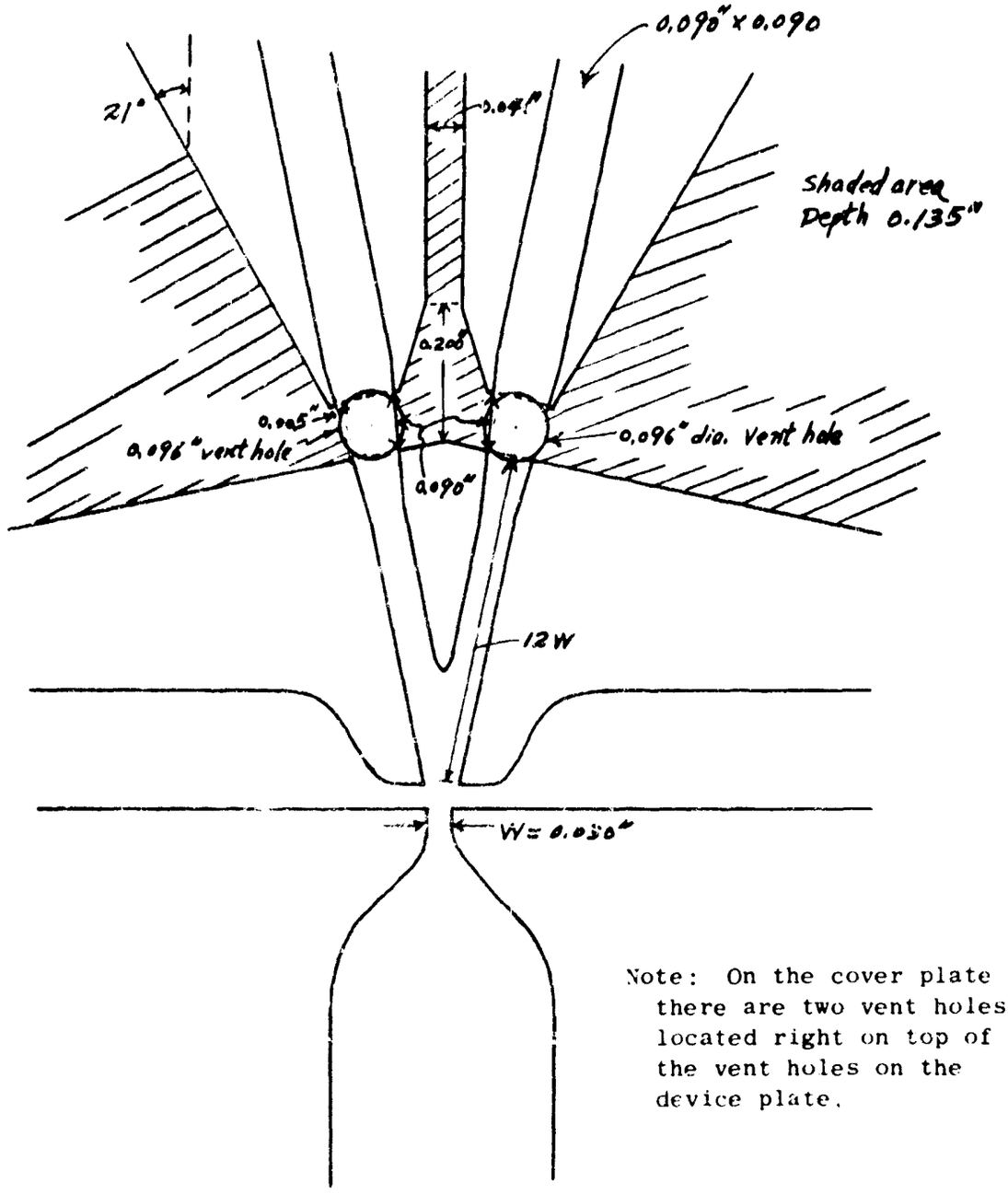

Note: On the cover plate there are two vent holes located right on top of the vent holes on the device plate.

Figure G-1. Isolation flip-flop showing the modification of HDL flip-flop (See figure A-1 for the original design.)

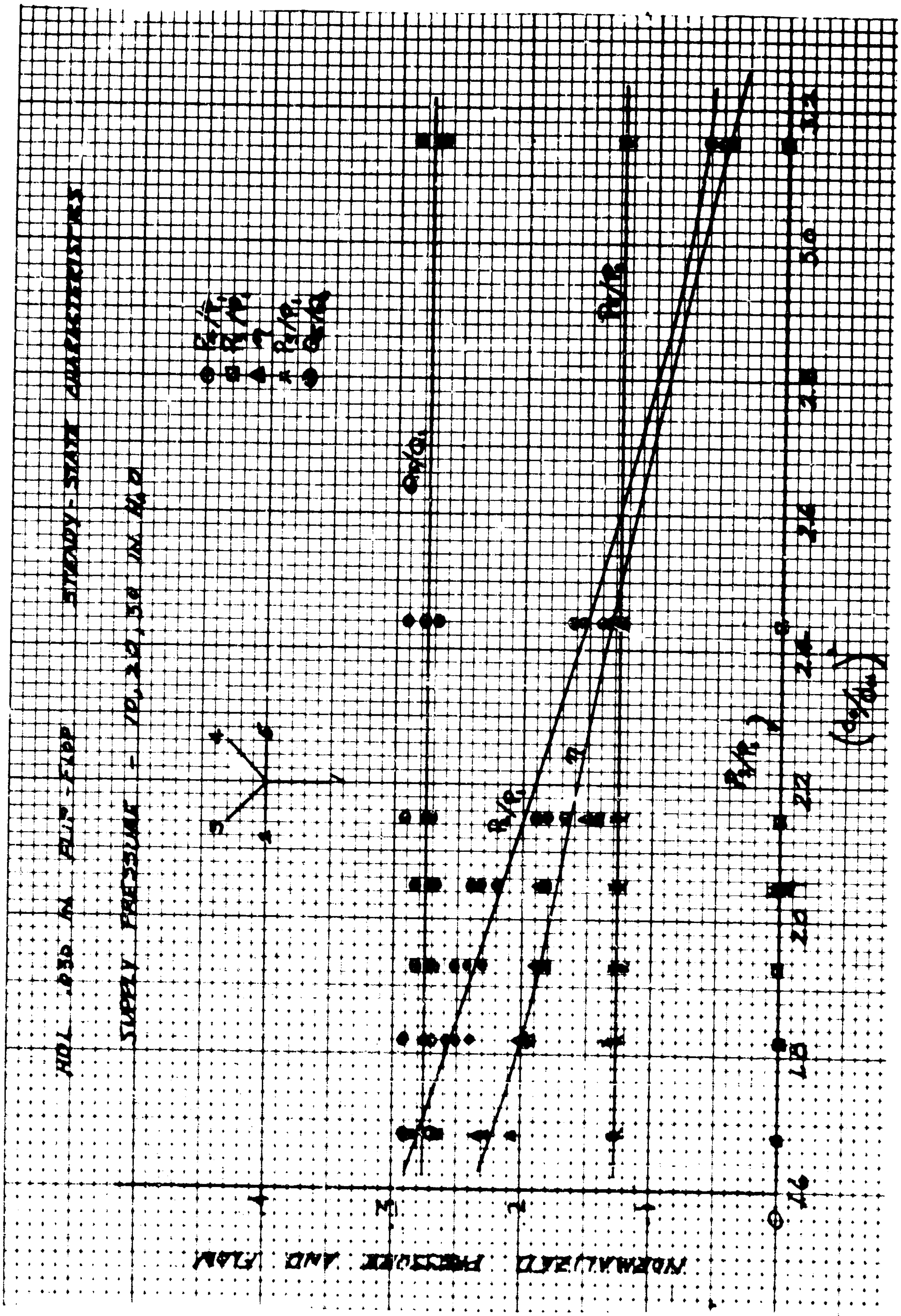
HDL .030 IN FLIP-FLOP
STEADY-STATE CHARACTERISTICS
SUPPLY PRESSURE - 10, 20, 30 IN H2O
NORMALIZED PRESSURE AND FLOW

Figure G-2

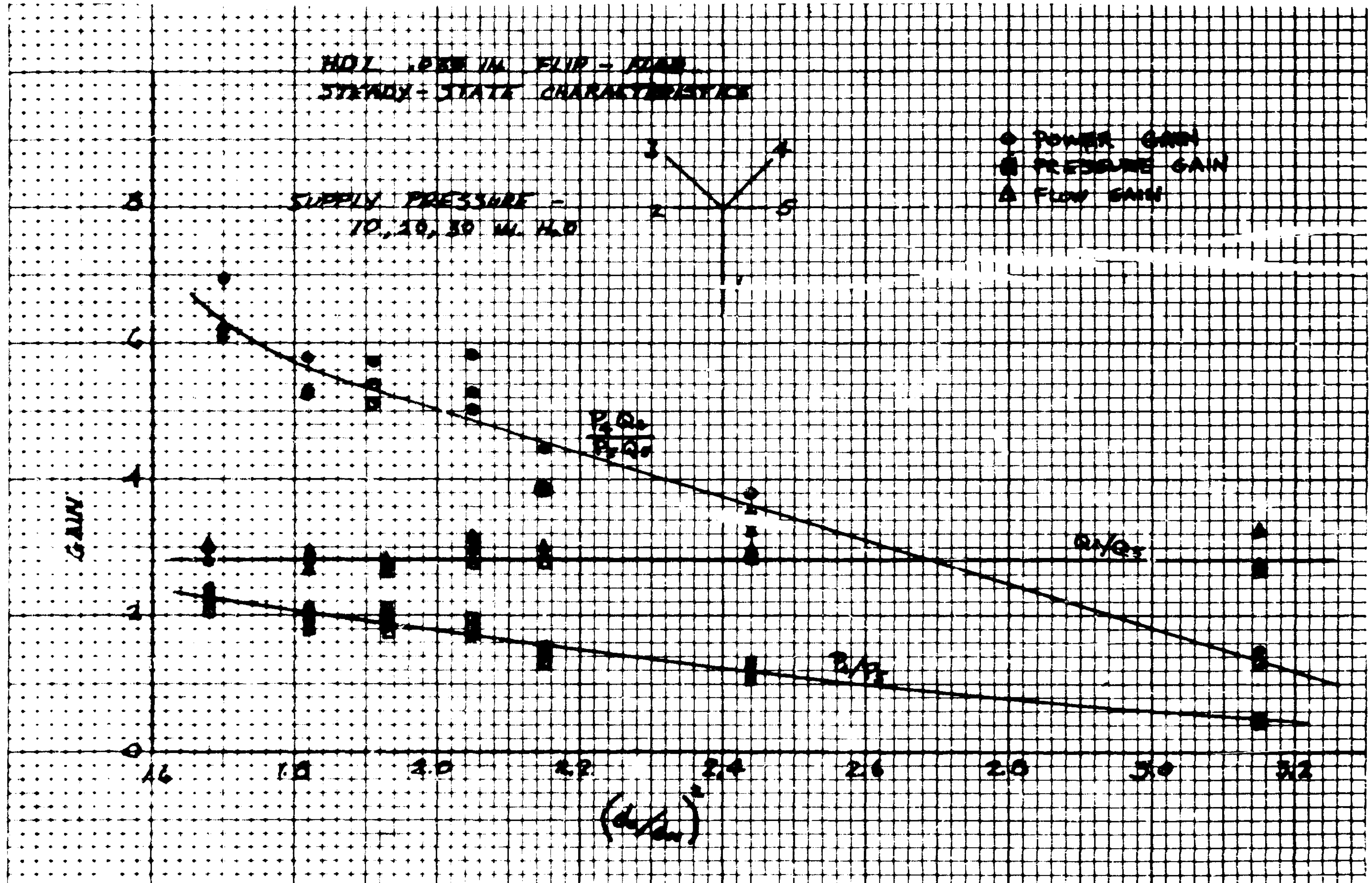
STEADY - STATE CHARACTERISTICS
SUPPLY PRESSURE -
10, 20, 30 IN. H2O
POWER GAIN
PRESSURE GAIN
FLOW GAIN
GAIN
0
2
4
6
8
1.6
1.8
2.0
2.2
2.4
2.6
2.8
3.0
3.2

Figure G-3

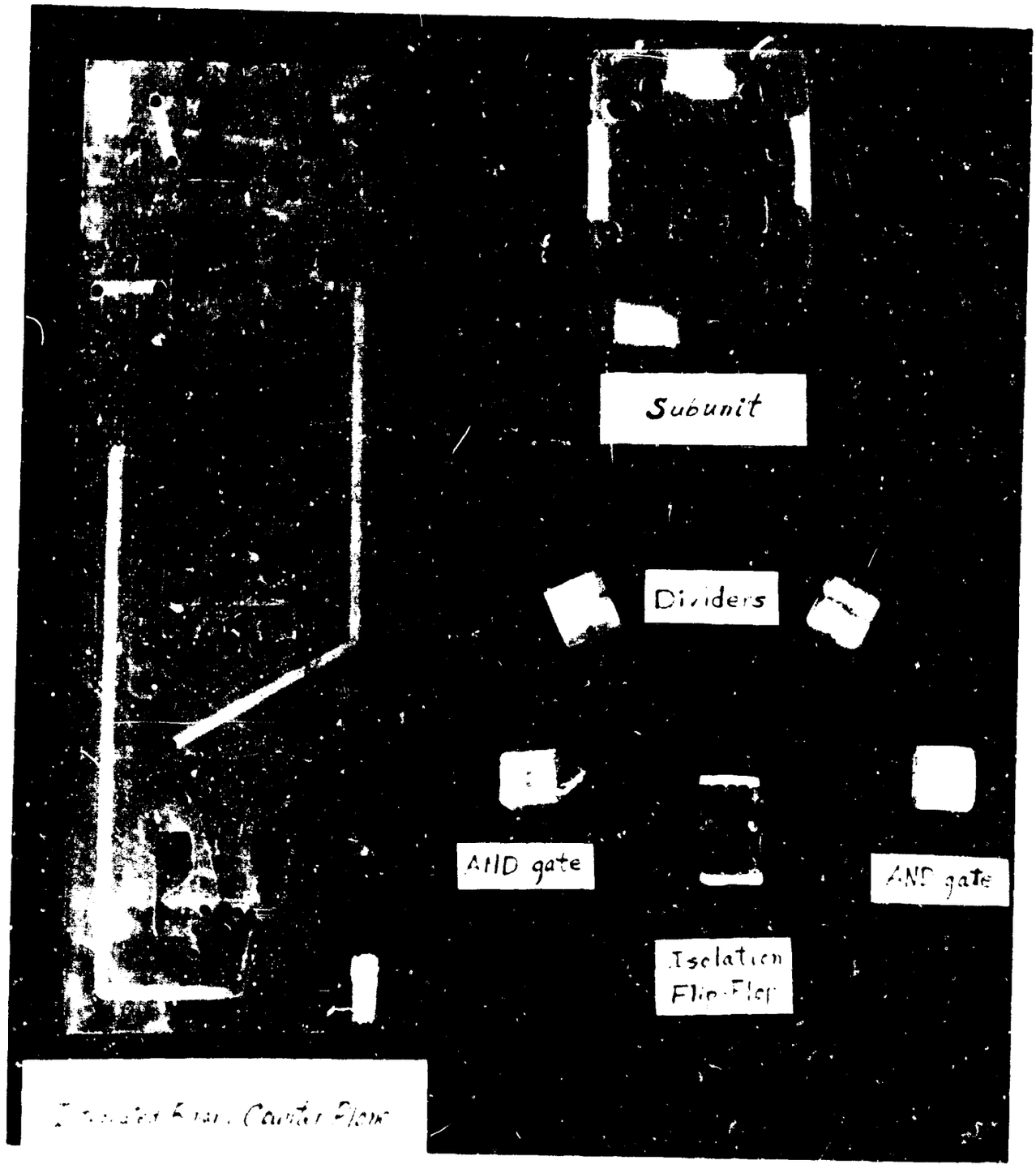

Figure G-4. Integrated binary counter plane, using isolation flip-flop.

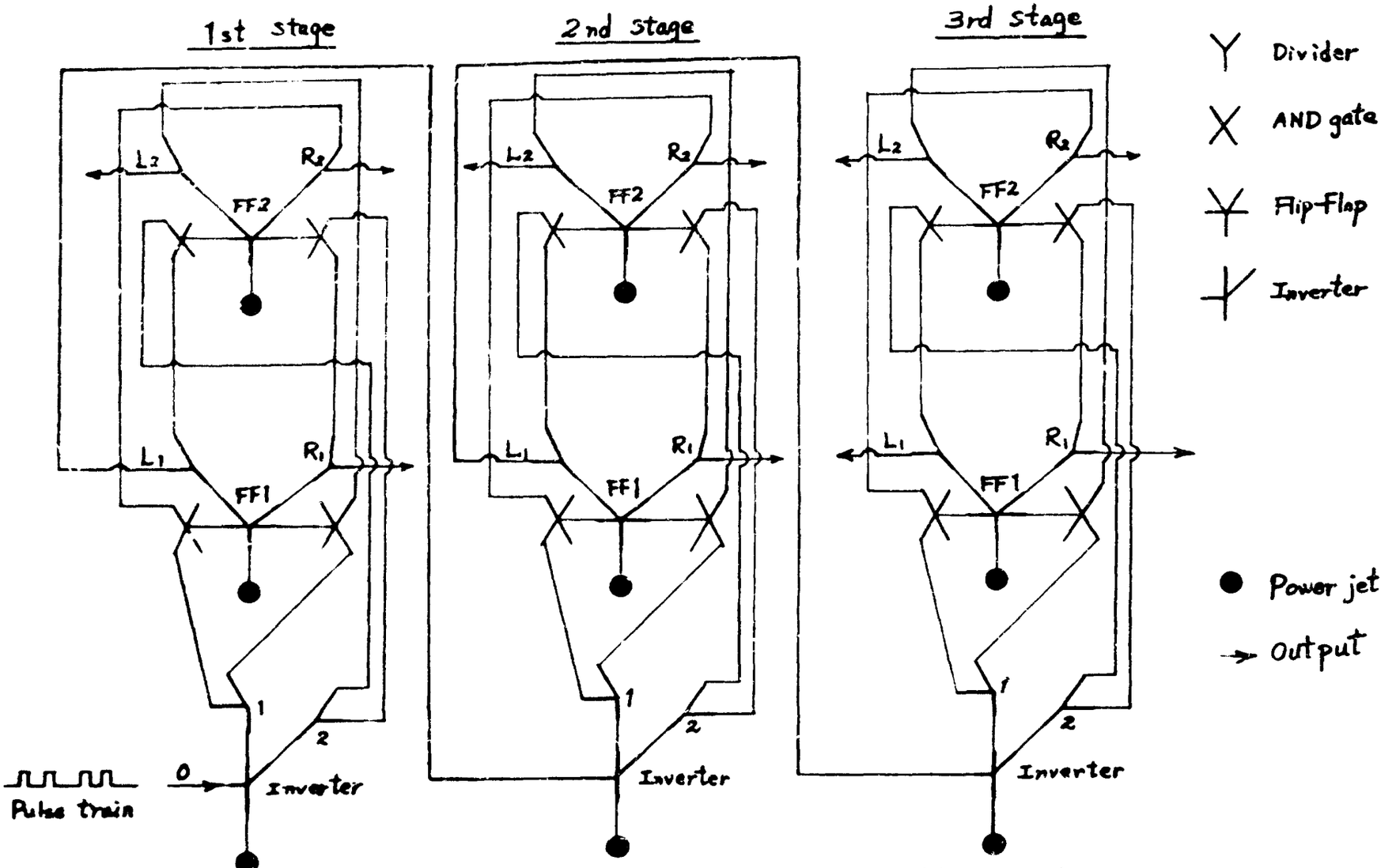

Figure G-5. Logical design of the three-stage binary counter.

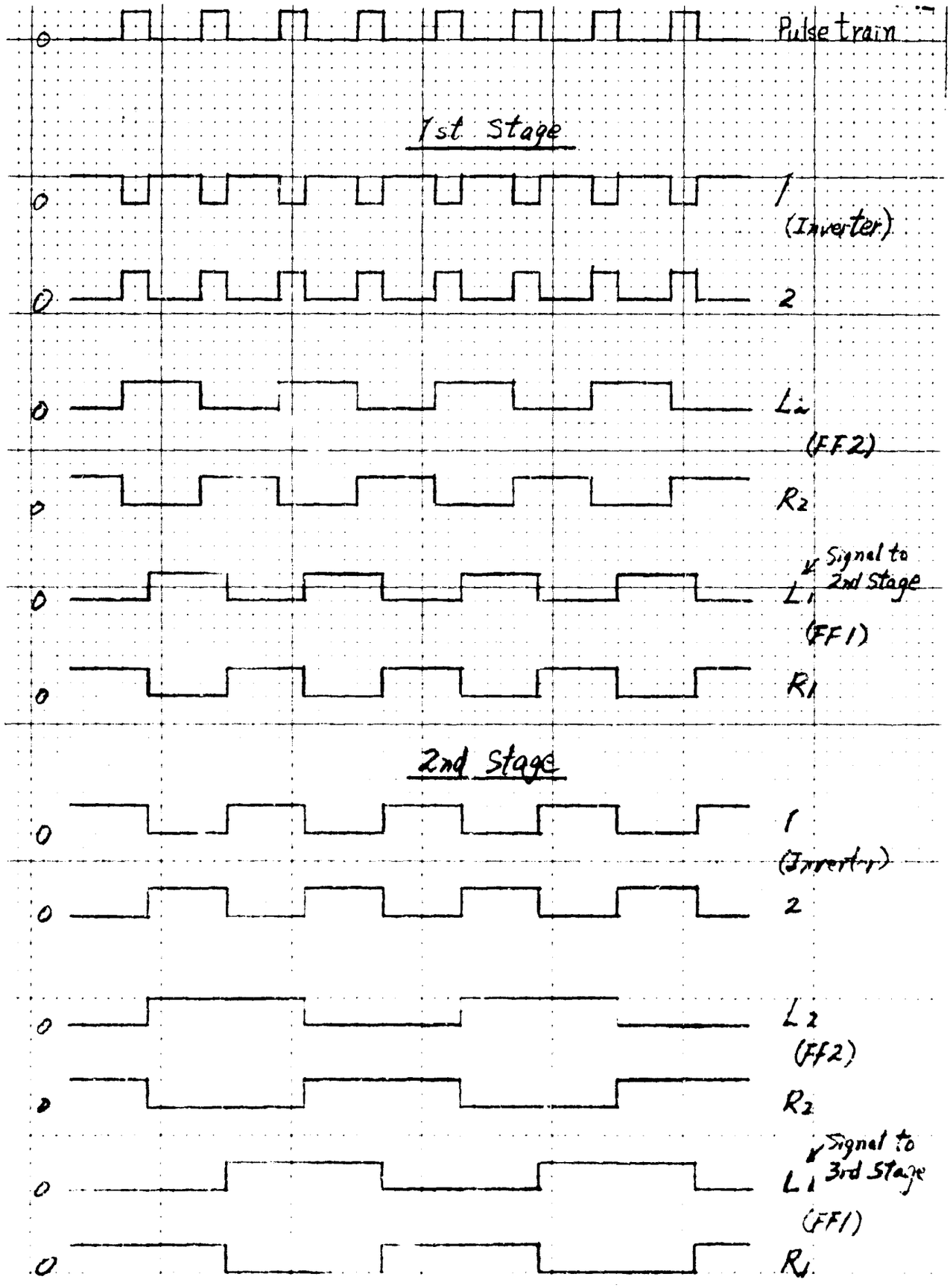
Pulse train
1st Stage
1
(Inverter)
2
L2
(FF2)
R2
L1
Signal to 2nd Stage
(FF1)
R1
2nd Stage
1
(Inverter)
2
L2
(FF2)
R2
L1
Signal to 3rd Stage
(FF1)
R1

Figure G-6(a)

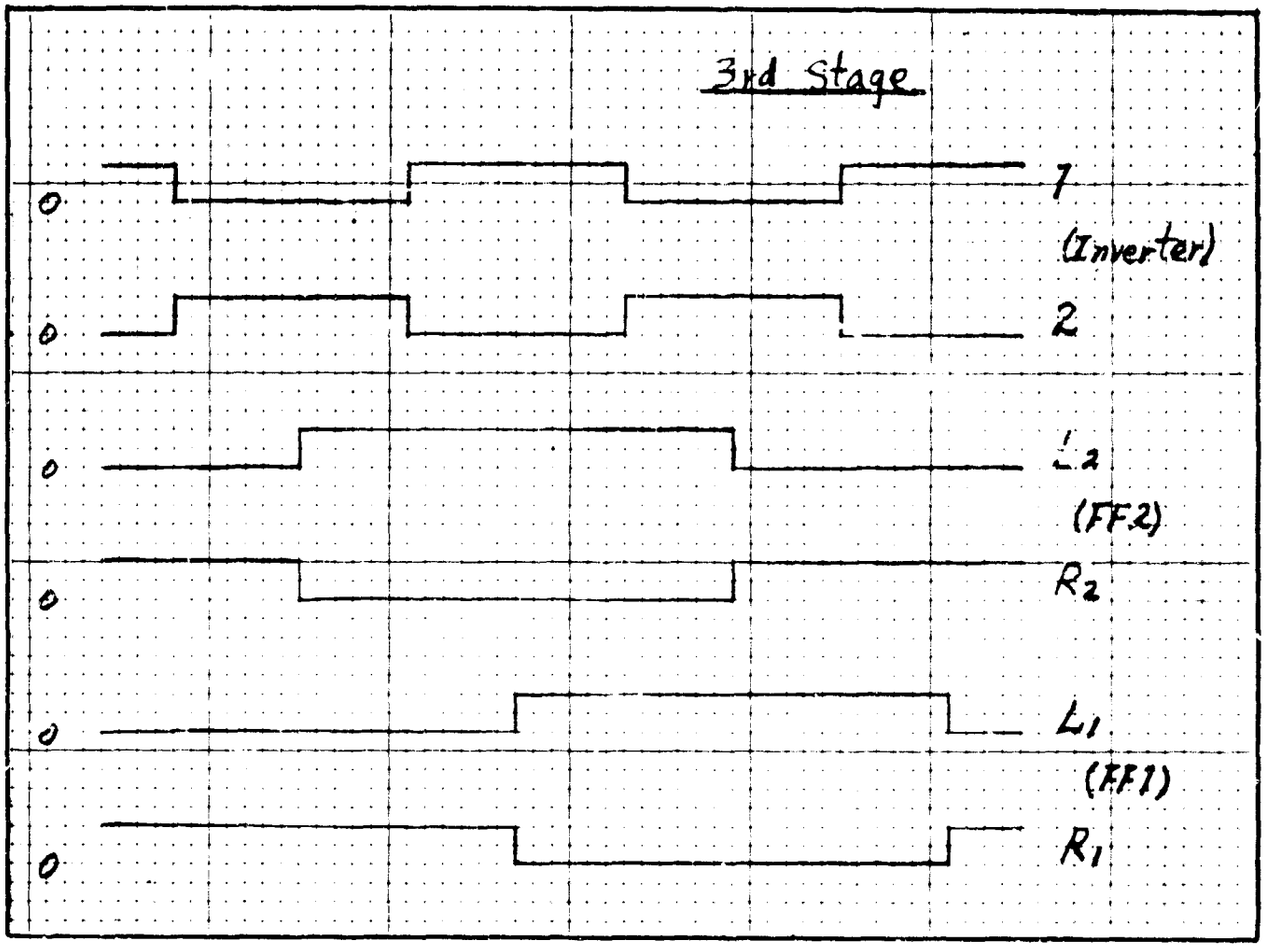

Figure G-6(b)

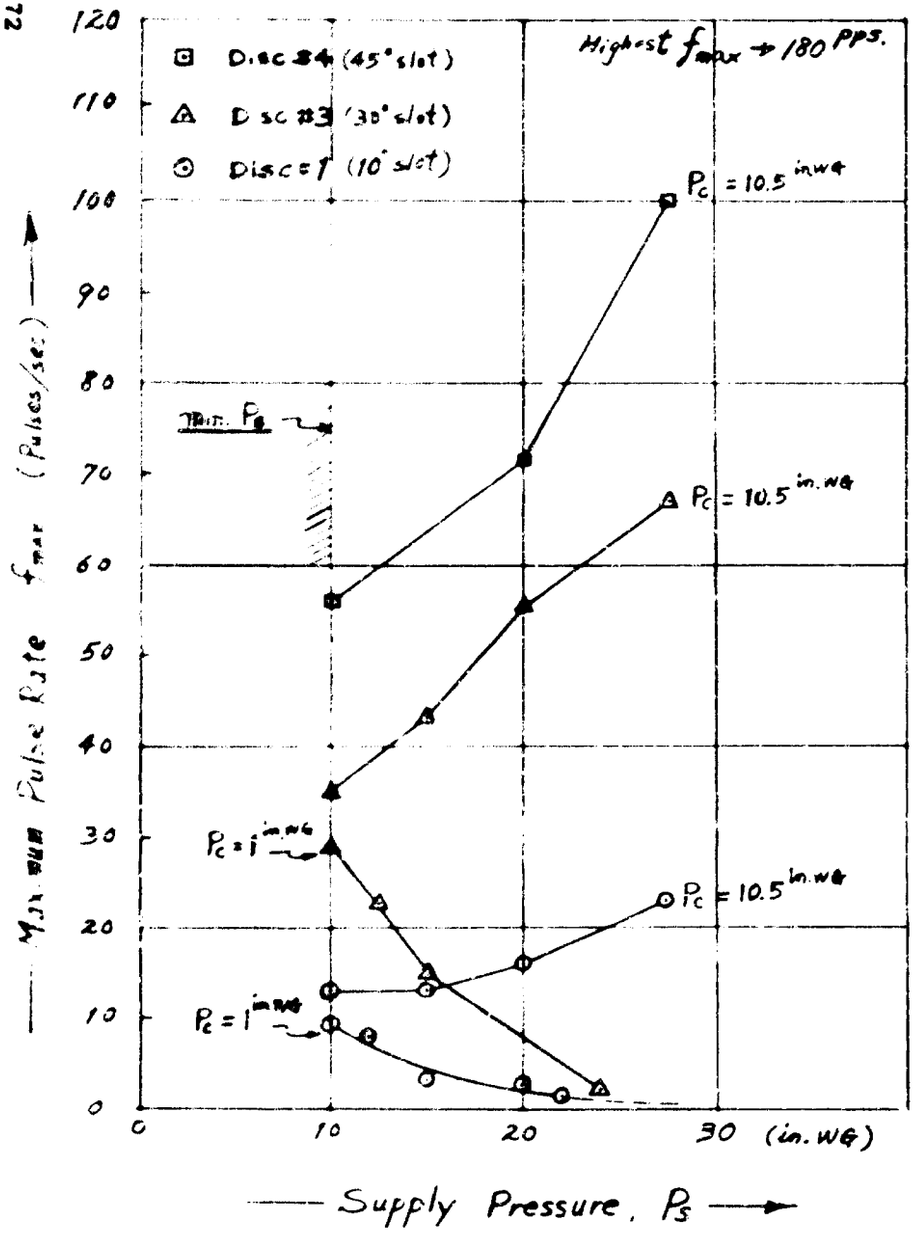

Figure G-7

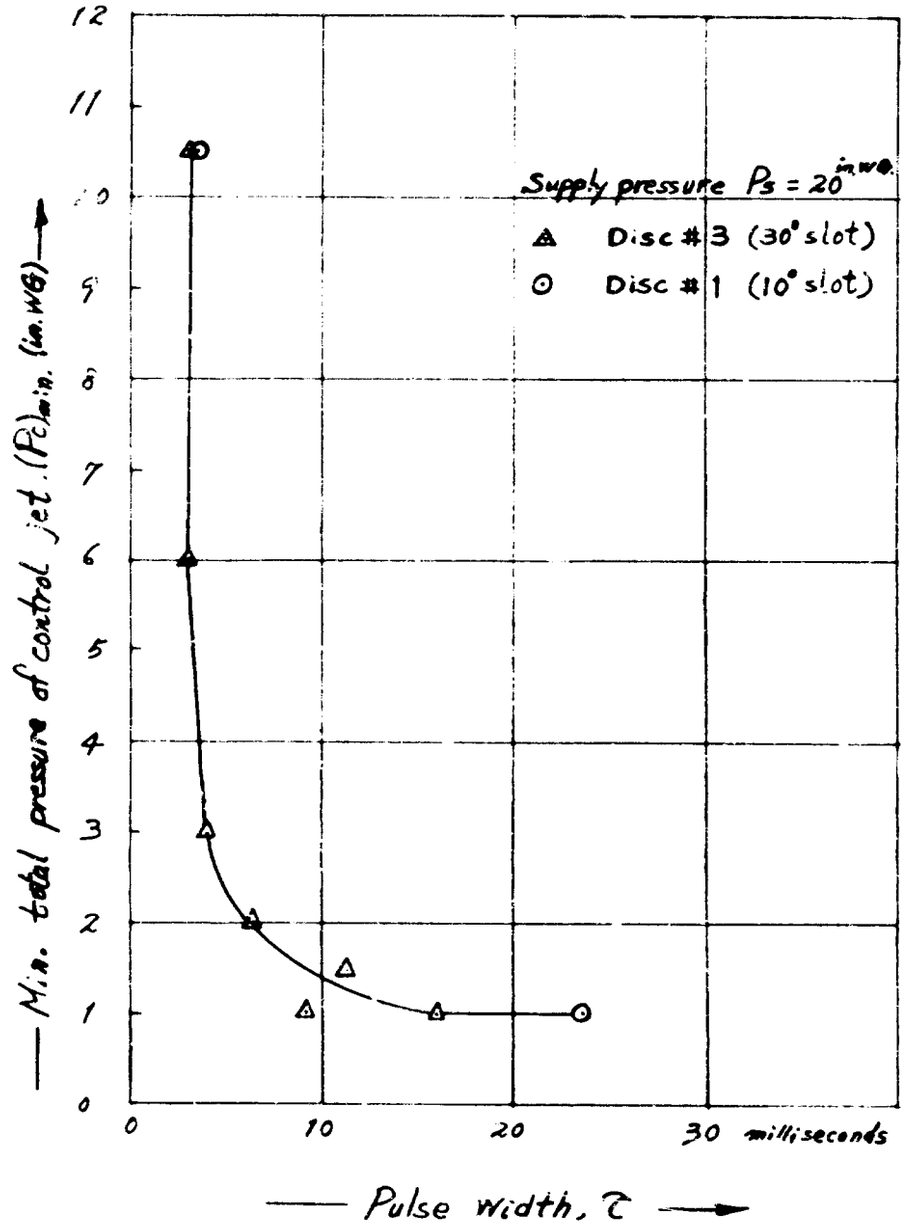

Figure G-8